UNIVERSITY
OF TRENTO - Italy
DEPARTMENT OF INDUSTRIAL ENGINEERING

XXVIII cycle

Doctoral School in Materials Science and Engineering

Production of strengthened copper materials by Mechanical Milling, Mechanical Alloying and Spark Plasma Sintering

Giulia Cipolloni

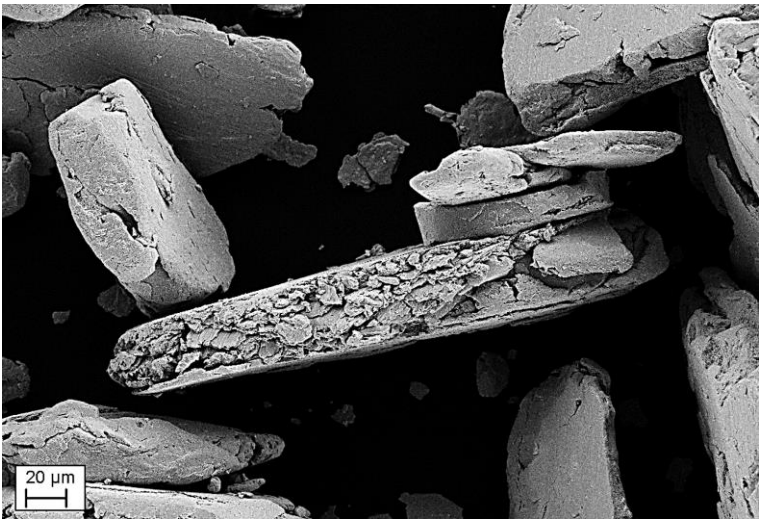

April 2016

PRODUCTION OF STRENGTHENED COPPER MATERIALS BY MECHANICAL MILLING-MECHANICAL ALLOYING AND SPARK PLASMA SINTERING

Giulia Cipolloni

E-mail: giulia.cipolloni@unitn.it

Approved by:

Prof. Massimo Pellizzari,
Department of Industrial Engineering
University of Trento, Italy.

Prof. Alberto Molinari,
Department of Industrial Engineering
University of Trento, Italy.

Ph.D. Commission:

Prof. Vigilio Fontanari,
Department of Industrial Engineering
University of Trento,
Italy.

Prof. Gino Mariotto,
Department of Informatics
University of Verona,
Italy

Prof. Eugene A. Olevsky,
Department of Mechanical Engineering
University of San Diego,
United State of America

University of Trento,

Department of Industrial Engineering

April 2016

University of Trento
Department of Industrial Engineering

Doctoral Thesis

Giulia Cipolloni - 2016
Published in Trento (Italy) – by University of Trento

To my beloved G. and L.

Abstract

Copper is widely used in many applications demanding high thermal and electrical conductivity, unfortunately its low hardness and wear resistance limit its performance. Work hardening has been proposed as a successful strengthening mechanism for the production of harder copper material, keeping the intrinsic conductivities. In this PhD thesis initially mechanical milling (MM) has been considered as suited strengthening technique due to the severe strain hardening and microstructural refinement induced by severe plastic deformation during the process. Then an enhanced hardening has been obtained by dispersion of a second harder phase in the copper matrix by mechanical alloying (MA), leading to the production of metal matrix composites (MMC). In this PhD thesis strain hardened and dispersion hardened copper materials have been sintered by Spark Plasma Sintering (SPS).

Firstly the MM behaviour of Cu as function of milling time has been studied, it consists in three stages: flaking, welding and fracturing process. Since stearic acid has been added as process control agent (PCA), its decomposition has been analysed to limit the residual porosity in sintered samples. Several focused attempts have been made and the best results have been obtained by using a fine particle size, decreasing the heating rate and applying the SPS pressure once the decomposition of PCA was completed. However the presence of copper oxide and microstructure defects induced by the severe strain hardening hinder the densification. The residual porosity is responsible of a decrease of hardness in sintered sample and consequently to a limited wear resistance, to a decrease of thermal conductivity and to a loss of ductility.

For the production of MMC a ceramic reinforcement (0.5wt% of TiB_2) has been selected. Increasing milling time the dispersion of the hard phase among the matrix becomes more homogeneous and refinement of TiB_2 is highlighted. The evolution of particle size and morphology during MA is similar to MM; also the densification mechanism during SPS are the same consisting in powder rearrangement, local and bulk deformation. The final density generally decreases by increasing milling time, by the way an increasing hardness confirms that strain hardening and dispersion hardening abundantly compensate the negative effect of porosity. Has been proved that the hard particles successfully enhanced sliding and abrasion wear meanwhile the copper matrix guarantees high thermal conductivity, satisfying the requirements.

Therefore considering the characteristics of the initial copper powder, promising results have been obtained for MMCs showing an increased hardness combined with a high wear resistance and a thermal conductivity comparable to atomized copper and much higher than the commercial Cu-Be alloy. On the other side mechanical milled samples exhibited some limits, but they allowed a deep understanding of the MM process of copper.

Table of contents

Chapter I
Introduction 1

Chapter II
Processing Technologies 5
2.1. Mechanical Milling (MM) 5
2.1.1. Development of advanced materials by MM 5
2.1.1.1. Selection of the strengthening mechanism 5
2.1.1.2. Evolution of particle size and morphology during MM 7
2.1.1.3. Achievement of a nano-structured material 8
2.1.1.4. Influence of MM parameters 10
2.2. Mechanical Alloying (MA) 12
2.2.1. Evolution of particle size and morphology during MA 13
2.2.2. Metal Matrix Composite (MMC) 15
2.2.2.1. Selection of the reinforcement for Cu MMC 15
2.2.2.2. Influence of the reinforcement 16
2.3. Spark Plasma Sintering (SPS) 19
2.3.1. Densification mechanisms 19
2.3.2. Sintering mechanisms 22

Chapter III
Wear Behaviour 25
3.1. Introduction 25
3.2. Copper applications 26
3.3. MMC: design and wear behaviour 30

Chapter IV
Materials and Experimental procedures 33
4.1. Materials 33
4.1.1. Copper 33
4.1.2. TiB_2 34
4.2. Processing route 34
4.2.1. Mechanical milling and Mechanical alloying 34

4.2.1.1. PCA, BPR and type of cycle 34
4.2.1.2. Milling time 35
4.2.2. Spark Plasma Sintering 36
4.3. Characterization of milled powder 37
4.3.1. Particle size 37
4.3.1.1. Image analysis 37
4.3.1.2. Sieve analysis 37
4.3.1.3. Metallography 37
4.3.2. Contamination 38
4.3.3. Microstructural evolution 38
4.4. Characterization of sintered samples 39
4.4.1. Density 39
4.4.2. Metallography 39
4.4.3. Hardness and microhardness 39
4.4.4. Tensile test 40
4.4.5. Wear 40
4.4.5.1. Sliding wear test 40
4.4.5.2. Abrasion wear test 41
4.4.6. Thermal conductivity 42

Chapter V
Mechanical Milling of Copper 43
5.1. Selection of the milling parameters 43
5.2. Effect of milling time 49
5.2.1. Morphology and particle size 49
5.2.2. Decomposition of PCA 53
5.2.3. Densification and sintering mechanisms 56
5.2.4. Characterization of sintered samples 58
5.3. Optimization of SPS process 65
5.3.1. Modification of SPS parameters 65
5.3.2. Modification of MM parameters 67
5.3.2.1. Evolution of powder morphology and microstructure 67
5.3.2.2. Effect of nanoparticle size and oxide during SPS 75
5.3.3. Modification of MM parameters and SPS cycle 85
5.4. Conclusions 86

Chapter VI
Mechanical Alloying of Copper and TiB_2 89
6.1. Effect of milling time on MA behaviour 89
6.1.1. *Selection of the MMC as function of milling time* 89
6.2. Spark Plasma Sintering of MMC 97
6.3. Conclusions 106

Chapter VII
Material characterization of MM-Cu and MA-Cu+TiB_2 107
7.1. Thermal conductivity 107
7.2. Tribological behaviour 111
7.2.1. Sliding wear behaviour 111
7.2.1.1. Effect of the load during dry sliding wear 129
7.2.2. Abrasion wear behaviour 133
7.3. Mechanical properties 137
7.4. Conclusions 142

Chapter VIII
Conclusion 145
8.1 Mechanical Milling 145
8.2 Mechanical Alloying 146
8.3 Properties of sintered MM-Cu and MA-Cu+TiB_2 147

List of abbreviation and acronyms 151
References 153
Scientific Production 161
Acknowledgements 163

Chapter I

Introduction

High electrical conductivity and thermal conductivity are two of the most attractive properties of copper. These advantages are the driving force for copper's new and challenging applications as high performance materials in thermal and electric fields such as plastic injection moulding, actively cooled component, continuous casting moulds, electrical contacts and welding electrodes (Avelar Batista et al., 2006; Barella et al. 2014; Futami et al., 2009; Samal et al. 2013). The high heat transfer capability leads a faster heating and cooling cycle of the moulds, therefore to a faster processing route and to a reduction of cost (Boey et al. 2005). In electrical contacts and welding electrodes a large contact force is desirable to maintain effective current transfer whilst, on other hand, it is advisable to have contact force as small as possible to reduce the wear (Futami et al., 2009; Samal et al. 2013). All these applications make copper as a competitive alternative to tool steels.

Unfortunately the low wear resistance and the high oxidation limit the copper performance pushing to the development of new advanced materials. Since wear resistance strongly depends on hardness different solutions to improve wear resistance without significantly affecting conductivity have been evaluated in the last years. Initially a surface hardening has been performed by surface coating, i.e. physical vapour deposition (PVD) coating leading to a low friction, high wear and oxidation resistance (Avelar-Batista et al. 2006; Barella et al. 2014). By the way the employment of a coating is limited by elastic and plastic deformation of the substrate, which the hard, thin and brittle coating cannot follow without failing. The difference between the thermal expansion coefficients of the two constituents increase the microstructural mismatch leading to easier and faster failure of the component. Moreover coating temperatures usually have a detrimental effect on the mechanical properties of the alloy, as they will over-age the substrate increasing the hardness mismatch between PVD coating and substrate. In addition defects produced by the deposition process, as voids, are very common and they can act as nucleation sites of cracks during service (Avelar-Batista et al., 2006). These drawbacks have been an additional driving force to further improvements and development of advanced processing routes for copper components.

In the last years, several processes based on severe plastic deformation (SPD) have been developed to refine the grain size and to improve hardness and strength

(Valiev 2004). This approach is based on heavily straining hardening by a microstructure refinement using severe plastic deformation induced by a high imposed pressure, in this way not only the properties of the surface are enhanced but of the entire component. Successful results have been obtained by SPD approaches as equal channel angular pressing (ECAP) and high pressure torsion (HPT) (Benchabane et al., 2011; Valiev, 2004). By the way the main limitation to these solution is the strong anisotropy showed by the products (Mishra et al., 2005; Setman et al., 2013).

At this point mechanical milling (MM) has been proposed as a successful SPD process for the production of strengthened nanostructured base materials (Suryanarayana, 2001). MM is of considerable interest as the microstructure is more uniform than that of other SPD methods especially due to the continuous change of deformation axis during processing (Setman et al., 2013). MM has been widely used to synthesize nano crystalline materials due to its simplicity, low cost, and applicability to most materials (Ruzic et al., 2013; Suryanarayana, 2001). During MM a nanometre sized microstructure characterized by high grain boundary surface and dislocation density can be achieved enhancing hardness and wear resistance by mechanical hardening (Ruzic et al., 2013).

An extended hardening can be obtained by dispersion strengthening, which consisting in the uniform dispersion of a harder second phase through the metal matrix by mechanical alloying (MA). This leads to the production of metal matrix composites (MMC), which have recently attracted substantially attention (Long et al., 2010 [1]; Stobrawa et al., 2009). In the specific case of this PhD thesis the hard particles have to withstand wear by grooving or indenting; the copper matrix has to guarantee high thermal and electrical conductivity and enough support for the hard particles. Work hardening by MM and dispersion hardening by MA are appropriate processing routes to give desired combination of high strength and low electrical resistivity to copper materials (Ashby, 2011). A similar benefit has to be expected also for thermal conductivity. Nevertheless, the dispersion hardening by MA will negatively affects conductivity more than MM only (Ashby, 2011). Beside microstructural defects generated by MM, i.e. dislocation, grain boundaries etc., also the reinforcement particles act as scattering centres slowing down the electric and thermal flows (Ashby, 2011). By the way dispersion hardening is an appropriate processing route since dispersion strengthened materials are superior in structural stability than precipitation hardened materials, because the second phase does not dissolve at high temperature (Ruzic et al., 2013). In addition MA is a solid state process performed at low temperature thus reducing or avoiding possible chemical reactions between the metallic matrix and ceramic phases (Suryanarayana, 2001; Suryanarayana, 2011). For these reason in this PhD thesis MM and MA of copper powder and titanium di boride (TiB_2) powder have been performed and deeply analysed. Moreover the selection of powder metallurgy as processing route is convenient also to avoid reinforcement segregation typical occurring in the ingot metallurgy process.

Segregation can adversely affect the properties of MMCs, and thus a homogeneous distribution of the reinforcement is essential for the improvement of mechanical properties of the composite (Ruzic et al., 2013; Suryanarayana, 2001; Suryanarayana, 2011). In order to reduce both the potential chemical reactions between the constituents and the possible growth of the nanocrystalline grain occurring at high temperature for prolonged time, the milled materials investigated in this study have been sintered by Spark Plasma Sintering (SPS). SPS technique is characterized by a shorter time and lower temperature compering to the conventional processes as hot isostatic pressing (HIP) (Elsayed et al., 2015; Tokita, 1993). The process offers accurate control of sintering energy as well as high sintering speed, high reproducibility, safety and reliability. Moreover SPS can easily consolidate a homogeneous, high quality sintered compact because of the uniform heating, surface purification and activation made possible by dispersing the spark points (Tokita, 1993).

The fundament goal of this PhD thesis is to study and to develop a copper based material showing high hardness, wear resistance and thermal conductivity. Two different processing routes have been considered: MM and MA in order to achieve a severe and homogenous strain hardening, the refinement of microstructure as well as particle size. In the first case a water atomized copper powder has been ball milled while in the second one 0.5wt% TiB_2 has been added to the Cu powder. In this way it has been possible to separately evaluate the effect of strain hardening and that of dispersion hardening. The PhD thesis is divided into three parts. The first one is aimed at the study of MM as function of different parameters and at the sintering of the milled powders through SPS. Firstly the investigation was focused on the effects of different MM parameters, e.g. process control agent (PCA), ball to powder ratio (BPR) type of cycle and milling time, on the milled powders. It is well known that the sintering processing route can be severely affected by particle size, morphology and contamination level (Bouvard et al., 2000; Suryanarayana, 2001). For this reason in the first part of this PhD thesis the attention has been focused on each single step of MM in order to guarantee their complete understanding and their optimization for the further stages of the study.

In the second part MA of copper and 0.5wt% of TiB_2 powders has been analysed as function of milling time and the sintered MMCs have been produce by SPS. MA has been proposed as an advantageous method for the production of composite characterized by a uniform distribution of the reinforcement.

The last part deals with the tribological behaviour of all the produced materials in order to evaluate the real competitiveness of copper MMC on tools steels. The severe wear service conditions of possible MMC applications request a deep wear analysis in order to improve the mechanical properties by an accurate choice of the materials, an appropriate design of the component and an optimized processing route. Also thermal conductivity has been evaluated and relations with the processing route and the material properties have been found and described.

Chapter II

Processing technologies

2.1 Mechanical Milling (MM)

Approximately two decades ago it had been demonstrated that the refinement of materials structure to nano scale by deformation processing and other means is the best way to improve mechanical properties of final products due to deformation and refinement of the crystallite structure (Suryanarayana, 2001; Zhao et al., 2002). By understanding of the underlying mechanism of strain-induced grain refinement is crucial not only from a theoretical point of view, but for technological development of advance plastic deformation techniques. From this point of view MM has been very thoroughly investigated; however, in the majority of cases the investigations are confined to areas like alloying in binary or multi component systems. Here comes the main difference between MM and MA: generally MM refers to the milling of a uniform composition powder which does not need any material transport for homogenization; in the other MA is the milling of a mixture of powders during which material transfer is required in order to guarantee a homogeneous microstructure (Suryanarayana, 2001). The first part of this PhD thesis is focused on the production of single copper system by MM. The first goal is to understand the behaviour of copper during MM and SPS in order to apply the acquired knowledge to MMC's production. The second goal is to separate the effect of strain hardening, i.e., the only strengthening mechanisms during MM, from that of dispersion hardening also working during MA analysed in the second part of this PhD thesis.

2.1.1 Development of advanced materials by MM

2.1.1.1 Selection of the strengthening mechanism

Grain refinement induced by SPD in metals is a well-known phenomenon to increase the properties of materials. On such purpose several type of techniques based on SPD have been developed involving complex stress state or high shear, resulting in a high defect density and equiaxed ultrafine grain size (d < 500 nm) or nanocrystalline structure (d < 100 nm). For example, ECAP and HPT have been used for synthesizing ultrafine-grained materials with a remarkably elevated mechanical strength (Benchabane et al., 2011; Valiev, 2004). By the way these techniques reduce

the grain size of bulk material, but it is not possible to act on the microstructure evolution of the raw materials. For this reason in the last years another SPD technology, i.e. MM has found considerable interest, because the repetition of flattening, cold welding and fracturing process causes the modification in the microstructure evolution of the raw powders, which can be kept by an optimized sintered process (Suryanarayana, 2001). Moreover MM process is of considerable interest because it assures a more homogeneous plastic deformation due to the continuous change of deformation axis during processing (Setman et al., 2013). For example Mishra et al. demonstrated the limits of ECAP technique by studying the microstructural evolution of copper processed by SPD. They obtain an ultrafine microstructure (<1μm) after several number of passes and they attested an inhomogeneity in deformation from one grain to the other and even within a grains. This inhomogeneity in deformation could lead to an unequal and detrimental distribution of grain size in the final microstructure (Mishra et al., 2005). These limitations of some SPD techniques, as in the case of ECAP, promote the success of MM processing route as an efficient alternative to induce work hardening. Different strengthening methods may have a very different influence on properties (Ashby, 2011) as report in Figure II-1.

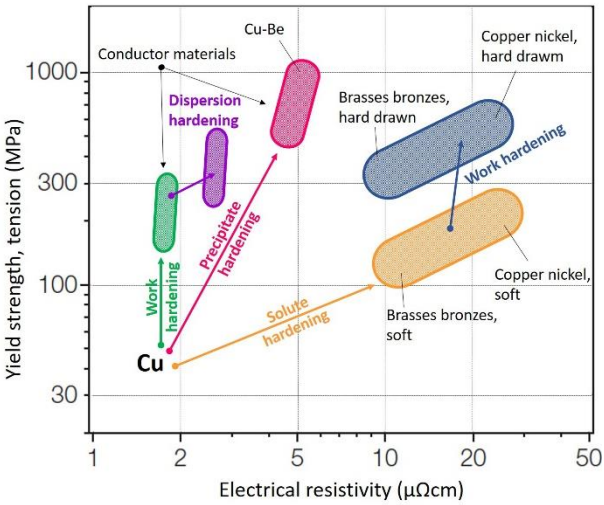

Figure II - 1. The strengthening mechanisms to increase strength without losing electrical conductivity for copper (adapted from Ashby, 2011).

In the case of copper (Figure II-1) it is clear that work hardening and dispersion hardening by MM or MA respectively represent a very promising way looking for materials having high strength and low electrical resistivity. A similar benefit has to be

expected also for thermal conductivity. Nevertheless, the dispersion hardening by MA will negatively affect conductivity more than MM only. Work hardening and precipitation hardening seem to be the best solutions to increase strength with a slight increase of resistivity. Dislocations and precipitates scatter less the electrons than the solute atoms (Fig. II-1). In fact by solute hardening the little gain in strength is accompanied by a drastically increase of resistivity (Fig. II-1) (Ashby, 2011). From Figure II-1 is clear that precipitates offer the greatest gain in strength with a slight loss of conductivity. By the way the precipitation hardening it is more difficult to control in comparison with MM and MA, because precipitation hardening relies on changes in solid solubility with temperature to produce fine particles of an impurity phase. With this respect, it is more appropriate to incorporate inert dispersoid particles such as oxide, carbides, borides into copper, thorough MA leading to the formation of copper based MMC's (Suryanarayana, 2001). The success of MM and MA as processing routes to perform work hardening has been the driving force for their use for several purposes.

MM has been widely used to refine the materials microstructure down to nano scale in order to increase their performance and also the reactivity for the sintering process. MM method is usually used to synthesize quasi-crystalline, nano crystalline and prolonging milling time the formation of amorphous materials is obtained (Suryanarayana, 2001). Later MM has been used also to perform mechano-chemical oxidation of copper by the synthesis of cuprous oxide nanoparticles (Khayati et al., 2013; Khitouni et al., 2009). In some case MM has been used to prepare metal flakes as pigment in various industry or to carry out surface mechanical attrition treatment (SMAT) for plastic strain induced grain refinement in copper (Xiao et al., 2008; Wang et al., 2006). In the recent years MM has been also used to produce harmonic structures having bimodal grain size distribution which allows achieving both high strength and high ductility (Orlov et al 2013). By the way the uses of MM reported above are only some of the several applications of these advantageous processing routes. It is clear the potential of MM opening a new field of research which drew much interest.

2.1.1.2 Evolution of particle size and morphology during MM

MM is one of the high strain powder metallurgy processes because high strain is introduced from multi direction into the powder-material. MM induces high energy impacts by collision between grinding medium and particles causing SPD, repeated fracturing and cold welding on the particle leading to nano crystalline materials (Suryanarayana, 2001).The energy transfer due to the impacts is responsible for the morphological and microstructural evolution of ductile material shown in Figure II-2.

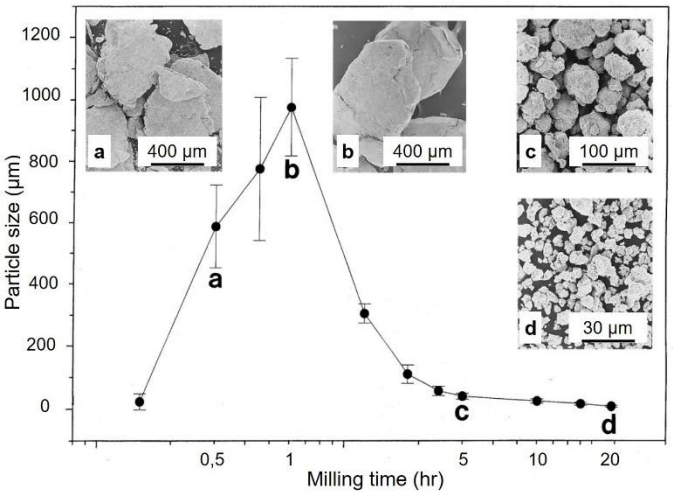

Figure II - 2. Morphological and dimension evolution of ductile material powder as function of milling time (adapted from Suryanarayana, 2001).

It is clear how for short milling time the morphology of the ductile milled powder changes into a flatten particles. The impact force causes the severe plastic deformation and the flattening of particles. The flaking level characterized by the ratio of the mean diameter to mean thickness drastically increases, as also particle size. In a later stage of the process the flakes tend to aggregate due to the predominance of cold welding events and particle dimension tends to increase. Increasing milling time the continuous work hardening leads to fracturing of the particles and a continuous powder refinement. Once fracturing and cold welding for long milling time reach an equilibrium any significant morphological and dimensional changes occur, the particle hardness remains constant and the size distribution is quite narrow (Suryanarayana, 2001). A finer mean particle size and narrower particle size distribution improve sintering allowing the production of highly dense materials (Pellizzari et al., 2011 [1]). A nano microstructure is also beneficial for sintering since small grain size enhances the grain boundary diffusion increasing the sintering rate (Diouf et al., 2012 [1]; Diouf et al., 2012 [2]).

2.1.1.3 Achievement of a nano-structured material

By literature it is known that solids deviating from their perfectly ordered structure may exhibit attractive features. The various deviations may be divided in the following two classes. The first class is obtained by thermally disordering the crystalline structure of a material and by freezing-in the disordered state by means of quenching, e.g. glasses. In the second class of disordered materials, the deviation from the perfect

crystal is induced by incorporating defects such as vacancies, dislocations, and grain or interphase boundaries. Nano-crystalline materials produced by MM belong to the second class and they have attracted considerable attention due to the improved physical and mechanical properties, which arise from the crystallite size refinement and consequent high density of interfaces as well as the significant increase of grain boundary produced by prolonging milling time (Gleiter, 1989)

The nanocrystalline material produced by MM can be considered as a coherent-precipitate strengthened two-phase alloy in which all grain boundaries merge into whole continuous matrix and each of the grains embeds in the matrix coherently. It is obvious that MM induces strain deformations which create significant amount of defects such as vacancies, dislocations, stacking faults and grain boundaries, which severely affect the physical, mechanical, optical and magnetic properties in comparison to the coarse-grained polycrystalline materials (Gheisari et al., 2013; Yousefi et al., 2013; Zhao et al., 2002). The electrical conductivity is severally related to the microstructure refinement, and a decrease of conductivity is expected after MM (Yusoff et al., 2011). The electrical conductivity decreases by MM because crystallite size refinement after milling produces a large number of interfaces which act as a source for electron scattering (Rajkovic et al., 2006). Nakamichi claimed that the grain boundary resistivity is mainly caused by the electron scattering from the grain boundary dislocation core region (Nakamichi, 1996). According to the reported literatures, the following expression could be used to estimate the contribution of grain boundaries to electrical resistivity

$$\Delta\rho_{GBs} = \frac{3}{2}\,\rho_{S-GBs}\,\left(\frac{S}{V}\right) \qquad (2.1)$$

Where S/V is the grain boundary surface area per unit volume and $\rho_{S\text{-}GBs}$ is specific grain boundary electrical resistivity, which was reported to be 3.12×10^{-12} Ωcm^2 for pure copper. De Hoff and Rhines reported that the ratio of grain boundaries surface area to volume was approximately equal to 2.37/d, where d is the mean grain diameter (DeHoff et al., 1968; Wang et al., 2014). It is clear that grain boundaries and defects are responsible of the change of microstructural parameters such as crystallite size, lattice strain and lattice parameter which drastically influence the electrical conductivity (Gleiter, 1989).

The achievement of a nanostructure material can be separated into two subsequent stages: continuous grain refinement and attainment of a constant grain size (Zhao et al., 2002). During the first stage, large amount of defects are introduced, causing the decrease of crystallite size, and the increase of the micro strain and the stored enthalpy. During the second stage, however, cycling changes of the micro-strain and the stored enthalpy are observed, which means that the microstructural cyclic variation of the milled powders occurs, even though crystalline size remains constant (Zhao et al., 2002). It has been demonstrated that the mechanical strained

structure of copper usually shows the formation of shear bands and a number of mechanical twins of two types, i.e. multiple and high-order twins (Huang et al., 1996). The generation of mechanical twins has been explained as follows: the shear stress induced by MM exceeds the critical shear stress for twinning and when the grain size decreases below to a critical value, twinning rather than slip becomes the preferred mode of deformation (Huang et al., 1996). Moreover it has been well documented that Cu coarse grains are refined upon continued straining by various dislocation activities (Wang et al., 2006). The dislocation density during MM of copper results from the balance between the rate of dislocation generation by plastic deformation and the rate of its annihilation by dynamic recovery (Khoshkhoo et al., 2014). Dynamic recrystallization generally occurs during hot deformation, which usually is accompanied by material softening (Khoshkhoo et al., 2014). Moreover the presence of this defect structure decreases the diffusion distances and increases the diffusivity of oxygen atom absorbed on the particle surface at low temperature. In view of the reduced particle size and the increased surface energy by MM, the surface oxidation of the powder is drastically enhanced (Poluboyarov et al., 2005). Mechanical activation of copper in presence of molecular oxygen, in particular that absorbed by the copper surface, may lead to the formation of defect-rich oxide (Wen et al., 2011). The presence of oxide severely affects the chemical, physical and mechanical properties of the final product (Menapace et al; 2016). Possible sources of oxygen during milling are the atmosphere, the process control agent and the powder composition, as well (Madavali et al., 2014; Zeng et al., 1999).

2.1.1.4 Influence of MM parameters

MM is influenced by many variables which determine the final material microstructure and properties. Generally speaking the parameters which influence the final products are the type of milling, the milling media (vial and balls), the milling time, the milling speed, the ball to powder weight ratio (BPR), the milling atmosphere, the extent of filling the vial, the temperature of milling and the process control agent (PCA), (Fig.II-3) (Zhang F.L. et al., 2008). All these parameters are responsible for the morphological and microstructural evolution of the milled powders (Suryanarayana, 2001; Zhang Y.F. et al., 1999).

Actually, there are many different types of milling machines and the selection depends on the type, the quantity and the composition of the milled powder. In this PhD study a planetary ball mill has been used. This type of milling machine contains a vial which can be rotated both around the axis of the supporting disk on which it is arranged and its own axis (Fig.II-3). The rotations create centrifugal forces acting on powder material and milling mediums. However, since the vial and the supporting disk rotate in opposite direction, the centrifugal forces alternately act in-phase or anti-phase. As consequence, the milling medium runs down to the “ground” (due to friction

effect) or lift off to collide against the opposing inside wall (impact effect) (Suryanarayana, 2001).

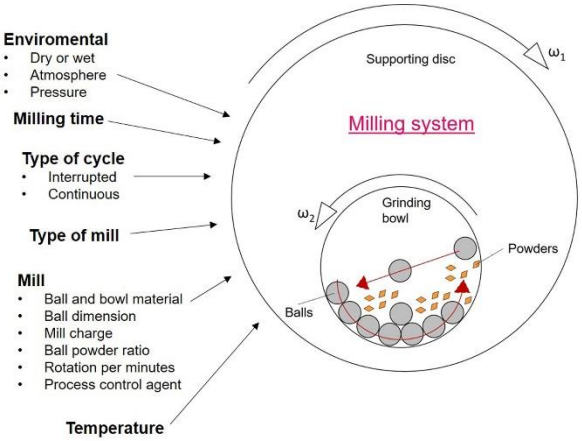

Figure II - 3. Schematic drawing of a high-energy planetary ball mill and MM parameters.

The typical materials used to fabricate milling vials and balls are: chrome steel, Cr-Ni steel, tungsten carbide (Suryanarayana, 2001). Wearing of the grinding media leads to the contamination of the powder (Marques et al., 2007). It has been demonstrated that mass wear of the media increases almost linearly by increasing milling time at the early stage, and then it starts to increase more rapidly (Sato et al., 2010). Also contamination from atmosphere is one of the major problems for mechanical milled materials (Luo et al., 2013; Madavali et al., 2014). By the way contamination from the atmosphere can be avoided or minimized by milling in an inert high purity atmosphere or in vacuum (Gordo et al., 2005; Suryanarayana, 2001). It has been demonstrated that an argon atmosphere is more preferable than air for the processing of copper powders (Madavali et al., 2014). On the other side contamination from the milling media cannot be avoided. The wear rate of milling media is dependent on the rotation speed, the diameter of the ball and the ball filling ratio (Sato et al., 2010). To minimize iron contamination arising from the milling medium some precautions can be employed as coating and step-fashion MA method (Luo et al., 2012; Luo et al. 2013). Also the use of a PCA reduces wear, and further contributes to achieve a suited equilibrium between fracturing and welding events. If a ductile metal or alloy is milled at room temperature without any PCA welding will predominate over fracture and particle size will steadily increase with milling time (Harris et al., 1995; Huang et al., 1995). Growth occurs by the continuous transfer of material from the smaller to the larger particle (Harris et al., 1995; Huang et al., 1996). To inhibit welding and to produce a fine powder, it is generally necessary to cool the vial and/or

use a PCA. Surfactant absorbed on the surface of the materials can reduce their hardness and can reduce the viscosity of the mixture (Zhang F.L. et al., 2008). The most used PCA's are benzene, stearic acid, ethanol and methanol (Long et al., 2010 [1]; Suryaranayana, 2001). The use of PCA's, however, is problematic, since they are organic compounds and inevitably increase the C, H and O levels in the powder (Bhattacharya et al., 2004; Gomez et al., 2006). It is well known that these impurities are detrimental to the ductility and conductivity of the compounds. By the way the addition of PCA leads to a decrease of average particle size, but increases the required milling time (Gheisari et al., 2013; Khayati et al., 2012; Zeng et al., 1999). Another benefit from the use of PCA is to reduce the temperature during the milling process. A limitation of MM is related to the temperature increase because only a small percentage of the total energy is used for the milling process, the major part of energy is turned in to heat (Suryaranayana, 2001). Higher speed means higher energy and therefore higher heating. The increase of temperature is strongly influenced by BPR. That is because a high BPR leads to an increase of number of collision per unit time resulting in a much higher energy transfer, which causes a higher increase of temperature and deformation (Suryanarayana, 2001; Wang et al., 2014). The use of increasing BPR considerably affects the microstructural evolution of the milled powder leading to a high dislocation density (Khoshkhoo et al., 2014). All the milling parameters are important and influence the milling process, by the way MM is strictly dependent on milling time in order to achieve the milled powder requirements. For every milling system there is an optimum milling time for which fragmentation and cold welding process are in dynamic equilibrium and MM can be considered completed.

2.2 Mechanical Alloying

MA is one of the solid state processes for the production of MMC combining strain hardening by microstructure refinement and dispersion hardening. MMC due to the complexity and to the high number of variables influencing their final behaviour their design is quite elaborate, but their promising properties encourage research in this field (Maurice et al., 1990). The goal is to combine the different properties of the two or more constituents in a new material with novel properties. The challenge is to increase the bonding strength of the interphase by controlling manufacture process and some particle features as size, morphology and volume fraction (Berns et al., 2003; Estrada-Guel et al., 2014; Zum Gahr et al., 1998).

MA is widely accepted as an appropriated technique for the development of MMC with better properties than those achieved by other methods (Akhtar et al., 2009; Long et al., 2010 [2]; Suryanarayana, 2001). By employing MA, the agglomeration of reinforced particles can be avoided and a homogeneous distribution of reinforcing phase within the matrix can be achieved. Compared to the liquid phase process, the

powder metallurgy technique allows better control of the reinforcement distribution and the production of more uniform matrix microstructure without the formation of segregations (Bouvard et al., 2000). Also the adhesion between the constituent must be guaranteed otherwise pulling out of the reinforcement may occur deteriorating the material properties. Moreover the presence of an interspace between the phases may acts as site of crack nucleation and it can be considered very detrimental for the mechanical properties of the component. MA due to the intense energy involved by impact events between the milling media and the powder assures a strong mechanical bonding among the constituents. A slight rise in the powder temperature during MA as a result of frictional forces and impact of the grinding balls against other balls and the vial facilitates alloy formation. Finally during the design of MMC the thermal and chemical stability between the constituents cannot be neglected because the formation of unwanted component it may not satisfy the chemical, mechanical and physical requirements. MA generally involves lower processing temperature thus reducing the reactivity between metal matrix and reinforcement phase. Therefore, due to these promising and suitable characteristics of MA, it has been selected as suited technique for the production of MMCs in the second part of this PhD thesis and its fundaments are described in the following section.

2.2.1 Evolution of particle size and morphology during MA

MA is a process that was developed by John Benjamin in the late 1960s to produce oxide dispersion-strengthened materials (Benjamin, 1970). Then due to its high performance and advantages has been widespread in several applications, for example some of the attributes of MA are: production of fine dispersion of second phase particles, extension of solid solubility limits, refinement of grain sizes down to nanometre range, synthesis of novel crystalline and quasicrystaline phases, development of amorphous phases, disordering of ordered intermetallic, possibility of alloying of difficult to alloy elements and inducement of chemical (displacement) reactions at low temperatures (Suryaranarayana, 2001). The process can be described as a high-energy milling process in which different types of powder particles are subjected to repeated cold welding, fracturing, and rewelding in order to obtain a uniform microstructure (Maurice et al., 1994; Maurice et al., 1995). Generally during MA the elemental powders are blended and formation of different types of phases occurs through a very fine and intimate mixture of the components. The effects of MA could be divided in two groups: on one side constitutional changes may occur leading to the formation of solid solutions, intermetallic phases, and amorphous phases in alloy systems; on the other side microstructural changes of the processed materials may occur developing ultrafine-grained and nanostructured phases, and an intense powder refinement.

Related to the second group of the MA effects, Gilman and Benjamin summarized the process into 4 stages (Gilman et al., 1983). Depending on the predominant process, each stage will exhibit a morphology that can describe the process taking place at that time (Fig.II-4) (Fogagnolo et al., 2003). These stages include: initial, intermediate, final, and completion stage.

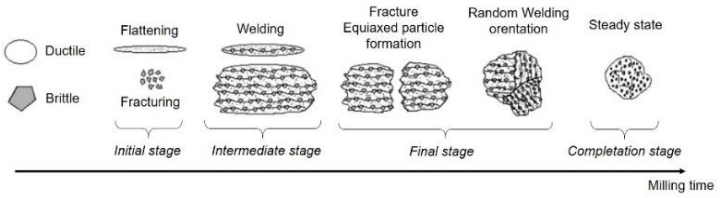

Figure II - 4. Various stages of ductile-brittle system during MA (adapted from Fogagnolo et al., 2003).

At the *initial stage* of MA, the starting soft particles generally tend to be flattened by compressive force. For ductile-brittle system, the hard particles tend to be less deformed while the ductile particles show high tendency of binding the hard particles together. Fracture is expected to be predominant in BCC and HCP metals (due to lower number of slip systems) with respect to cold welding in FCC metals (12 slip systems). As a result of difference in ductility between brittle and ductile phases, particle size distribution is wide during the initial stage of MA. A more homogenized particle size distribution is anticipated upon prolonging the milling duration. At the *intermediate stage* of MA, significant changes in particles' morphology occur. Cold welding is now more substantial than in the previous stage. Greater plastic deformation results in formation of layered structures. Also, within this stage of milling, laminated structure can be further refined once fracture is taking place (Fogagnolo et al., 2003; Gilman et al., 1983). Considerable particle size reduction can be detected at the *final stage* of MA, where the layered structure is no more detected and the microstructure becomes very homogeneous. At this stage, further deformation is almost impossible since particles already reached very high hardness induced by accumulation of strain energy (Gilman et al., 1983). At the end of the process, i.e. *completation stage*, the particles show a heavily deformed meta-stable structure. Further prolonging the milling time will not improve the particles distribution anymore (Gilman et al., 1983; Ruzic et al., 2013).

In some cases the presence of harder oxides in the powder mixture enhances the brittleness of the system leading to a finer particle size at the end of MA (Menapace et al., 2016; Rajkovic et al., 2008). The presence of oxide can be attributed to different causes: for example to the grade of purity of the starting powders, to the formation of oxide compounds during MA or to the severe oxidation of the reactive surface of the

milled powders. It is essential to notice that during MA, as for MM, due to heavy deformation and to numerous defects introduced into particles, the diffusivity of solute atoms into the matrix by preferential path is increased. Besides, both the reduction of diffusion distances and the slight rise in temperature during milling also aids the diffusion oxygen behaviour and consequently, selective reaction takes place among the matrix and oxygen elements (Suryanarayana, 2001). Moreover, due to an increase in the free energy of the system caused by a reduction of particle size and consequence increase in surface energy, the surface oxidation of the powder is drastically enhanced (Poluboyarov et al., 2005; Wen et al., 2011).The formation of oxide can be promoted affecting both the MA kinetic and the final composition of the MMC (Marques et al., 2007; Prasad et al., 2004; Ritasalo et al., 2010; Wen et al., 2011).

2.2.2 Metal matrix composite (MMC)

2.2.2.1 Selection of the reinforcement for Cu MMC

The success of MMC is associate to the possibility to design and to improve the characteristics of the component by a projected synergy of the properties of the constituents. The selection of the reinforcement during the design of MMC must be optimized in order to limit possible secondary reactions of undesired products, to enhance the adhesion between the matrix and the second phase and guarantee the tailored properties (Groza et al., 1993). The two constituents of MMCs have different duties: the hard particles have to withstand wear by its higher hardness; the matrix has to guarantee toughness and enough support for the hard particles. In the specific of copper MMCs the matrix has to keep its intrinsic thermal and electrical conductivity, meanwhile its low wear resistance must be enhanced by the homogeneous dispersion of a hard second phase. Since Cu MMCs are becoming attractive materials for specific thermal and electrical applications, different studies have been conducted in the last years in order to deeply investigate and improve their performance.

Several types of reinforcement have been dispersed in copper matrix (Al_2O_3, WC, TiC, SiC, TiB_2, Cr, NbC, carbon-nanotube, etc.), in most of the cases ceramic powders are used due to a very high hardness and a good chemical stability in comparison with metal reinforcements (Khaleghi et al., 2012; Sahani et al., 2011; Stobrawa et al., 2009). For example, even if the addition of a small amount of Cr and Zr seems to be effective to improve copper composite properties, it leads to unwanted precipitation of hard secondary phases. One of the limitations of such precipitation-hardened alloy is the lack of strength above 500°C, related generally to the structural instability associated with the coarsening of precipitation particles (Girish et al., 2012; Tjong et al. 2000). Also Cu-graphite composite have been widely studied for applications requiring highly electrical conductivity in addition to low friction and wear,

but the processing complexity and the poor mechanical properties limited its diffusion. In addition it is not easy to fabricate a fully dense Cu graphite composite due to the poor wettability between the two phases, as well as their significant differences in densities. Among various ceramic dipersoids NbC has been used as reinforcement in copper matrix but the electrical conductivity was dramatically affected by the presence of NbC because the material did not reach the electrical conductivity requirements (at least 50% IACS) (Long et al., 2010 [2]). Also Al_2O_3 particles are commonly used to reinforce copper producing superior elevated temperature strength, increased hardness and improved creep resistance (Rajkovic et al., 2008). But the surface of the mechanically milled Al_2O_3 particles are covered by oxide nanometer-thick layers that gives rise to some problems during consolidation. Recently as copper's reinforcement, a family of layered ternary carbides, including Ti_3AlC_2, Ti_3SiC_2 and $Zr_2Al_3C_4$ which possess good thermal and electrical conductivities as well as high strength and modulus, have been added to copper and significant improvements in both hardness and strength were observed (Zhang J. et al., 2009).

Titanium diboride (TiB_2) particle has been also considered as a possible interesting candidate to reinforce copper because of its high melting point, high hardness, superior wear resistance and thermal conductivity (Kwon et al., 2006; Suryanarayana, 2001; Tjong et al., 2000; Tu et al., 2003). Moreover the yield strength of Cu-TiB_2 composite produced by in situ reaction and after a suitable heat treatment, it is found to be higher than that of Cu-Al_2O_3 composites (Biselli et al., 1994, Ma et al., 2000). This has been attributed to the good microstructural stability, arising from the chemical stability of TiB_2 phase (Biselli et al., 1994, Ma et al., 2000). Guo et al. produced successfully a dispersion strengthened Cu-TiB_2 alloy combining mechanical alloying with heat treatment (Guo et al., 2013). Increasing milling time the interface boundaries between the phases become vanish or disappear completely, and finally forming homogeneous microstructure. Also the creep resistance of the composite is several order of magnitude higher than that of the unreinforced Cu (Ma et al., 2000). At this point TiB_2 can be considered as a suitable reinforcement for copper matrix composites.

2.2.2.2 Influence of the reinforcement

As already discussed, in order to achieve high strength and high wear resistance, it is necessary to alloy copper with reinforced ceramic particles. However, while most of ceramic reinforcements can enhance significantly the strength of the MMC with respect to that of the matrix, they tend to decrease thermal and electrical conductivity of composite material (Elsayed et al., 2015; Long et al., 2010 [2], Stobrawa et al., 2009; Uddin et al., 2010).

Thermal and electrical conductivities are determined by many factors, such as: the electrical and thermal conductivities of the constituent phases, the volume fractions

and the distribution of the constituent phases, the size, shape, orientation and spacing of the phases, interaction between phases, and the preparation method (Andrews et al., 1969; Zhang J. et al., 2009). The electrical conductivity of MMC is related to the electrical resistivity of the system and several models have been developed to predict its value. The electrical resistivity can be calculated approximately by the rule of mixture (Landauer, 1952). Others more accurate models have been proposed for the prediction of electrical resistivity of composite materials for example Maxwell model and P.G. Klemens model (Girish et al., 2012). In all these methods the electrical resistivity is calculated by different elaboration based on the electrical resistivity and volume fraction of the dispersion particles and matrix. Usually the theoretical values of electrical resistivity of MMC are underestimated because several approximations are made and some phenomena are neglected. For example the presence of porosity and interspace between the two phases, the interfacial thermal resistance, the occurrence of electron scattering by thermal vibration and microstructural defects are some of the phenomena totally ignored. As demonstrated in previous section also grain boundary affects electrical conductivity according to equation 2.1. Although the limitations of these methods, the effect of a second phase on the electrical resistivity of the composite is clear, increasing the fraction of reinforcement, the electrical resistivity of the composite increases (Andrews et al., 1969; Nakamichi et al., 1996; Wang et al., 2014).

Similar behaviour is obviously shown by thermal conductivity because the problem of heat conduction in heterogenic materials is mathematically analogous to the problems of electrical conductivity of such materials. Several analytical expressions have been formulated, the solutions of Maxwell and Rayleigh were the first of many attempts to determine the effective thermal conductivity of heterogeneous material. Maxwell's expression is as follows:

$$\frac{K_{eff}}{K_m} = 1 + \frac{3\Phi_1}{\left(\frac{k_1+2k_m}{k_1-k_m}\right)} \qquad (2.2)$$

Where, k_m is the thermal conductivity of the matrix, k_1 the thermal conductivity of the filler, Φ_1 is filler volume fraction. In Maxwell approximation the thermal interactions between filler particles is ignored. Later on also the shape, size and type of arrange of the inclusions have been considered by several researchers. A lot of implementations have been carried out in the years, and an empirical model quite popular in literature is Lewis–Nielsen model (Pietrak et al., 2015). The effective thermal conductivity (K_{eff}) of a composite according to the Lewis-Nielsen model is given as:

$$K_{eff} = \frac{1+AB\Phi_1}{1-B\varphi\Phi_1} \qquad (2.3)$$

$$B = \frac{\frac{k_1}{k_m} - 1}{\frac{k_1}{k_m} + A} \quad (2.4)$$

$$\varphi = 1 + \left(\frac{1-\Phi_m}{\Phi_m^2}\right) * \Phi_1 \quad (2.5)$$

Where, k_m is the thermal conductivity of the matrix, k_1 the thermal conductivity of the filler, Φ_1 is filler volume fraction, Φ_m is maximum filler volume fraction as function of the type of packing, and A is the shape coefficient for the dispersed particles (Pietrak et al., 2015). These approximations are very useful to evaluate the effect of the second phase on the thermal conductivity, but also other characteristics can be detrimental for this property, for example porosity. The most common approximation of the dependence of thermal conductivity on porosity is the modification of Maxwell's expression (Khaleghi et al., 2012; Ondracek et al., 1973). The modified equation is of the type:

$$K_{eff} = K_0 \frac{1-P}{1+\beta P} \quad (2.6)$$

Where K_0 is the thermal conductivity of nonporous material and β is the geometrical factor of pores. When pores are spherical β is equal to 0.5 (Khaleghi et al., 2012; Ondracek et al., 1973).The effect of porosity is detrimental as the effect of the addition of a second phase, a lower density leads to a lower thermal conductivity.

Also other properties are affected by the dispersion of reinforcement, for example strength (Suryanarayana, 2001). The analysis of strength for composites is associated to the fraction of grain boundaries and hard particles. On one side the formation of grain boundaries is related to the occurrence of grain refinement. The effect of grain size refinement on strength improvement is estimated by Hall-Petch equation, by which decreasing grain size the strength is enhanced. On the other side the contribution to strength originating from hard particles can be divided into two types according to the particle size: Orowan mechanism for nano particles and dislocation pile-up mechanism for coarse particles (Anderson et al., 1993; Wang et al., 2014). Independently of the mechanism the dispersion of a second phase leads to an increase of strength of the final product. In general at a given content of hard phase, a finer size of reinforcing particles results in smaller interparticle spacing and leads to a higher tensile and bending strength but to a lower toughness in comparison with coarse particles (Berns et al., 1996; Srivatsan et al., 2000).

2.3 Spark Plasma Sintering

Nanostructured materials have unique properties with respect to their micrometric scale counterparts, and SPS is a promising technique for their consolidation. The need to preserve the advantages given by these materials when subjected to SPS has driven the attention of many researchers. In fact in order to reduce the potential chemical reaction occurring at high temperature for prolonged time and to keep the fine microstructure obtained by MA, SPS is a diffused technology. In addition it has been demonstrated that SPS is very promising for the production of advanced materials which are difficult to produce by conventional sintering methods, like for example MMCs, fibre reinforced ceramics, nanocrystalline materials, intermetallic compounds and functionally graded materials (Dash et al., 2012; Tokita, 1993). The process produces a highly dense compact in a shorter sintering time and offers ease of operation and accurate control of sintering energy as well as high sintering speed, high reproducibility, safety and reliability. Moreover SPS can easily consolidate a homogeneous, high quality sintered compact because of the uniform heating, surface purification and activation made possible by dispersing contact points (Tokita, 1993).

The base concept of SPS is to apply beside pressure sintering system an electric current, this provides an enhancement of densification without microstructural change working at lower temperature ad in shorter time than conventional sintering processes (Tokita, 1993). The application of an electrical discharge leads to the generation of Joule heating, electric field diffusion, spark plasma and spark impact pressure. Recently the absence of plasma has been demonstrated during the process (Hulbert et al., 2009). By the way even without plasma, the pressure sintering system and the application of direct continuous pulsed current guarantee the production of fully dense high quality materials. Beside Joule effect and electric field diffusion, it has been proved that a localized melting may occur at the contact points due to a temperature increase caused by the limited contact area (Diouf et al., 2012 [2]; Song et al., 2006). All these phenomena promote the formation of necks allowing the formation of metallurgical bonds and consolidation.

The SPS system is formed by a controlled vacuum chamber, a uniaxial vertical pressurization mechanisms, a sintering DC-pulse generator, and conductive designed punches which act also as electrodes. An advanced control unit is integrated in the SPS system for position, temperature, applied pressure and vacuum measuring (Tokita, 1999).

2.3.1 Densification mechanisms

Densification of powders is strictly characterized and affected by the particle size distribution, morphology, number of contact points and type of contact points

(Bonnenfant et al., 1998; Bouvard, 2000; Delie et al., 1998). When densification concerns different type of powders as in the case of MMC, also other factors become relevant such as the volume fraction of the hard phase, the particle size ratio between the powders and the entity of the dispersion of the reinforcement among the matrix (Bonnenfant et al., 1998; Bouvard, 2000; Delie et al., 1998). When powders are processed by MM and MA, the subsequently severe strain hardening and dispersion hardening hinder densification. The induced severe strain hardening limits the deformability of the milled powder so that in some cases the effect of the particle morphology and size distribution becomes negligible (Gan et al., 2008; Praminik et al., 2008). Especially in powder metallurgy the properties of a component are directly related to densification. It is important to optimize and predict the densification behaviour during sintering because the presence of defects such as porosity, poor interparticle bonding, impurities and high internal stresses due to the processing stage may lead to premature failure, for instance under tensile or bending stress (Berns et al., 2003).

Densification is closely related to the application of the pressure which initially promotes powder rearrangement followed by the local and bulk deformation of the powders. According to Bouvard's study, under applied pressure hard particles are assumed to be non-deforming, while the soft powders behave in a visco-plastic manner promoting densification (Bonnenfant et al., 1998; Bouvard, 2000; Delie et al., 1998). The mechanisms of densification depend on the value of applied pressure related to the yield pressure of the soft powders (Bouvard, 2000; Delie et al., 1998). Since the pressure applied to the powders is lower than their yield pressure the densification advances by powder rearrangement (Anselmi-Tamburini U., 2013; Bouvard, 2000; Munir, 2006). Powder rearrangement is severely affected by the packing density of the powders which is related to the particle size distribution (German, 1992 [1]; German, 1992 [2]). The packing density is maximum for wide distribution because the smaller particles can fill the gap between the bigger particles. Although the higher packing density, a wide particle distribution do not assure the highest final density, which is more promoted by a small particle size and a narrow distribution (Pellizzari et al., 2011[1]; Pellizzari et al., 2011[2]). The role of particle size distribution is very significant because it influences the thermodynamic driving force for sintering which is proportional to the specific surface area. Moreover particle size affects the number and extension of the contact areas, in turn, the local pressure and electrical resistance which are of great importance in SPS due to the specific heating mechanism (Anselmi-Tamburini et al., 2005). When applied pressure is higher than the yield pressure of the soft powders plastic or viscous deformation are the main mechanisms of densification. On one side soft powders promote densification on the other side hard particles hinder it (Bonnenfant et al., 1998; Bouvard, 2000; Nikzad et al., 2012). Three situations may occur depending on the volume fraction of hard particles and on the size ratio: (1) for low fraction hard particles may be mostly isolated

from each other, (2) for medium fraction may form aggregates or (3) for large fraction may create a percolating network (Bouvard, 2000) (Fig.II-5). Since hard particle are limited and well dispersed densification can be completed because soft particle are mostly responsible for densification. When hard particles are able to aggregate, the pores between them are difficult to close, and these excluded volumes are responsible for residual porosity. When the fraction of hard phase exceeds the limit, a percolation network is created and deformation of soft particles is obstructed (Bouvard, 2000). This situation is indeed the most critical because the densification can only proceed by rearrangement, plastic deformation or fragmentation of the hard particles, and the effect of soft particles can be neglected. In this case the applied load is sustained by the percolation, subsequently hard particle have to rearrange in order to obtain a full dense material (Bouvard, 2000).

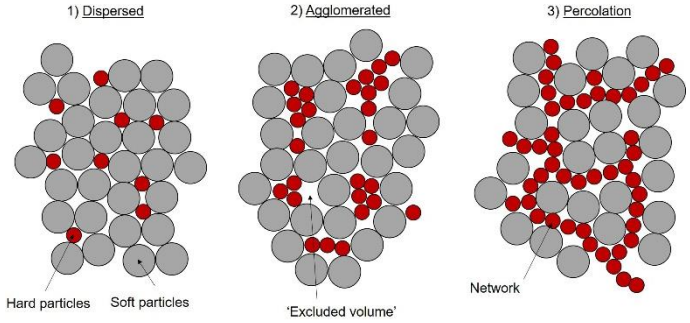

Figure II – 5. Possible type of particles dispersion depending on the fraction of hard phase (adepted from Bouvard 2000).

The rearrangement of the powder is strictly related to the type of mechanical and chemical contact between the hard particles (German, 1992, [2]). If the contact are weak densification is facilitated, otherwise the strong rigid structure of hard particle drastically hinders densification. All these three cases depend on the particle size ratio defined as the ratio of the mean diameter of soft particles on the mean diameter of hard particles. Generally speaking, as particle size ratio decreases, i.e. using large dispersoids, densification rate increases and the maximum fraction of hard particles which allows densification by soft particle deformation increases (Fedrizzi et al., 2012). Moreover the use of very small reinforcements would give problem of agglomeration leading to a poor dispersion and subsequently to deteriorated mechanical properties. On such attempt MA has been demonstrated to be a suitable processing route to reduce or even avoid agglomeration problems of fine hard phase powders. At the same time MA leads to a much fine particle size and to a narrower particle distribution favouring the densification of the milled powders and also sintering behaviour is improved (German et al., 1992 [2]; Pellizzari et al., 2011 [2]).

In Diouf study it has been demonstrated that the densification of atomized copper powders consists in three stages: rearrangement of the powder, local deformation and bulk deformation (Diouf et al., 2012 [1]; Diouf et al., 2012 [2]). A pressure of 25MPa is applied at the beginning of SPS cycle and then is increased up to 60MPa at different temperature: 450, 650 and 900°C. From 450°C up to 650°C the fracture morphology clearly indicates that most of the particles are increasingly packed but not yet sintered, only a local deformation of the contact area occurred as demonstrated also by Song et al. (Diouf et al., 2012 [2]; Song et al., 2006). The absence of dimples of the fracture surface indicates that sintering phenomena responsible for the formation of metallic bonding between particles did not occur even if density significantly increases. Only at 900°C a dimpled fracture surface is evident, which is indicative of an effective consolidation of the material. It may be concluded that for atomized copper powder even if densification proceeds during the entire SPS cycles, mass transport phenomena responsible for the formation and growth of sintering necks mainly occur between 650°C and 900°C. In other words, in some case the material can be densified, but not yet sintered.

2.3.2 Sintering mechanisms

If on one side densification is related to the applied pressure and mostly depends on the rearrangement and on the deformability capability of the powders; on the other side sintering is governed by different mechanisms activated by the applied external load, the heating and the electric current. The consolidation of powders during SPS consists in the activation of four stages in series: (1) activation and refining of the powder; (2) formation of the sintering neck; (3) growth of the sintering neck and (4) plastic deformation (Tokita, 1993; Zhaohui et al. 2008). The first two stages are promoted by the heating and electrical discharge and they are enhanced by the occurrence of oxide breakage and the overheating of the contact surfaces between the particles (Diouf et al., 2012 [2]; Song et al., 2006). The growth of the neck and plastic deformation are promoted by application of the load and the Joule effect. Even if the electrical current is mostly associate to the Joule effect, experimental studies indicate that it gives a direct contribution also to the diffusion mass transport (Munir et al., 2006).

Four sintering mechanism are responsible of the formation and growth of the necks: plastic deformation, power law creep, grain boundaries diffusion and Nabarro-Herring and Coble creep (Olevsky et al. 2006). It has been demonstrated that in the early stage of SPS, when relative density is lower than 90%, the densification mechanism is related to the *plastic deformation* of the contact areas between the particles. Since the local pressure is higher than the yield pressure of the particles the consolidation is activated by plasticity, once pressure decrease due to an increase of the contact area the plasticity densification stops. When pressure is constant end high

sintering temperature is reached, consolidation proceeds by two major diffusion mechanisms that contribute to mass transfer during SPS: *power-law creep* and *grain boundaries* diffusion mechanisms for conductive materials (Olevsky et al. 2006). These diffusion mechanisms are strictly related to the high levels of grain-pore and grain-grain interface areas in the material. Since SPS is a process involving hot deformation of powder under pressure power law creep plays an important role, especially it always dominates the consolidation process when porosity is higher than 30% and grain size is in micro-size range (~40μm). When the level of porosity and the grain size of the powder decrease grain boundaries and bulk diffusion mechanisms predominate. The driving source for these material transport mechanisms are: external applied load, sintering stress and steady-state electron migration (Olevsky et al., 2006). Depending on the value of porosity and grain size of the powders the magnitude of the contributions of the three different factors accordingly changes. Since the grain size is around 40μm the external load is the dominant transport mechanism in the material. For porosity lower than 30% electronmigration and surface tension become the main contributions to shrinkage depending on the average grain size. When the grain size decreases down to 1 μm the consolidation is aided by electromigration, if the grain size reaches nanometric dimensions close to 100 nanometres the mechanism governing sintering is the surface tension (Olevsky et al., 2006). By the way for very small porosity, an external load must be applied in order to close all the voids. The last mechanism during SPS is the densification by *Nabarro-Herring and Coble creep* which acts only when the grain size is much smaller than the particle size. All these mechanisms are strictly related to the particle size and to the SPS parameters (temperature, pressure, time and heating rate). The particle size determines the number of contact points and the extension of contact areas and consequently the electrical resistance. Moreover the particle size is responsible of the overheating of the particle surface layers in the contact region (Diouf et al., 2012 [2]; Song et al., 2006). Finally the particle size influences mass transport phenomena because the finer the particle size, the larger the grain boundaries surface, which results in an enhanced mass transport towards the neck region. In general increasing temperature, applied load and time the consolidation of the powders is enhanced because the plastic deformation and the mass transport phenomena responsible for sintering are promoted. Also heating rate affects the SPS cycle, increasing the heating rate the grain boundary diffusion is enhanced and grain growth diminishes (Olevsky et al., 2007).

In the case of copper powders has been demonstrated a prevailing effect of temperature on the consolidation of the particles, followed by particle size and pressure (Diouf et al., 2012 [1]; Nefedova et al., 2015). Temperature affects resistance to plastic deformation and the mass transport phenomena responsible for sintering. Only when the sintering temperature was increased up to 900° the consolidation by the formation of neck occurred (Diouf et al., 2012; Song et al., 2006). Particle size

influences the electrical resistance, the overheating and the mass transport phenomena as mentioned above (Zhaohui, 2008). The temperature reached on the surface of the coarser particle is significantly higher than that on the finer one. Consequently, localized melting, thermal softening of the subsurface layers and field activated mass transport phenomenon in the contact regions are enhanced. The local overheating increases slightly with heating rate, in terms of both actual values of temperature and thickness involved (Diouf et al., 2012 [1]; Diouf et al., 2012 [2]). The effect of pressure in negligible due to the high deformability of the copper powder since they are not mechanical strain hardened (Diouf et al., 2012 [1]; Nefedova et al., 2015).

In the case of mechanical milled powders on one side the nano microstructure aids the consolidation by the high surface energy of the powder and the large amount of grain boundaries; on the other side a common problem pointed is the presence of contaminations arising from the milling media and atmosphere which hinder the consolidation. Very recently the influence of oxygen and nitrogen contaminations on the densification of cryomilled copper powders during SPS has been evaluated (Wen et al., 2011). The authors found the difficulty to obtain full density related to the thermal decomposition of O and N based compounds to gaseous species which lead to porosity formation. Also copper oxide acts as a barrier to the thermal and electrical flows during SPS hindering the consolidation process (Menapace et al., 2016; Zhang R. et al., 2003). Fortunately SPS significantly reduces the grain boundary resistivity through the reduction of impurity segregation at grain boundaries (Chen et al., 2004; Diouf et al. 2013). This results in the purification of grain boundaries and in the improvement of the bonding quality (Risbud et al., 1994; Srinivasarao et al., 2009). Such advantage of SPS is of great interest specially in the processing of powders which suffer from contamination as an unavoidable issue during their production.

Chapter III

Wear behaviour

3.1 Introduction

Wear is usually discussed in terms of its damaging effect on change of topography of the surface, volume of material removed, transition in wear behaviour, and the effect of wear debris on performance of engineering applications. It must be considered that wear is one of the three most commonly encountered industrial problems leading to the replacement of the components, the others being fatigue and corrosion (Eyre, 1981). Several wear mechanisms have been reviewed by Eyre as responsible of the wear behaviour: adhesion, abrasion, fretting, corrosion, delamination and fatigue (Eyre, 1981). Wear under abrasive and adhesion metal-to-metal sliding conditions are the most often encountered in industrial components as wear mechanisms. Abrasive wear occurs when hard particles penetrate a surface and displace material in the form of wear debris. Adhesive wear occurs when surfaces slide against each other, and the pressure between the contacting asperities is high enough to cause local plastic deformation and material transfer by a process of solid-phase welding or by a localized bonding between contacting surfaces. Adhesion is favoured by clean surfaces, non-oxidizing conditions, and by chemical and structural similarities between the sliding couple. Particles, which are removed from one surface, are either permanently or temporarily attached to the other surface resulting in a tribolayer, usually a tribo-oxidative layer.

It must be considered that friction and wear are not intrinsic material properties but are characteristic of the engineering system. The tribological behaviour of a component is influenced by the characteristic of itself and by the conditions of service. In Figure III-1 a schematic representation of the engineering approach to the design of a component under wear is reported. Firstly the characteristics of the component must be carefully designed, in the case on MMCs both matrix and reinforcement could affect the tribological behaviour by different parameters. The matrix has the task of supporting the hard phase and to incorporate them in the microstructure. Therefore, the matrix should have not only a high hardness but also a high yield point and a certain degree of ductility (Fig. III-1) (Theisen, 2008). It must be also considered that the presence of defects in the matrix such as pores, cracks, inclusions or a not adequate adhesion between the two MMC constituents could affect the wear resistance. At the same time the selection of the type of reinforcement, and in

particular its size, volume content, hardness and dispersion must be optimized. The tribological behaviour depends also on the type of wear system (sliding, rolling etc.) and on the corresponding service parameters such as load, temperature, sliding velocity, time, the type of environmental and the presence or not of lubricant. The tribological behaviour of a component under wear is revealed by the predominance of certain wear mechanisms, (Fig.III-1) (Eyre, 1981). By the accurate analysis of the outputs of the wear system the tribological behaviour can be identified and described. The analysis of the worn surface, of the wear debris, and of the counterface allow a qualitative evaluation of the wear damage. To have a quantitative analysis the friction coefficient, the temperature in exercise, the mass loss and the derived wear rate coefficient must be considered.

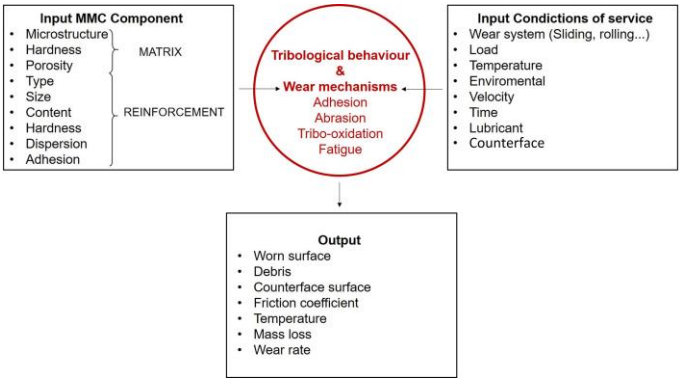

Figure III - 1. Schematic representation of engineering approach to tribology.

The study of wear is now day widespread and considerable efforts are being made to develop improved surfaces because an improved tribology design leads to a potential saving in maintenance and replacement costs, to a reduction of losses consequential upon breaking down and to a saving in investment through increased life of machinery (Eyre, 1981). These benefits are the driving force toward a more selective and accurate choice of the materials and of the processing route of a component according to the specific service life conditions.

3.2 Copper applications

Copper has always attracted considerable interests because of its high electrical and thermal conductivities, producing welding electrodes, electrical switches and injection/casting moulds (Avelar Batista et al., 2006; Barella et al. 2014; Futami et al., 2009) (Fig.III-2). Until recently, conventional mould materials would mainly

comprise tool steels. The development of high thermal conductivity Cu alloy allowed these materials to be considered as an alternative to steels leading to a faster heating and cooling injection cycle. By the way Cu has some distinct shortcomings such as low hardness, strength and wear resistance, restricting its applications (Fig.III-2). From Figure III-2 it is evident how materials having high thermal conductivity are very soft, and materials showing high hardness are not good heat exchanger.

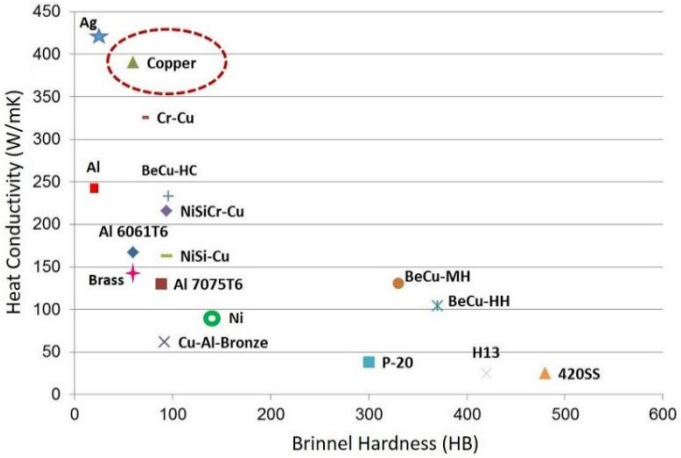

Figure III - 2. Brinnel hardness versus heat conductivity.

Neglecting polymer materials, also wear resistance is tightly related with hardness, as reported in Figure III-3. In the last years several attempts have been made to improve the hardness of copper because the service conditions during injection/casting moulding are very severe. During injection moulding abrasive wear occurs as hard fillers in the polymer are pressed and slid against the barrel and screw surfaces. In addition, the screw may also vibrate in the barrel leading to metal-metal contact between them, so that impact wear and adhesive wear may occurs. Finally attack by corrosion is possible from the polymer matrix or any other additives (Boey et al., 2005). Meanwhile during casting the mould is subjected to an extreme temperature gradient causing geometrical distortions. Moreover, long high temperature exposition combined with possible thermal fluctuation causes creep and thermal fatigue damage (Barella et al. 2014).

In order to improve the wear resistance there are mainly two options based on two totally different concepts: the first one consists on surface treatments or coatings which involve only a thin layer of the component, and the second one is a massive strengthening of the bulk material by precipitation hardening or dispersion hardening.

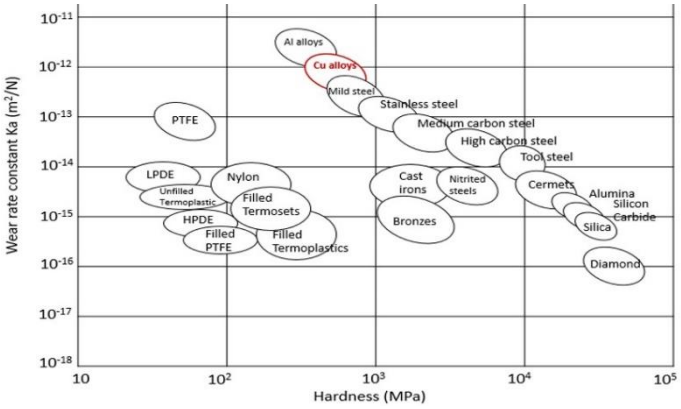

Figure III - 3. Hardness versus wear rate constant for different materials.

In the first case tailoring the surface to match the operating conditions is becoming increasingly important. There is a wide range of techniques now being used, including recently developed processes such as physical vapor deposition (PVD), ion implantation, and laser treatment, etc. Surface treatments which increase the hardness and place the surface in a condition of residual compressive stress are widely used. For example PVD of TiN, CrN and CrAlN on Cu coating can provide low friction, high wear and oxidation resistance, which can improve the deficient wear and corrosion characteristics of Cu alloy in moulding operations without significantly affecting the thermal conductivity of the Cu substrate (Avelar-Batista et al., 2006; Bull et al., 2001). At the same time coatings have been used also for copper casting moulds (Barella et al., 2014). Usually casting copper moulds are coated with chromium or nickel to provide a harder working surface and to avoid copper pick-up on the surface of the cast strand, which can facilitate the development of the surface cracks on the cast product (Barella et al., 2014). In general the employment of a coating is limited by elastic and plastic deformation of the substrate, which the hard, thin and brittle coating cannot follow without failing (Barella et al. 2014). In addition the difference between thermal expansion coefficients of the two constituents increases the microstructural mismatch leading to easier and faster nucleation and propagation of cracks on the surface of the component and at the interface between substrate and coating (Barella et al. 2014). Moreover coating temperatures usually have a detrimental effect on the mechanical properties of the alloy, as they will over-age the substrate and reduce its hardness. This will further increase the hardness mismatch between PVD coating and substrate. Finally, under the application of a very high load, fragmentation of the coating may occurs especially because defects produced by the deposition process are very common and they can act as crack nucleation sites. The breakage of the

coating leads to the formation of debris which promote a severe abrasion of the substrate and this limits the coating applications (Avelar-Batista et al., 2006).

A second strategy for microstructure design and properties improvement is the strengthening of metals and alloys through grain refinement. In fact, most nanostructured metals exhibit enhanced wear resistance in comparison with their corresponding coarse-grained samples (Zhang Y.S. et al., 2006). Initially, as in this study of Zhang et al., a nanocrystalline surface layer on a Cu plate is achieved by means of surface mechanical attrition treatment (SMAT) (Zhang Y.S. et al., 2006; Zhang Y.S. et al., 2008). The thickness of the deformed layer is 500 micron, much deeper than the thickness achievable by common coating. In addition the thickness of the strengthened layer can be tailored according to the specific requirements. The tribological properties of the SMAT Cu are remarkably improved at all applied loads and sliding speeds due to the stability of mechanical mixed layer and to the high hardness of the nanocrystalline structure. In addition prolonged SMAT enhances the wear resistance of the component because a thicker and deeper mechanical hardened layer is formed enhancing the load bearing capability of the substrate (Zhang Y.S. et al., 2007). By the way an abrupt increase of the wear volume is detected, which corresponds to the remove of the nanocrystalline layer. At this point in order to increase the thickness of the nanocrystalline layer, the use of MM is introduced for the production of bulk-nanostructured mechanical strengthened materials showing improved wear performances.

In the last years the addition of a second hard phase by MA is a suitable processing route to further improve wear resistance of components. The introduction of a second harder phase in a soft metal matrix enhances the effectiveness of MM, increasing the hardness and the tribological behaviour of the alloy (Elsayed et al., 2015). The introduction of copper matrix composites can be challenging in several applications, for example for injection/casting mould MMC can be used as an intermediate layer between the Cu substrate and the ceramic coating. MMC is characterized by an intermediate thermal coefficient due to the coexistence of the two constituents, i.e. matrix and ceramics. This could reduce the thermal and the stress gradient typical of coated components. A reinforced copper intermediate layer produced by MA could enhance the load bearing capability of the substrate, prolonging the permanence of the coating and slowing down the crack nucleation and propagation. Other applications in which Cu matrix composites play an important role are welding electrodes, contact wires and forming tools. The use of Cu is request in these components because process or frictional heat has to be removed rapidly. All of these applications work under dry sliding wear condition. Usually abrasion, adhesion, oxidation and plastic deformation are the main wear mechanisms. The addition of a hard phase opposes itself to the penetration of the abrasive particles of the counterpart and the material removal is limited (Eyre, 1981). Also the adhesion is prevented because the contact between the component and the counterface is not continuous

anymore, but hard particles stand proud of worn surface of composite sample avoiding solid-phase welding or localized bonding between contacting surfaces (Eyre, 1981). Another important wear mechanism involved during sliding wear is oxidation, which in some case is desirable (Eyre, 1981). The occurrence of oxidation leads to the formation of a continuous tribo-film which improves the wear behaviour reducing the friction coefficient (Straffelini et al., 2005; Zhang Y.S. et al., 2008). A harder material is characterized by a higher capability to sustain the oxide layer and therefore by a higher wear resistance. For this purpose the production of a material which facilitates the oxide production and increases the load bearing capability to outstand the protective oxide layer, is a challenging chance for material engineers, and MMC are suitable candidates for this goal.

3.3 MMC: design and wear behaviour

When ductile materials are subjected to sliding wear a severe plastic deformation of the near surface region is induced and the microstructure and properties of the sub surface metals change accordingly (Yao et al., 2015). When the unreinforced specimen rubs against medium carbon steel disk, the hard asperities on the steel counterpart penetrated and cut deeply into the surface of alloy, which results in a large amount of material removal and scratches. Increasing the hardness by dispersion hardening can be a successful solution to improve wear resistance (Zum Gahr, 1998). From the mechanical and tribological point of view not all the hard particles (HP) and metal matrix combinations are good for producing a tough and wear resistant composite. Both properties depend on different microstructural parameters (Berns et al., 1997; Berns et al., 1999; Berns, 2003). A good compromise must be found by tailoring accurately the characteristics of the two or more constituents. Dispersed HP protect the metal matrix against abrasion and the metal matrix provides the toughness. Oxide, carbides and borides have been successfully incorporated in the soft matrix to reduce the extent of surface plastic deformation and related metallic wear phenomena (Suryanarayana, 2001). In order to guarantee a positive effect, the HP have to be harder than the abrasive material and should also have a high fracture toughness so that the grooving particles of the counter face will tend to fracture rather than the HP (Theisen, 2008). It is believed that during the initial stages of the abrasive wear process, the abrasive particles from the counterface are capable of gouging the soft metal matrix, thus, protruding the HP to the composite surface. At this stage, the HP come in contact with the abrasive particles of the counterface. Several intrinsic factors but overall the relative hardness of the HP (H_{HP}) and of the abrasive (H_a) particles govern the wear mechanism (Deshpande et al., 2006, Berns et al., 1999). The relative abrasive wear rate of composite tends to decrease when H_{HP} exceeds about $0.8H_a$. When $H_{HP}<0.8H_a$, the abrasive particles of the counterface indent and

penetrate into the composite surface. When $H_{HP}>0.8H_a$, the abrasive particles are strained and blunted (Richardson, 1968).

Also the size of the HP affects the wear behaviour of the composite (Berns, 2003, Zum Gahr, 1998) especially when subjected to abrasive wear. In order to improve the wear resistance HP must be bigger than the abrasive particles, this reduce the abrasion depth if they are well bonded to the matrix (Zum Gahr, 1998). Moreover the mean free path between the HP must be smaller than or at least as large as the width of the abrasive particle, if possible to act as an obstacle to the scratching abrasive (Akhtar et al., 2009; Zum Gahr, 1998). If the HP are too small they will be easily pulled out unless they are present in large quantities obstructing the penetration of the abrasive grain into the softer matrix. By the way it must be considered that over a certain volume fraction percolation of HP may occurs forming brittle network leading to a premature failure of the component (Bouvard, 2000; Zum Gahr, 1998). Moreover micro-cracking can occur if material contains internal notches such as cracks, pores, embrittled grain boundaries and inhomogeneous distribution of reinforcement particles, especially when a high normal load is applied (Deshpande et al., 2006, Akhtar et al., 2009). All these considerations are related only to the abrasive wear contribution of counterface against MMC, but once HP particle are pulled out the wear mechanism changes from two-body abrasion to three-body abrasion (Onat, 2010). The wear process thus generates a hard plastically deformed surface layer on top of a tougher zone that continuously renews itself as wear progresses. This leads to the formation of very hard wear debris, which together with the pulled out HP change the abrasive behaviour from two–body to three body abrasion (Zum Gahr, 1998). In some other case the debris and HP are compacted as a result of the load applied and a self-protecting layer prevents deeper penetration of the hard particles into the surface and also avoid deeper grooves (Berns et al., 1999; Zhang Y.S. et al., 2008).

In the specific copper base alloy are characterized by the presence of a high initial friction coefficient, typical of the adhesion mechanism, followed by the attainment of a lower value when wear become tribo-oxidative (Straffelini et al., 2005). Adhesion wear mechanism appears due to the formation of micro-joints between the sample and counter parts. As consequence of their relative movement, the softer sample is broken, leaving voids in the Cu alloy and transferring some material to the disc. Some cracks may be nucleated in the small void and grow until the delamination of the worn surface occurs (Gao et al., 2015, Onat 2010). As the hardness of the reinforcement particle is higher than that of conterface, this reduce the cutting efficiency of the abrasive particle and consequently the abrasion wear loss. Once reinforcing particle fracture or loosen from the copper matrix because bonding between the matrix and reinforcement becomes weak, they can be easily removed from the matrix, contributing to the mass loss as abrasive body. Increasing the content of reinforcement the wear resistance increases independently from the type of reinforcement (Akhtar et al., 2009; Lu et al., 2012; Tu et al., 2003). In Cu-TiB_2 composite increasing the content of hard phase,

wear resistance increased considerably if distribution of reinforcement in the matrix is uniform (Kwon et al. 2006; Tjong et al 2000). In some cases localized fracture easily occurred at brittle and weak TiB_2 reinforcement-matrix interface under high load conditions especially for larger reinforcement particle size (Tjong et al., 2000). Prolonging sliding time a reduction of friction coefficient is due to the lubricating action exerted by the surface oxide. Usually the attainment of a tribo-oxidative wear mechanism is associable to the increased contact temperature (Straffelini et al., 2005). Increasing sliding speed or normal load or prolonging sliding time the flash temperature increases, which promotes the formation of a mixed surface layer rich in oxygen preventing the contact metal-to-metal during sliding, thus help to reduce the friction coefficient and the wear rate (Straffelini et al., 2005; Straffelini et al., 2004; Zhang Y.S. et al., 2007, Onat, 2010).

Chapter IV

Materials and Experimental procedures

4.1 Materials

4.1.1 Copper

In this study a water atomized copper powder was considered. Figure IV-1 shows a scanning electron micrograph of the atomized Cu powder (AT-Cu) and a light optical micrograph of a polished metallographic cross-section. Cu particles are characterized by an irregular morphology and by the particle size distribution reported in Table IV-1. Most of the powders have a particle size in the range of 45 and 75 microns. The oxygen content in AT-Cu is equal to 0.2%, others information about the composition cannot be declared as request by the company providing the powder.

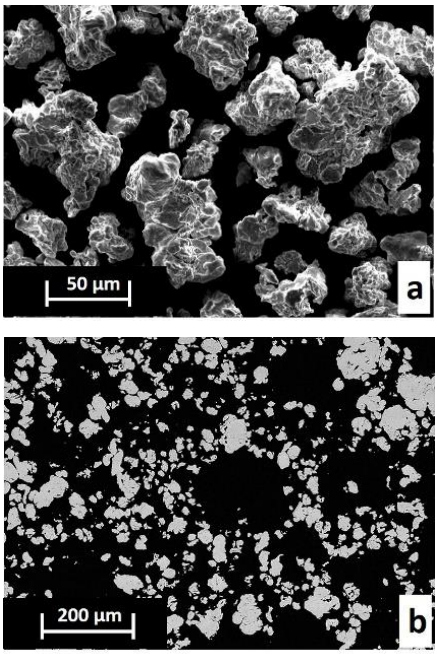

Figure IV - 1. SEM (a) and OM (b) micrographs of AT-Cu powder.

Table IV - 1. Particle size of AT-Cu powder.

Particle size	% Cumulative
> 75 µm	8,7
> 45 µm and < 75 µm	57,6
< 45 µm	33,7

4.1.2 TiB_2

The TiB_2 powder was produced by continuous chemical process that controls stoichiometry and particle size (≈ 3µm) to create high purity powder (Fig.IV-2).

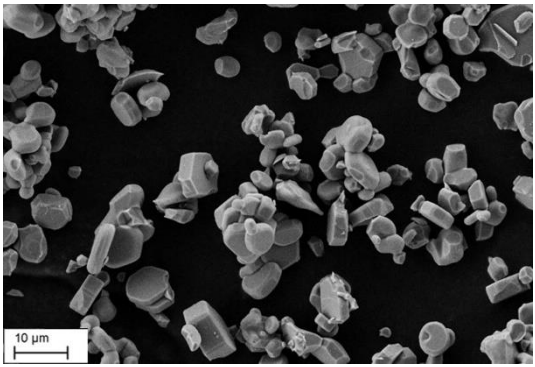

Figure IV - 2. TiB_2 powder

4.2 Processing route

4.2.1. Mechanical milling and mechanical alloying

4.2.1.1 Process control agent, ball powder ratio and type of cycle

All the MM and MA process were conducted in a Fritsch Pulverisette 6 planetary mono mill at 400 rotation per minute. Vial and sphere with 10 mm diameter of 100Cr6 (63 HRC) were used. The system was evacuated down to 10^{-1}torr to reduce the interaction between powders and oxidizing agent during milling.

Initially three different milling parameters have been selected for MM: the type of process control agent (PCA), the ball to powder ratio (BPR) and the type of cycle. Firstly the effects of three different PCAs on the size, morphology and contamination content of the milled powder have been estimated. MM has been conducted in absence of PCA and with 0.5wt% of PCA (toluene or stearic acid ($CH_3(CH_2)_{16}CO_2H$)).

In a first set of experiments the powder has been milled using a BPR equal to 33:1 and an interrupted cycle (Table IV-2). In a second set, once the best PCA has been selected, the BPR was reduced to 10:1 keeping an interrupted cycle. In the third set two different milling strategies were investigated:

1. Interrupted milling involving 2min on and 9min off for an effective total milling time comprised between 20 (time I) and 200 minutes (time II);
2. Continuous milling for a total milling time between 20 and 200 minutes.

Table IV - 2. Different milling parameters.

Stage	Sample	PCA	BPR	Cycle	Effective MT (min)
1	A-I	None	33	Interrupted	20
	A-II	None	33	Interrupted	200
	B-I	Toluene	33	Interrupted	20
	B-II	Toluene	33	Interrupted	200
	C-I	Stearic acid	33	Interrupted	20
	C-II	Stearic acid	33	Interrupted	200
2	D-I	Stearic acid	10	Interrupted	20
	D-II	Stearic acid	10	Interrupted	200
3	E-I	Stearic acid	10	Continuous	20
	E-II	Stearic acid	10	Continuous	200

4.2.1.2 Milling time

Once the optimized combination of milling parameters has been found, copper powder and 0.5wt% of stearic acid have been mechanical milled for six milling times: 20, 120, 200, 240, 360 and 720 minutes continuously. After proper considerations, also interrupted milling has been carried even for longer milling time: 3000 and 6000 minutes, (Tab.IV-3). In the case of MMC nine powder batches were prepared using 9 different milling times to find the condition leading to proper particle size, morphology and uniform dispersion of reinforcement. The milling times were from 5 up to 240 minutes conducted in continuous as reported in Table IV-3. Each milling cycle has been carried out using a new powder batch in order to keep a constant filling ratio. The labels of all the different batches of milled powder are reported in Table IV-3.

Table IV - 3. Labels of the different milled powders.

Process	Milling time (min)	Type of cycle	Symbol
MM AT-Cu + 0.5wt%PCA	20	Continuous	MM-20'
	120		MM-120'
	200		MM-200'
	240		MM-240'
	360		MM-360'
	720		MM-720'
MM AT-Cu + 0.5wt%PCA	20	Interrupted	MMi-20'
	120		MMi-120'
	200		MMi-200'
	720		MMi-720'
	3000		MMi-3000'
	6000		MMi-6000'
MA AT-Cu + 0.5wt%PCA + 0.5wt%TiB_2	5	Continuous	MMC-5'
	10		MMC-10'
	20		MMC-20'
	40		MMC-40'
	80		MMC-80'
	120		MMC-120'
	160		MMC-160'
	200		MMC-200'
	240		MMC-240'

4.2.2. Spark plasma sintering

The powders were sintered in a DR.SINTER® SPS1050 (Sumitomo Coal & Mining, now SPS Syntex, Inc.) apparatus using graphite punches and dies. Samples of 20mm external diameter and 5mm height were produced. SPS was performed at a nominal temperature (measured with a thermocouple inserted into a blind hole in the die wall) of 950°C, with a uniaxial pressure of 30MPa applied at 700°C. The selection of the loading temperature has been made on the base of the complete decomposition of PCA during the heating process, in order to avoid residual porosity. The heating rate was 100°C/min up to 900°C and 50°C/min up to the sintering temperature. Initially the maximum temperature and pressure were held for 1 and 3 minutes, respectively,

before allowing the furnace to cool to room temperature. Then, in order to improve the densification the pressure was increased up to 60MPa. This last setting parameters have been used for the production of the tensile and wear tests. During the whole SPS sintering cycle, the voltage, current, displacement of the upper punch and temperature were recorded. The displacement of the upper punch was used to follow the densification process. The first derivative of displacement (ds/dT) against temperature is representative of the densification rate

4.3 Characterization of milled powder

4.3.1 Particle size

4.3.1.1 Image Analysis

The powder morphology was characterized by quantitative image analysis on a polished metallurgical cross section molded in epoxy resin. To obtain statistical support, at least 10 optical micrographs for each sample were considered. Two distinct parameters were analyzed, namely, the particle cross sectional area and the aspect ratio, i.e., the ratio between the maximum and minimum length of each particle. The first parameter is representative of the particle size, while the second resumes the particle morphology.

4.3.1.2 Sieve analysis

A sieve analysis was carried out to determine the particle size distribution under different milling conditions for the MMC powders. Powder samples (50g) were poured on the top of the sieve (355 to 25μm, 355, 250, 180, 125, 90, 45, 25μm). The column was then placed in a mechanical shaker, model FRITSCH 3 Spartan4 for 30minutes. The powder on each sieve was finally weighed by a precision balance (0.0001g). The weight of powder sample located on each sieve was then normalized by the total weight to obtain the particle sizes distribution.

4.3.1.3 Metallography

Milled powder have been cold molded in epoxy resin. Then standard metallographic preparation was also accomplished, including grinding with SiC papers up to 4000grit, final polishing with 3μm and 1μm diamond pastes. The powder morphology and dimension were evaluated by optical (OM) and Scanning Electron microscopy (SEM, model Philips XL30).

4.3.2 Contamination

The iron and chromium contaminations of the powder arising from the milling media were measured by an inductively coupled plasma mass spectrometry (ICP). The oxygen and carbon content was measured by combustion analysis (LECO).
The study of PCA decomposition has been carried out by thermo-gravimetrical analyses (TGA) combined with quadrupole mass spectrometry (QMS) using STA409CD by Netzsch. TGA of the milled powders was carried out in a protective argon atmosphere up to 1060 °C and at a heating rate of 20 °C/min. These analyses were combined with QMS which consists of four cylindrical rods, set parallel to each other forming a quadrupole. The quadrupole is the component of the instrument responsible for filtering sample ions according to their mass-to-charge ratio (*m/z*). QMS allows to detect all the gaseous products coming from the decomposition of PCA. The organic nature of PCA leads to the emission of C, H and O compounds that have been recorded applying the correct ratio of voltage to the quadrupole. All the same batches of powder have been used to minimize possible experimental errors (130 mg).

4.3.3 Microstructural evolution

X ray diffraction was carried out and the experimental data were elaborated with the Rietveld method using the Materials Analysis Using Diffraction software (MAUD) (Rietveld, 1969; Lutterotti 1997). The phase identification of the products was determined using Cu Kα radiation (λ= 0.15418nm). The crystallite size, the lattice strain of the MM-powders and the amount of dislocations were determined. The formers were evaluated using the X-ray peak broadening techniques. After proper corrections taking into account the instrumental effect, crystallite size and lattice strain can be calculated applying the Scherrer formula,

$$\beta \cos\theta = \frac{0.9*\lambda}{D} + \eta \sin\theta \qquad (4.1)$$

Where β is the peak width at half height, λ is the radiation wavelength, D is the crystallite size, η is the lattice strain and θ is the Bragg angle. This equation represents a straight line, where the lattice strain η is the slope and the intercept is $0.9\lambda/D$. This method has been proved to be quite accurate for measuring crystallite size in the range of 10-100 nm (Suryanarayana, 2001). Dislocation density δ was calculated by the crystallite size and the lattice strain derived from Bragg reflection - profile analysis as follows:

$$\delta = \frac{2\sqrt{3}*\ \varepsilon^{1/2}}{(D*b)} \qquad (4.2)$$

Where b is the Burger vector of dislocation (for Cu 0.25562 nm) and ε the lattice strain (Zhao et al. 2002; Xiao et al., 2008; Menapace et al., 2016).

4.4 Characterization of sintered samples

4.4.1 Density

The density of the SPS-processed pellets was measured according to Archimedes' principle (ASTM B962-08). For mechanical milled samples the relative density was calculated considering the theoretical densities of Cu as 8.96g/cm^3. In the case of MMC the theoretical absolute density was calculate according to the linear rule of mixture,

$$\rho_{MMC} = v_{Cu}\rho_{Cu} + v_{TiB2}\rho_{TiB2} \quad (4.3)$$

Where *v* is the volume fraction and ρ is the absolute density of each constituent. For mechanical alloyed samples the relative density was calculated considering the theoretical densities of TiB_2 as 7.76 g/cm^3.

4.4.2 Metallography

Metallographic cross section of the sintered samples was obtained by precision micro-cutting with a diamond blade. Standard metallographic preparation, including grinding with SiC papers up to 4000grit, final polishing with 3μm and 1μm diamond pastes, was also accomplished and chemical etching with 120mL of distilled water, 30mL of hydrochloric acid and 10g of iron chloride (Petzow, 1999).

4.4.3 Hardness and microhardness

After standard metallographic preparation Vickers micro-hardness was measured on the top flat surface of the sintered disc and even on cross-section, Figure IV-3. A micro-hardness tester, model Anton Paar MHT4 was used using an applied load of 0.5N, holding time of 10 seconds and a loading rate of 0.05N/s according to ASTM standard E9-08. Measurements were taken in 8 different positions and the average value and standard deviation were reported. The Brinell hardness was also measured using HB5 scale (F = 306.5N and ball tip's diameter D = 2.5mm) according to ASTM E10 – 01.

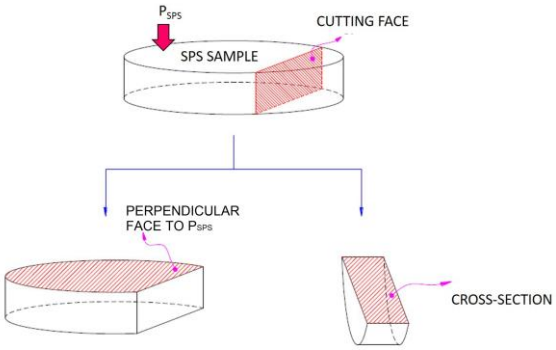

Figure IV - 3. Sample geometry and cut cross section.

4.4.4 Tensile test

Tensile test specimens of 4.9 x 4.9mm^2 cross section and a gauge length of 12.50mm length were produced directly by SPS, (Fig.IV-4). Mechanical characteristics were studied by means of tensile tests using an Instron 8516 SH device. Tensile tests were carried out with a strain rate of 0.1^{s-1} and an extensimeter was used to measure deformation. The fracture surface morphology was evaluated by SEM.

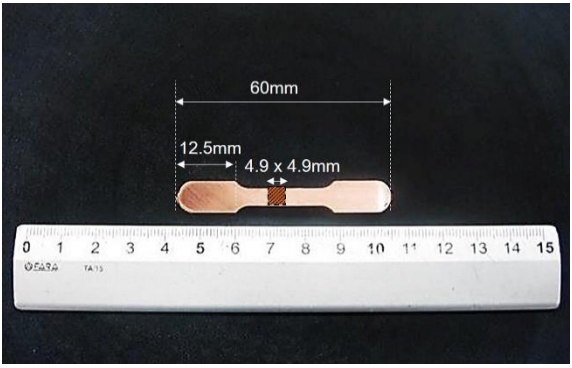

Figure IV - 4. Tensile test specimen produced by SPS.

4.4.5 Wear

4.4.5.1 Sliding wear test

The sintered samples were machined from the tensile test into block samples with the dimension of 9x13x5mm and the 9x13mm faces were employed as the wear

surfaces. The wear surface have been polished up to 1micron diamond paste. The dry sliding tests were carried using a block-on-disc configuration against AISI M3:2 (65HRC) steel counterface with a rotating speed of 300 rotation per minute, a load comprised between 50N-200N and a sliding time of 15, 30 and 240 minutes. The configuration of the test is reported in Figure IV-5.The worn abrasive disc and the copper based samples were substituted by a new one for every sliding time and load. During the experiments, the friction coefficient was recorded and the contact temperature were continuously measured by a thermocouple placed in a hole at 2mm depth from the contact surface. The wear curve was recorded by weighing the specimens, using a precision balance (0.0001g). By the volume loss (V) and the sliding distance (s.d) the wear rate (Ka) has been calculated by the Archard's equation (Straffelini et al., 2005):

$$Ka = \frac{V}{s.d.} \tag{4.4}$$

The wear tracks, the counterface and worn debris were observed by optical (OM) and a scanning electron microscopy (SEM). Semi-qualitative chemical analysis was carried out by energy-dispersive X-ray spectroscopy (EDXS). All the wear tests have been carried out also on AT-Cu and on a copper beryllium alloys (Cu-Be) as reference.

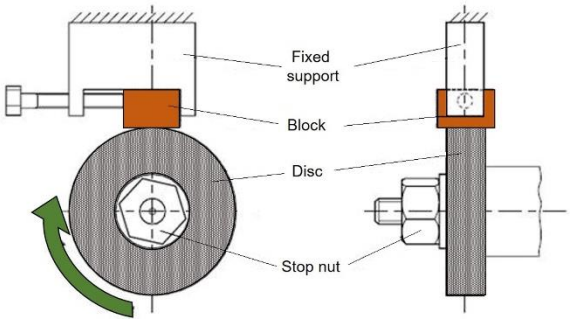

Figure IV - 5. Sliding wear test configuration.

4.4.5.2 Abrasion wear test

The abrasion wear resistance has been evaluated by scratch tests at different loads. The test specimens were machined from the sintered samples. Each test plane was polished to make a mirror surface prior to testing. The press surface, i.e., the sintered plane perpendicular to the pressing direction during SPS was indented/scratched (Fig.IV-3). The indenter was a Rockwell diamond indenter with

200μm of diameter. The loads of 1, 2 and 3N were applied for an abrasion distance of 5mm and with a sliding speed of 10mm/min. In scratch testing, after applying a specific normal load, the specimens is horizontally slid with a programmed traveling speed on a monitored linear stage. The output of the test is the penetration depth with the accuracy of ±1μm.

4.4.6 Thermal conductivity

Samples were cut into disk-shaped specimens of Φ10 × 2.7mm and the thermal conductivity (k) of the samples was derived by the equation:

$$k = \alpha \cdot \rho \cdot C_p \tag{4.5}$$

Where α is thermal diffusivity, ρ is the bulk density, and C_p is specific heat capacity. The thermal diffusivity and the specific heat were measured using the NETZSCH laser flash apparatus LFA 467 *HyperFlash*. The unit is equipped with a furnace which is capable for operation from -100°C to 500°C. The front surface of the sample is heated by a Xenon flash lamp with variation of energy by voltage and pulse-length. The resulting temperature increase on the rear face is measured using an IR-detector. Data acquisition and evaluation are accomplished by using the extensive software package. All samples were tested with the LFA between 400 and 500°C with 20 °C temperature steps. The measurements were carried out in a standard sample holder (Ø 10 mm). Each sample was measured five times at each temperature step. Prior to the measurement the front and the back of the samples were coated with graphite to enhance the emission/absorption properties of the sample. The specific heat was determined by the reference method given by ASTM-E 1461-2011. Therefore the LFA was calibrated with a Cp-standard (Pure-Copper: Ø 10 mm, thickness 2 mm).

Chapter V

Mechanical Milling of Copper

Part of this chapter has been published in:

G. Cipolloni, M. Pellizzari, A. Molinari, M. Hebda, M. Zadra
"Study of the processing route of copper powder by mechanical milling and Spark Plasma Sintering"
Proc. Of the 2014 European Powder Metallurgy Congress & Exhibition
21-24 September 2014, Salzburg, Austria

G. Cipolloni, M. Pellizzari, A. Molinari, M. Hebda, M. Zadra
"Contamination during the high-energy milling of atomized copper powder and its effects on spark plasma sintering"
Powder Technology, volume 275 (2015) pp 51-59

C. Menapace, G. Cipolloni, M. Hebda, G. Ischia
"Spark plasma sintering behavior of copper powder having different particle size and oxygen contents"
Powder Technology, volume 275 (2016) pp 170-177

5.1 Selection of the milling parameters

A major issue with MM is the contamination that arise from the milling media, the PCA and the atmosphere (Gordo et al., 2005; Madavali et al., 2014, Suryanarayana, 2001). Contaminations are generally deleterious and, in copper they negatively affect the electrical and thermal conductivity and for this reason must be minimized (Long et al., 2010 [2]). Process parameters such as the use of a PCA, the BPR and the milling time control the nature and the formation kinetics of contaminations (Suryanarayana, 2001). In this chapter the effects of the milling parameters are discussed according to the experimental process summarized in Table IV-2. Even if the PCA is a possible source of contamination, its use cannot be generally avoided because it delays the welding events especially in ductile materials (Harris et al., 1995; Huang et al., 1995; Suryanarayana, 2001).

In Figures V-1 optical micrographs of the cross section of the powders milled in absence of PCA (A) and with 0.5wt% of toluene (B) or stearic acid (C) are reported. Initially all powders have been milled using BPR equal to 33:1 (chapter IV) and an

interrupted cycle with an effective time of 20 and 200 minutes (I-II respectively). It is evident that the size of the powder milled without PCA is much bigger that of AT-Cu (Fig.IV-1). The intrinsic ductility of copper favours the predominance of welding over fracturing (Harris et al., 1996; Huang et al 1995). The powder morphology changes towards a flake-like shape, especially for short milling time (Luo et al., 2012; Suryanarayana, 2001,).

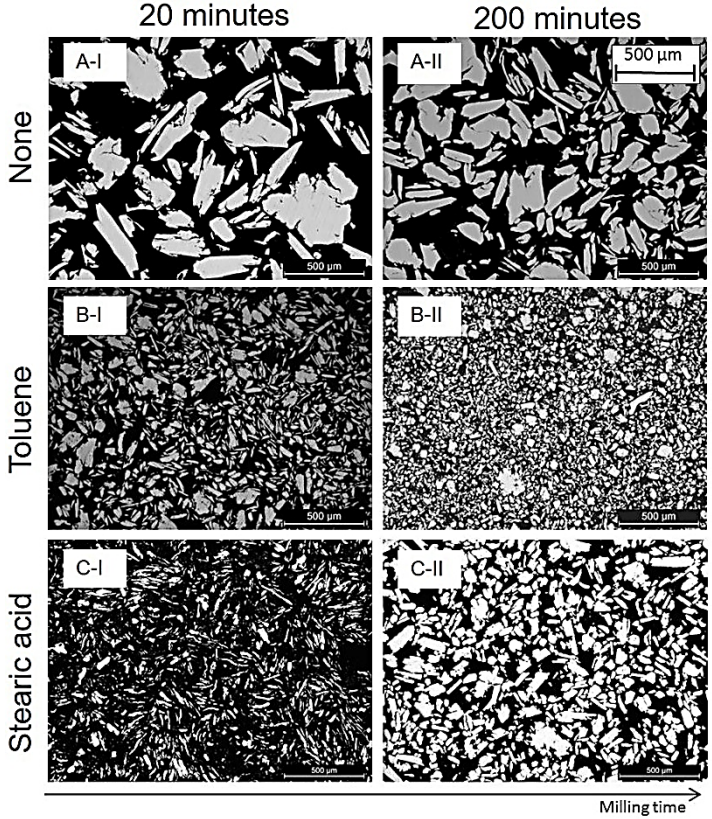

Figure V - 1. OM micrographs of the variation of the powder morphology as a function of milling time (I–II) and PCA: (b) none, (c) toluene, and (d) stearic acid.

The increased particle size is due to the temperature increase during MM and the predominance of welding events over fracturing ones. The benefit from using a PCA is evident because it impedes the clean metal-to-metal contact and leads to the dispersion of aggregates (Bailon-Poujol et al., 2011; Khayati et al., 2013, Zhang Y.F. et al 1999). A finer particle size is evident in powder milled with toluene even for prolonged MM. Using stearic acid the particle size after 200 minutes is intermediate between that using toluene and without any PCA (Fig.V-1). Although the smaller

particle size of powder milled with stearic acid for 20 minutes, the morphology of the particles is clearly flake like. All the assumptions made by looking at the OM micrographs are confirmed by image analysis. The cumulative distribution of area and aspect ratio (ratio between the maximum and the minimum length of each particle) of the milled powder as function of PCA and milling time are reported in Figure V-2.

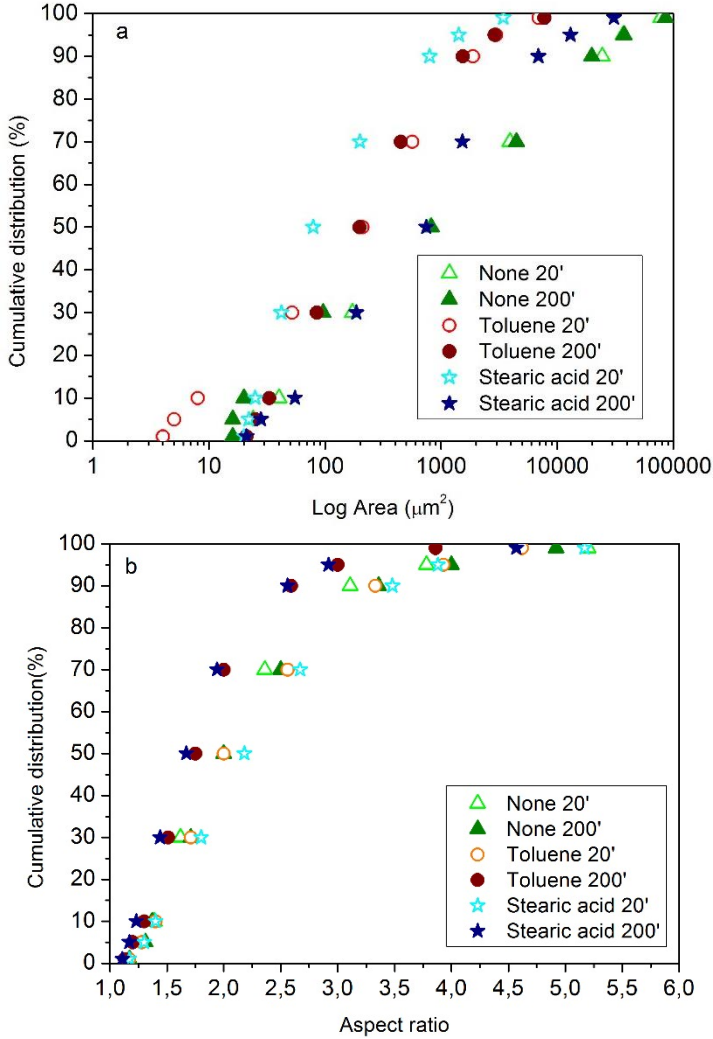

Figure V - 2. Cumulative distribution of area (a) and aspect ratio (b) of milled powders as function of process control agent and milling time (adapted from Cipolloni et al. 2015).

The effectiveness of PCA in reducing the particle size is evident (Fig. V-2a). Although the smaller particle area of powder milled with stearic acid after 20 minutes, toluene seems to be the best PCA because particle size is smaller even for long milling time. From a morphological point of view both toluene and stearic acid show a lower aspect ratio leading to a more equiaxial particle shape. This is due to the intense plastic deformation and the repeated welding events during MM. The achievement of a suitable particle size and morphology is very important because densification behaviour during SPS is severely affected by them. A round morphology is more suitable for sintering than a dendritic one because contact points between the powders are less in the former case (Gan et al., 2008). A lower amount of contact points between spherical particles limits the friction, enhancing the rearrangement of the powder, which is an important mechanism of densification during SPS. (Diouf et al., 2012 [1]; Diouf et al., 2012 [2]). Powder rearrangement is severely affected by the packing density of the powders which is related to the particle size distribution (German, 1992 [1]; German, 1992 [2]). The packing density is maximum for wide distribution because the smaller particles can fill the gap between the bigger particles. Although the higher packing density, a wide particle distribution do not assure the highest final density, which is more promoted by a small particle size and a narrow distribution (Pellizzari et al., 2011[1]). From a dimensional and morphological point of view, toluene is the best PCA due to its high wettability, which allows the achievement of equilibrium between welding and fragmentation for a longer milling time. By the way the purpose of using PCA is also to limit the contamination by the milling media. In order to evaluate the effectiveness of the different PCAs, ICP test have been carried out to determine the Fe and Cr content coming from wear of the vial and of the balls. The content of Fe end Cr impurities in the milled powder increases when the milling time increases (Fig.V-3) (Long et al., 2010 [1]; Marques et al., 2007; Sato et al. 2010). The composition of vial and balls (100Cr6) leads obviously to a lower amount of Cr than Fe. The lowest contamination is observed using stearic acid: for example, with reference to dry milling, the iron contamination decreases from 0.25% and 0.35% after 20 and 200 min, respectively, to 0.04% and 0.06%. Due to the relatively high viscosity, stearic acid promotes the formation of a protective layer all over the balls and the vial reducing wear of the milling media (Bailon-Poujol et al., 2011; Sato et al., 2010). On the other hand, toluene doesn't offer a similar protection mechanism leading to stronger contamination (Fig.V-3). In can be stated that, for those applications demanding high electric and thermal properties, the use of stearic acid is more effective for mechanical milling of copper. Therefore, in spite of the better particle size and morphology obtained with toluene with respect to stearic acid, the latter PCA was selected for the next step in this PhD thesis

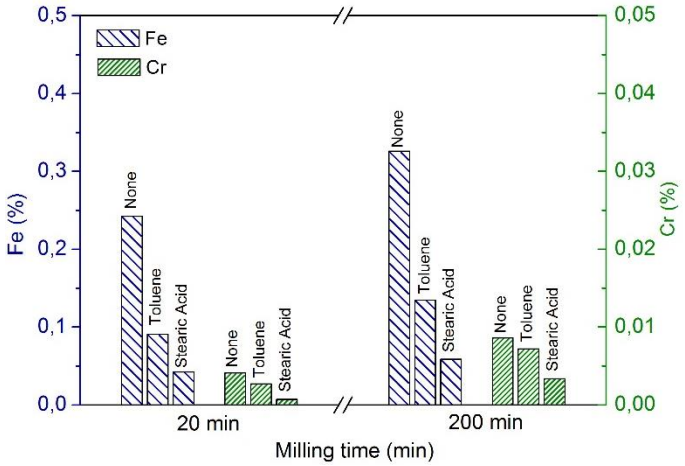

Figure V - 3. Fe and Cr contamination as function of process control agent and milling time (adapted from Cipolloni et al 2015).

At this point the effects of different BPR and the change of the type of cycle have been analysed in order to increase the milling efficiency and reduce the contamination level in the milled powders. OM micrographs of the as milled powder are reported in Figure V-4.

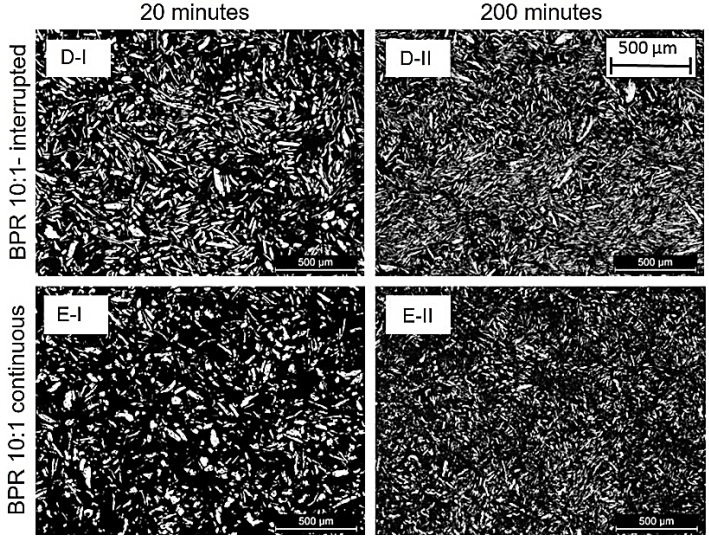

Figure V - 4. OM micrographs of powder milled with stearic acid using a BPR 10:1 for 20 min interrupted (D-I), 200 min interrupted (D-II), 20 min continuous (E-I) and 200 min continuous (E-II) (adapted from Cipolloni et al. 2015).

Firstly BPR has been decreased in order to reduce the milling energy, the impact frequency and thus the temperature, as well (Zeng et al., 1999). A drastic change in particle size and morphology is evident comparing Figure V-1 with Figure V-4. The decreased BPR leads to a more pronounced flake like morphology and a finer particle size of the powder especially after 200 minutes interrupted milling (D-II). For short milling time the difference is not relevant. The use of a lower BPR leads to a lower internal temperature, to a reduced formation of larger aggregates and to a finer particle size. At the same time the lower BPR leads to a lower contamination as reported in Table V-1.

Table V - 1: Fe contamination as function of type of milling cycle.

Fe contamination (%)					
Milling time (min)	A*	B*	C*	D*	E*
20 (I)	0.24	0.09	0.04	0.01	0.01
200 (II)	0.33	0.13	0.06	0.01	0.01

*Letters A-E are referring to micrographs in Fig. V-1 and Fig. V-4.

The Cr contamination is not reported because it was practically negligible compared to the previous results (Fig.V-3). The negative influence of a high BPR may be explained in view of the increased collision frequency resulting in a much higher wear of the milling media. Definitely, as far as contamination is concerned, the choice of a lower BPR is the most reasonable (Tab. V-1). Moreover the lower heat input does not require cooling pauses allowing for the replacement of the interrupted cycle with the continuous one shortening the production time. The use of a continuous cycle means a decrease of milling time of 80% in comparison with interrupted cycle (20 and 200 minutes continuously instead of 110 and 1100 minutes interruptedly). By the way the milled powder must also have a suitable particle size and morphology. Looking at Figure V-4, switching from interrupted to continuous cycle affects considerably the particle morphology especially for long milling time. The particle size of powder milled for 200 minutes results finer and less flake-like. From the contamination point of view the amount of Fe is the same of the interrupted cycle.
At this point stearic acid, a BPR equal to 10:1 and a continuous cycle have been selected for the further stage.

5.2 Effect of milling time

In order to deeply analyse the effect on copper powder the continuous milling time has been increased up to 720 minutes, all the studied milling time are reported in Table IV-3.

5.2.1 Morphology and particle size

Figure V-5 shows the morphology of as-atomized powder (AT-Cu). In Figure V-6 the evolution of the powder milled up to 720 minutes is shown. In detail, up to 200 minutes micro-forging is evident, leading to changes in particle shape without significant cold welding. The particle shape changed towards a flake like morphology in accordance with other studies (Luo et al 2012, Suryaranayana, 2001; Xiao et al. 2008). These changes derived from the high ductility of Cu under repeated collisions caused by milling medium, increasing the aspect ratio. With increasing milling duration, from 200 up to 240 minutes, the powders are progressively fractured and a smaller particle size is evident looking at Figure V-6d.

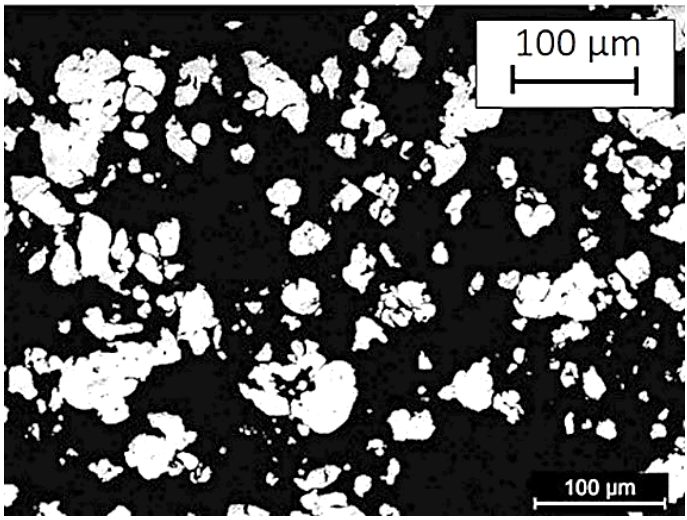

Figure V - 5. Starting copper water atomized powder.

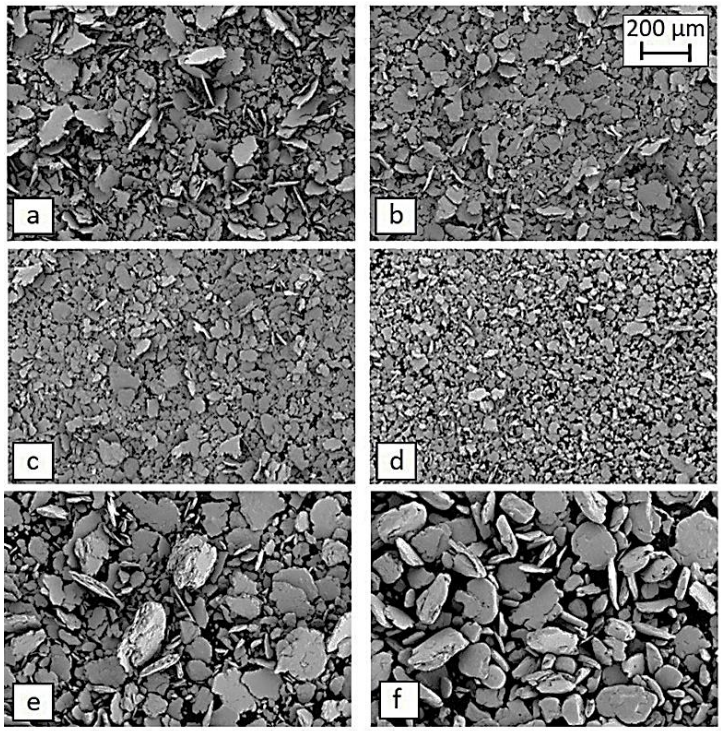

Figure V - 6. Variation of powder morphology as a function of milling time: (a) 20, (b) 120, (c) 200, (d) 240, (e) 360 and (f) 720 minutes conducted in continuous.

At this stage powder particles underwent increasing strain hardening, their fracture was activated resulting in a finer and progressively less dispersed size distribution. By prolonging milling, as a result of predominance cold welding, the particles showed a marked increase in size and their morphology became more equi-axed, Figure V-6e-f. The severe change of milling behaviour can be attributed to an increase of internal temperature inside the vial due to the continuous cycle configuration. For long milling time the repeated collisions of the grinding medium enhance the temperature inside the vial promoting welding. Looking at the large particle size a decrease of the effectiveness of PCA may be supposed and for this reason when the ball milling was extended to 720 minutes, the powders repeatedly tore and cold welded one other forming a matrix of randomly welded thick and highly deformed layers as shown in Figures V-7. An estimation of the aspect ratio of the powder can be made for a qualitative understand of the morphology evolution of the milled powder during milling. A very high aspect ratio is associated to powder milled for 120 and 200 minutes due to the intensive plastic deformation, meanwhile the

aspect ratio is gradually decreased with the increase of the milling duration (Luo et al., 2012; Xiao et al., 2008).

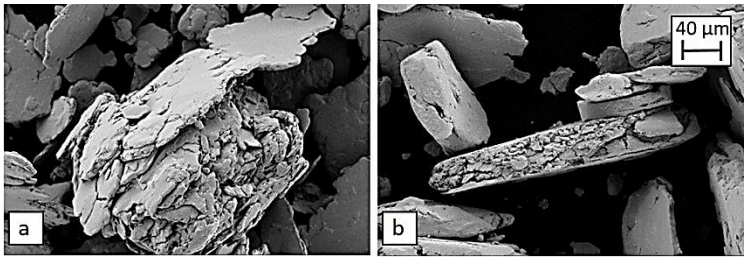

Figure V - 7. Highlight of powder compaction as a function of milling time: (a) 360 and (b) 720 minutes conducted in continuous.

Looking at Figure V-7 it is clear how the high energy impacts induced by the grinding balls tend to compact and smooth the particles forming shiny beads. The use of a not protective atmosphere leads to larger particle size than in the case of argon atmosphere (Madavali et al., 2014). Moreover the powder does not undergo to the typical milling process, but a continuous increase of particle size occurs instead of a severe refinement of the milled powder (Suryanarayana, 2001).

As explained previously an important feature of this PhD thesis is to analyse the effect of different milling parameter on the contamination level of the powder. In this chapter the effect of milling time on contamination from grinding media and PCA have been take in account. Firstly in order to limit the contamination coming from the milling media, the milling process has been interrupted when the level of Fe exceeded 0.1% even if much lower than some data reported in literature (Long et al., 2010[1]; Luo et al., 2013, Marques et al. 2007). This decision comes from the necessity for some thermal and electrical copper applications to have low amount of contaminations. The level of Fe in the powders measured by ICP analysis is reported in Table V-2 as function of milling time.

Table V - 2. Fe and Cr content in copper milled powders.

Milling time (min)	Label	Fe%
20	MM- 20’	0.008
120	MM-120’	0.011
200	MM-200’	0.009
240	MM-240’	0.019
360	MM-360’	0.030
720	MM-720’	0.117

Increasing milling time the level of Fe slightly increases up to 360 minutes than a drastically increase up to 0.12% has been attest after 720 minutes of milling. This can be attributed to the change of particle size of the milled powder and to the reduction of specific surface area. When the particle are smaller and flake like their adhesion on the grinding media is facilitated. A sort of protective layer is created and the wear of milling media is limited. Increasing milling time, when the lubricant action of PCA is lost, the particle size increases and powder change towards a more equiaxed morphology. At this point specific surface area decreases and the adhesion between milling media and copper powder is avoided; contact between sphere-sphere or sphere-vial are more frequent and the abrasion between them is enhanced. As mentioned above, by a drastically increase of the temperature inside the vial and the consequent predominance of welding events prolonging milling time, it is possible to deduce that the effectiveness of stearic acid is lost. The use of a continuous cycle leads to an overheating of the milling system and to a partial decomposition of stearic acid, as reported in Figure V-8.

Figure V-8 shows the influence of the duration of MM on the oxygen and carbon contents. The carbon content increase from 0.1% in the AT-Cu to 0.45% during the first 120 minutes because stearic acid takes time to be homogenized trough the milled powder. Increasing milling time a slight decrease of C content attests a partial decomposition of stearic acid (Kleiner et al., 2005). By the way the presence of such amount of PCA cannot be neglected for the further sintering process. The residual stearic acid must be correctly decomposed before sintering avoiding any gas entrapment which will favour residual porosity in the final products.

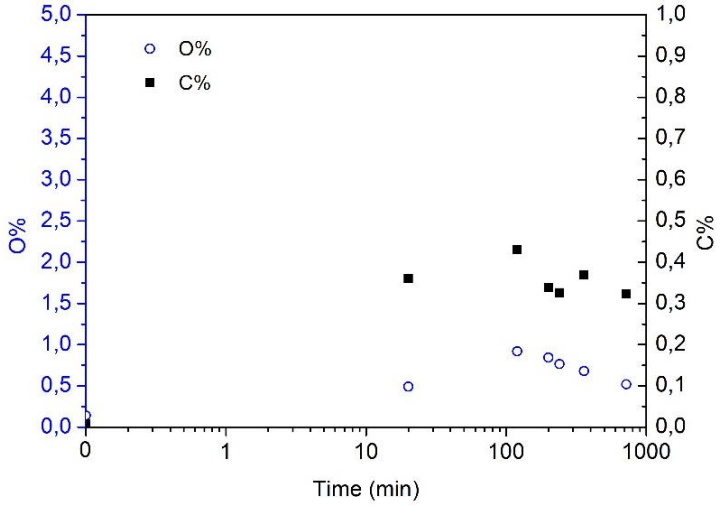

Figure V - 8. Oxygen and carbon content as function of milling time.

At the same time oxygen level must be considered because the presence of oxide on powder during SPS can affect considerably the process (Diouf et al., 2012 [2], Diouf et al., 2013). By Figure V-8 a slightly increases of oxygen content for short milling time is reported then decreases accordingly with C content trend. By the way, even if a linear increase of oxygen content in powder milled in air atmosphere was expected, this different trend is associated to the intense variation of particle size involved during milling (Raghu et al. 2001). The ratio between specific surface area/volume of the powders must be considered because oxidation of the particles during handling is intimately related to it. The ratio increases during the flaking process instead when welding process predominates the ratio decreases. This has severe effects on the amount of oxygen absorbed by the powder during milling and during handling. An increase of the dimension of the powder leads to a smaller oxidation phenomena. For this reason the oxygen level prolonging milling time decreases. The failure to attain complete densification of Cu powder during SPS is not completely related to the selection of densification parameters but instead it is related to changes in the chemistry of the powder too. The absorption of oxygen at powder surfaces and subsequent formation of thermally unstable compounds during milling and handling, and the subsequent thermal decomposition of these compounds during SPS generating gaseous species, leads to porosity formation, and consequently incomplete densification (Wen et al., 2010). Almost all gases generated during SPS can be trapped in the powder compact. The trapped gases contribute to a higher porosity and a reduced final density. The special surface structure and the high no equilibrium energy state induced by MM may enable absorption of oxygen on Cu powder surfaces. If SPS pressure is properly applied this phenomenon can be limited.
At this point in order to optimize the SPS parameters TGA and QMS of some milled powder has been conducted to evaluate the decomposition process of stearic acid during heating.

5.2.2 Decomposition of PCA

Initially QMS analysis has been carried out on powder milled for 0 and 200 minutes. This choice has been made thinking that the morphology and the size of the milled copper powders wouldn't have affect considerably the decomposition of stearic acid (Kleiner et al., 2005). In Kleiners work the decomposition of 2.5wt% of stearic acid occurs always in the same range of temperature ~350°C, indicating that the milling time does not affect the decomposition process. Moreover increasing milling time the mass loss during TGA decreases deducing that a partial decomposition of stearic acid already occurs during MM and a lower amount of PCA's contamination must be correctly decomposed. In Figure V-9 the TGA and the QMS curves for AT-Cu and MM-Cu-200' are reported.

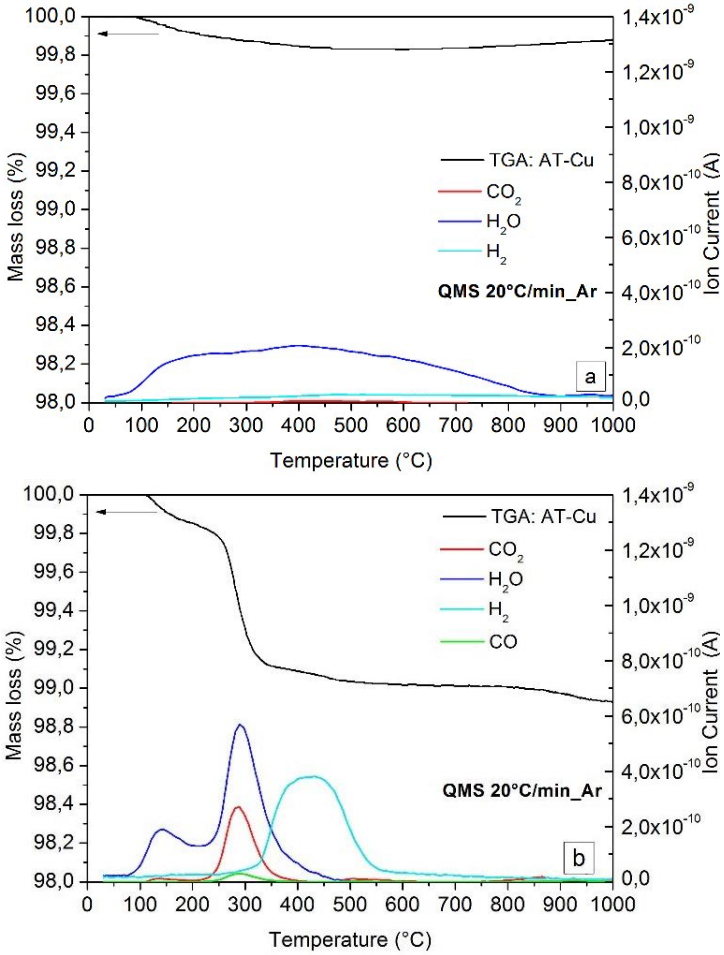

Figure V - 9. TGA and QMS curves of AT-Cu and MM-200' powders.

The TGA curve of AT-Cu shows a continuous mass loss until 500°C. Conversely, the milled powder shows a higher mass loss indicating three different events, associable to the decomposition of stearic acid that occur at different temperatures, i.e., 150, 300 and 450°C in agreement with Kleiner (Kleiner et al., 2005). According to QMS, these three events could be correlated with different gas emissions:

- *100°C-1000°C, continuous water evaporation;*
- *300°C, water evaporation and production of CO and especially CO_2;*
- *450°C, H_2 production.*

In the case of AT-Cu, only water evaporation up to 500°C has been revealed by QMS and TGA, since no stearic acid was used for milling. During preparation steps, the powders were exposed to the environment leading to an inevitable humidity adsorption on powder surfaces (Wen et al., 2010).

In the case of MM-200' three peaks corresponding to the three different gas emissions have been recorded by QMS. Accordingly TGA shows three different slopes of the curve depending on the atomic mass of the evaporated element. For this reason, the second segment (300°C) presents a higher slope due to the higher atomic mass of CO and CO_2 than H_2O and H_2.

The first peak is associated to the evaporation of H_2O. The second peak, at about 300°C, may be correlated to thermal decomposition of stearic acid. According to reaction (6.1) and (6.2) both CO/CO_2 gases and H_2O vapour might be formed as possible decomposition products,

$$C_{18}H_{36}O_{2\,(S)} + 27O_{2\,(g)} \rightarrow 18CO_{2\,(g)} + 18H_2O_{\,(g)} \quad (6.1)$$

$$C_{18}H_{36}O_{2\,(S)} + 18O_{2\,(g)} \rightarrow 18CO_{\,(g)} + 18H_2O_{\,(g)} \quad (6.2)$$

Peak III at about 450°C can be associated to the reaction between stearic acid and the iron and chromium contaminants. As a consequence, larger quantities of gas are generated according to the reactions described by equations (6.3) and (6.4).

$$2CH_3\text{-}(CH_2)_{16}\text{-}COOH_{\,(vapour)} + Fe_{\,(S)} \rightarrow [CH_3\text{-}(CH_2)_{16}\text{-}COO]_2Fe_{\,(S)} + H_{2\,(g)} \quad (6.3)$$

$$6CH_3\text{-}(CH_2)_{16}\text{-}COOH_{\,(vapour)} + 4Cr_{\,(S)} \rightarrow 2[CH_3\text{-}(CH_2)_{16}\text{-}COO]_3Cr_{2\,(S)} + 3H_{2\,(g)} \quad (6.4)$$

From results in Figure V-9 it is clear that any possible gas emission will be completed at around 600°C. Accordingly, in order to allow proper decomposition of the stearic acid and to avoid any gas entrapment the pressure during SPS have been applied a 700°C, when almost all the QMS curves tend to zero. The optimized SPS cycle is shown in Figure V-10.

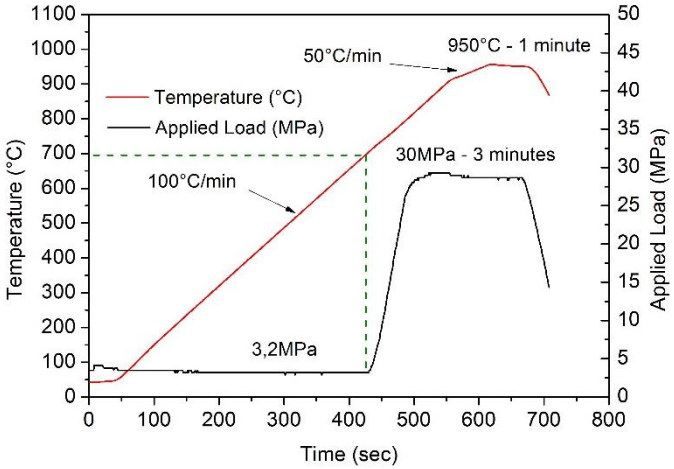

Figure V - 10. Optimized SPS cycle.

5.2.3. Densification and sintering mechanisms

Even if all powders milled for six milling times have been sintered by SPS the displacement and the displacement rate of MM-200' and MM-720' are reported in this section in order to facilitate the understanding (Fig.V-11). The selection of these samples has been made considering the two main particles morphologies obtained by milling, i.e. flake and large equiaxed. Moreover the displacement and the derivative of displacement of AT-Cu is always reported as reference. The displacement curve is widely accepted as a densification measure as a function of the sintering temperature. The densification behaviour changes depending of the milling time but especially of the particle morphology. The densification behaviour can be analysed considering two parts of the displacement curves, namely before and after the application of pressure at 700°C.

Before the load application a progressive increase of displacement for AT-Cu increasing temperature is observed. Comparing the densification rate of AT-Cu with the behaviour showed by Diouf, the peak at 100°C of powder rearrangement is absent but this can be attributed to the lower initial pressure (3MPa versus 23MPa) during the first stage of the SPS cycle. The slight increase of the displacement curve and the presence of a densification rate peak at 600°C can be ascribed to a powder rearrangement and to the local deformation (Diouf et al., 2012 [1]). The morphology and the particle size distribution of the AT-Cu powder and especially their higher ductility due to the absence of the MM treatment, enhance this behaviour. Moreover AT-Cu is characterized by a wider particle size distribution and this enhances the

powder rearrangement by a higher packing density (German, 1992 [1]; German, 1992 [2]).

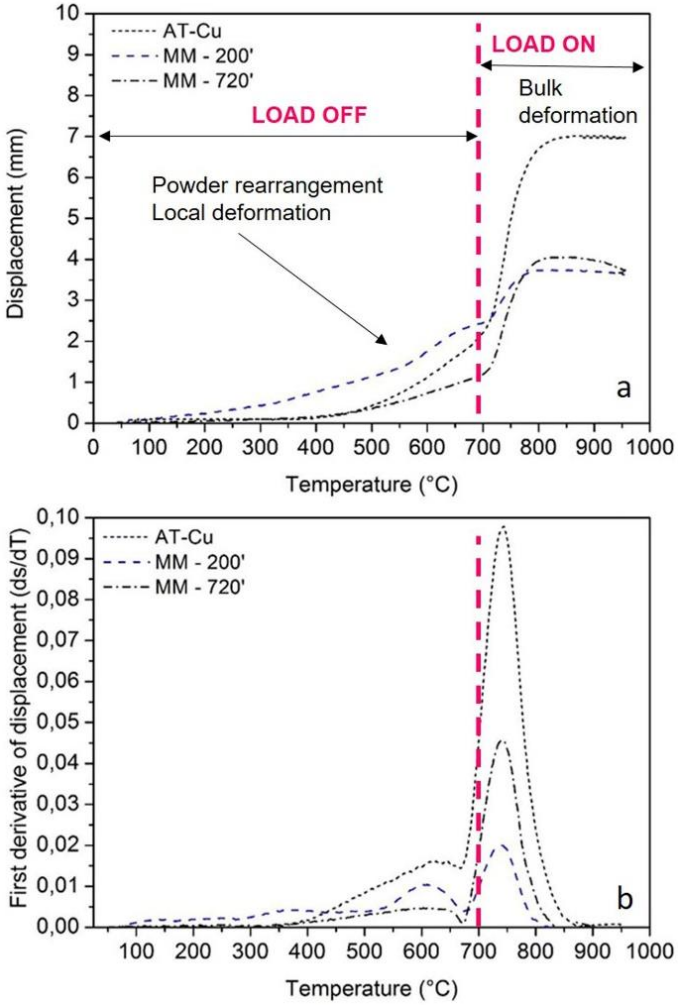

Figure V - 11. Displacement of lower punch and its first derivative during SPS.

In addition ductile copper powder leads to an easier compressibility of the powder during SPS. For this reason at 600°C the first derivative of AT-Cu is the highest in comparison with the other materials. During milling powders are subjected to a severe plastic deformation leading to a severe strain hardening. Therefore the densification mechanism should be retarded by a lower deformability of the powders under pressure. By the way before the application of the load MM-200' shows a greater

increase of the displacement almost at the beginning of the SPS cycle in comparison with AT-Cu and MM-720'. A contribution to the larger displacement may be attributed to the more irregular morphology of the flake like particles shown in Figure V-6. For MM-200' apparent density decreases with respect to that of AT-Cu and, in turn, increases the filling height in the die cavity. Under the application of the pressure, even if it is limited to 3 MPa, the packing of the flake like particles is therefore more pronounced (Diouf et al., 2013). This effect is responsible for the higher displacement of MM-200', at least until the application of the pressure. It is also believed that the presence of residual stearic acid in the milled copper powder aids the particle rearrangement by its lubricant action. For MM-720' the densification of the powder before the load is very little, demonstrating that powder rearrangement and local deformation are not active due to the higher hardness of powder milled for long milling time. The absence of a bimodal distribution especially for MM-720' does not facilitate the filling of the inter particle space therefore the densification of the powders is limited.

Once the load is applied, the AT-Cu rapidly densifies thanks to the lower hardness and favourable deformability. The sintering rate peak is the highest because densification is enhanced by smaller and more ductile particles (Pellizzari et al., 2011[1]; Ting et al., 1994; Ting et al., 1995). The higher reactivity of MM-200' before the application of the load leads to a limited displacements as well as to a lower displacement rate after 700°C. MM-720' recovers part of the densification when the load is applied and for this reason in this part of the SPS cycle the densification rate is higher than for MM-200'. All the displacement curves reach a plateau at 850°C, meaning that the maximum densification allowed to the powder has been reached.

5.2.4 Characterization of sintered samples

In table V-3 the density and the hardness on the cross section surface (Fig.IV-3) of the six sintered samples are reported.

Table V - 3. Real density, relative density and hardness of sintered samples.

Sample	Real density (g/cm^3)	Relative density (%)	HB 5
AT- Cu	8.76	99	91±2.1
MM-Cu-20'	8.76	99	88±1.8
MM-Cu-120'	8.67	97	93±1.5
MM-Cu-200'	8.67	97	106±2
MM-Cu-240'	8.37	94	121±2.3
MM-Cu-360'	7.83	89	102±2.4
MM-Cu-720'	7.88	89	113±1.9

It is evident that by increasing milling time the hardness increases due to the incremental strain hardening induced by MM. MM leads to a drastic increase of defect such as dislocations, vacancy, grain boundaries, which enhance hardness. The stronger plastic deformation limits the deformability and therefore densification, as confirmed by the lower density measured by increasing milling time (especially beyond 200 minutes). In Figure V-12 and Figure V-13 the OM micrographs of all the sintered samples are reported. The sample sintered from AT-Cu powder shows a uniform microstructure (Fig.V-12). Figure V-12 suggests that AT-Cu powders have already reached the final stage of sintering where surface areas of pores decreased through closing off of pore channels and decreasing their connectivity to minimize the surfaces corresponding to high level of densification. Some pores are still evident and give a pinning effect for the grain growth (Fig.V-12) (Diouf et al., 2012 [2]; Zhang Z.H. et al., 2008).

By looking at the density values a very high porosity is expected in the sintered microstructures, especially for MM-360' and MM-720'. However, the OM micrographs do not confirm this result (Fig.V-13).

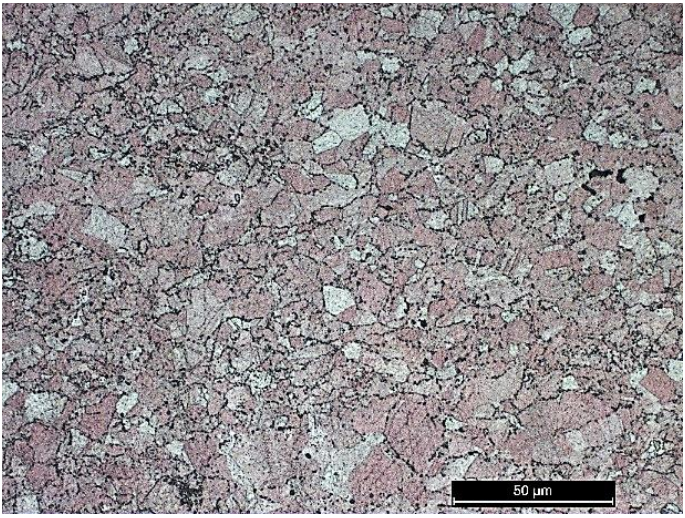

Figure V - 12. AT-Cu microstructure by OM micrograph.

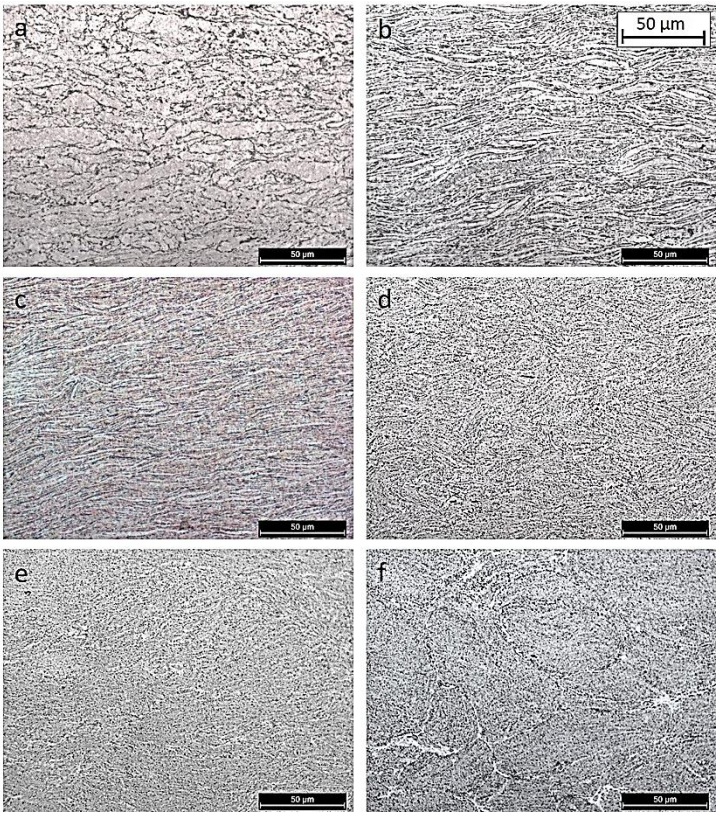

Figure V - 13. Variation of microstructure as a function of milling time: (a) 20, (b) 120, (c) 200, (d) 240, (e) 360 and (f) 720 minutes conducted in continuous.

The microstructure of the milled powders is severely affected by the powder morphology after MM. The samples from milled powder for 20, 120 and 200 minutes show an intrinsic anisotropy due to their flaky morphology. This kind of particles enhance the densification process by their rearrangement with elevate packing factor once pressure is applied, align them self in perpendicular direction to that of punch stroke leading to the distribution of porosity following the direction. This sintered products show a higher number of either longitudinal or interconnected pores, which distributed mostly along deformed particles' boundaries (Fig.V-13abc). MM-240' (Fig.V-13d) shows a stronger opposition of the particles to densification. These flake-like powders might express an ineffective rearrangement stage. The compressed flakes would not be perfectly aligned in one preferable direction as for shorter milling time (MM-120' and MM-200'). Therefore, instead of stacking "layer by layer", these flakes tended to be wrapped up leading to the less proper contact between particles

when sintering, and a microstructural anisotropy is less evident (Fig.V-13d). Increasing milling time the microstructure becomes more uniform (Fig.V-13ef). A remarkable feature that should be pointed out is the white region located at particles' boundaries in MM-720', (Fig.V-14)

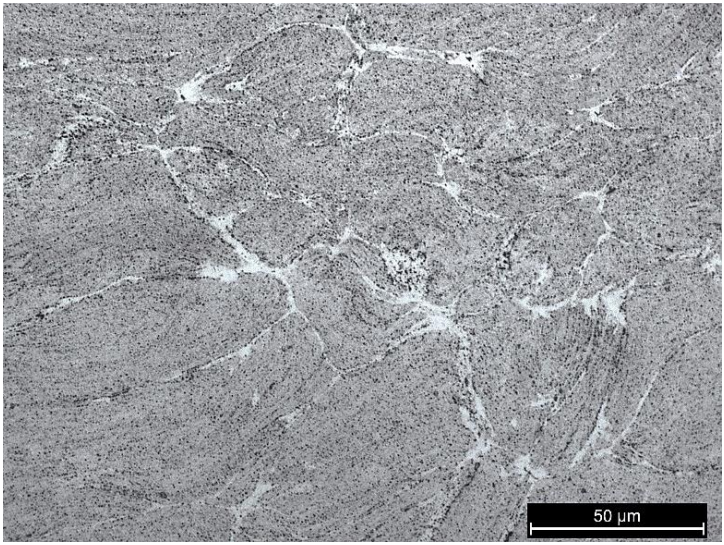

Figure V - 14. OM micrograph of MM-720'.

These white area can be associated to the occurrence of overheating at the contact points between the particles (Rajkovic et al., 2006; Rajkovic et al., 2008). Diouf claimed that increasing the contact area between the particles the electrical resistance decreases and consequently the current flow and the contact temperature increase according to $R=\rho h/S$ where ρ is the resistivity of copper, h is the thickness of the particles and S is the contact area between the particles (Diouf et al., 2012 [1], Yanagisawa et al., 2003). This behaviour lead to Joule effect, which promotes the sintering during SPS by a local overheating at the contact points between the particles, especially for coarse particles. The temperature increase at the surface of particles is very pronounced and raises on increasing particle size, overheating involves a very thin surface layer. Such a localized overheating causes thermal softening and localized melting at the surface, both enhancing deformation and the formation of necks by the activation of mass transport phenomena in the contact regions. By increasing particle size the local overheating increases dramatically and local thermal softening and melting support densification. At SPS temperature of 400°C it has been demonstrated by Diouf that the overheating of lamellar particle is confined within a very thin surface layer, becoming negligible at 0.2 micron of depth with a ΔT of 50°C.

On the other side the coarse powder shows an overheating (ΔT) of 500°C at 0.2 microns from the surface layer, reaching 900°C as nominal temperature at the contact points (Diouf et al., 2012 [1]). Despite the occurrence of overheating, densification of MM-720' is partially prevented because overheating does not affect the particle bulk temperature and, in turn, bulk deformation. Moreover also the severe strain hardening of the powder hinders densification. By the way by the micrograph of MM-720' any porosity comparable to an 11% could be associated to the limited densification.

LECO analysis has been carried out in order to evaluate the occurrence of the correct decomposition of PCA during the SPS cycle. In Figure V-15 carbon content before and after SPS as function of milling time is reported.

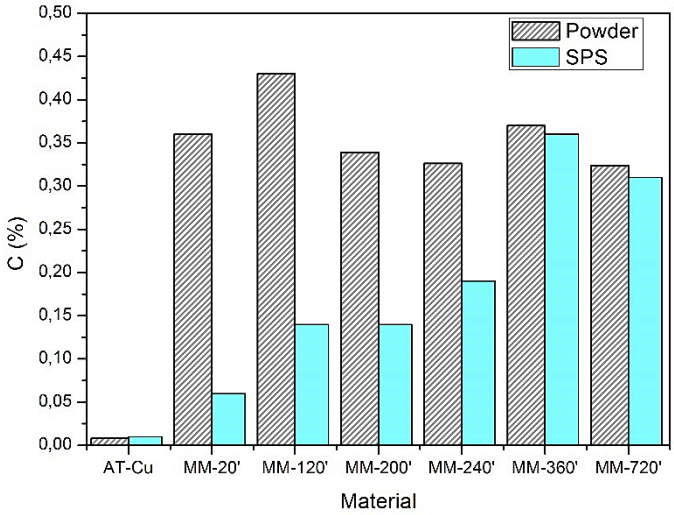

Figure V - 15. Carbon content before and after SPS by LECO analysis as function of milling time.

After the SPS cycle the level of carbon is reduced for all the samples, especially for MM-20'. This sample shows the highest loss of carbon, because stearic acid still not well homogenised and most of it covers the powder surfaces. Therefore its decomposition is facilitated. By the way the amount of carbon lost during SPS decreases with milling time. For MM-120, MM-200 and MM-240, when flake morphology is dominant the level of carbon loss is lower than MM-20. During MM process particles are deformed by impact contacts, and by welding events the flakes overlap entrapping part of the attached stearic acid between their surfaces. This slows down the decomposition kinetics of PCA reducing the level of carbon decomposed during SPS. Looking at Figure V-15 it is clear that for milling time longer than 360 minutes the decomposition of stearic acid is practically avoided, the amount of carbon

before and after SPS stays almost the same. The stearic acid, due to the intense overlapping of the particle, is constrained between them and not reduced during SPS. This means that the decomposition of PCA before the application of the load at 700°C did not occur. At this point it is clear that the morphology and the dimension of the milled powder affect considerably the decomposition process of stearic acid. On such attempt the QMS analysis has been conducted for all the milled powders, and in Figure V-16 the QMS analysis of MM-200' and MM-720' are reported for comparison.

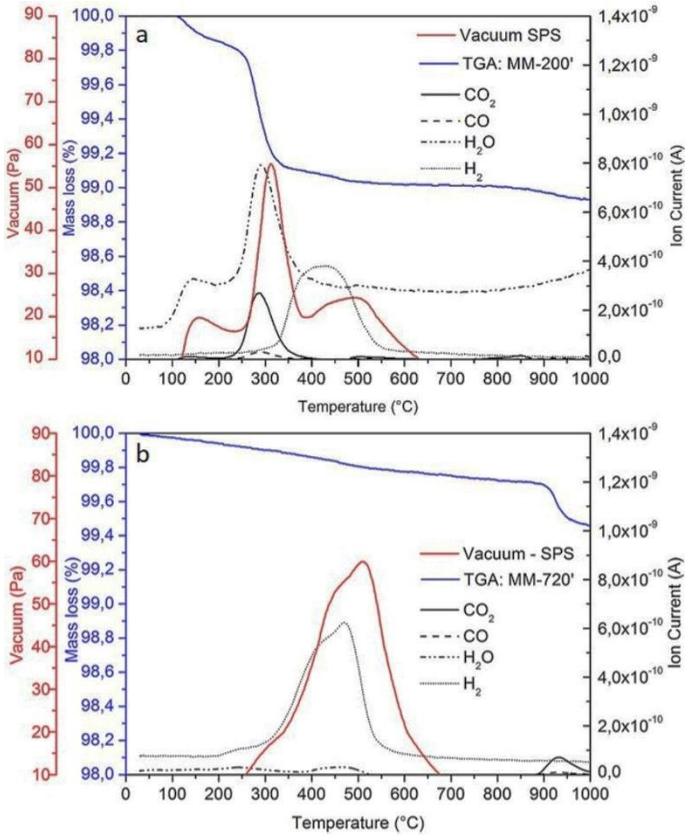

Figure V - 16. TGA and QMS curves of MM-200' (a) and MM-720' (b) powders.

In MM-720 the decomposition of stearic acid is not complete at 700°C but a CO_2 peak is evident at 950°C. Accordingly the TGA curve (solid blue line) shows an intense mass loss at 950°C. The peak of H_2, associated with a slight and continuous decrease of mass, is reported by both powders. The occurrence of the decomposition of stearic acid at 950°C can be attributed to the particle size and morphology as

mentioned above. This delays the decomposition of PCA so that the application of SPS pressure at 700°C is no longer adequate. The information obtained by QMS can be monitored during SPS by the vacuum trend (solid red line). In fact the excellent correspondence between the vacuum trend and the ion current recorded by QMS (Fig. V-16a) highlights the reliability of the vacuum level as useful measurement for the analysis of gas emission during SPS. The slight delay of the vacuum curve in comparison to the QMS curves can be attributed to the different heating rate, 100°C/min and 20°C/min respectively. In Figure V-16b is evident that the CO_2 emission at 950°C during QMS is not detect by vacuum recording during SPS. The decomposition of stearic acid occurs but CO_2 remains entrapped in the sintered sample. The presence of CO_2 is the reason of the high level of carbon detected by LECO analysis after SPS and responsible of the low density value

It has been demonstrated that the absorption of oxygen and other elements at the powder surfaces leads to the formation of thermally unstable compounds. Their decomposition during SPS releases gaseous species that cause the formation of pores and reduce the final density (Wen et al., 2010). This found also confirmation by the SEM micrograph displayed in Figure V-17.

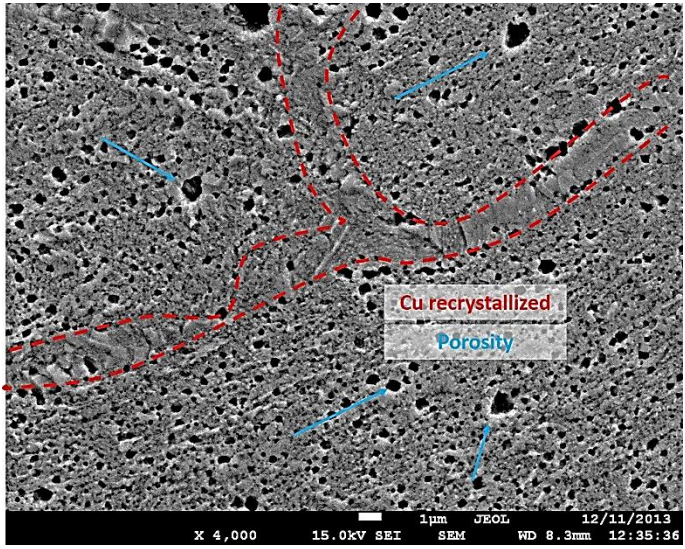

Figure V - 17. SEM micrograph of MM-720' microstructure.

A uniform and round shaped porosity is evident in MM-720' sintered sample. The round shape is typical of porosity coming from gas emission. Moreover the SEM micrograph confirms the presence of a continuous copper recrystallize zone between the large particles caused by the overheating phenomena, as highlighted by a red

dashed line (Fig.V-17). Therefore the particle size of MM-720 is suitable to enhance the Joule effect responsible of an appropriate sintering process, but it prevents the decomposition of stearic acid leading to a high residual porosity.

At this point in order to increase the density of the sintered sample three different solutions have been proposed:

i) The optimization of the SPS cycle by changing the loading temperature in order to allow the proper decomposition of the PCA;
ii) The optimization of the particle morphology and size of the milled powder in order to facilitate the densification process.
iii) The combination of i and ii.

5.3 Optimization of SPS process

5.3.1 Modification of SPS parameters

The old (black lines) and the new optimized SPS cycles (blue lines) are plotted in Figure V-18. The main difference is that the pressure is applied at 950°C instead of 700°C to allow the gas emission from the decomposition of stearic acid for MM-720' powder. Moreover high temperature soaking time has been prolonged to four minutes (instead of two minutes) to maintain the same loading time (3 minutes).

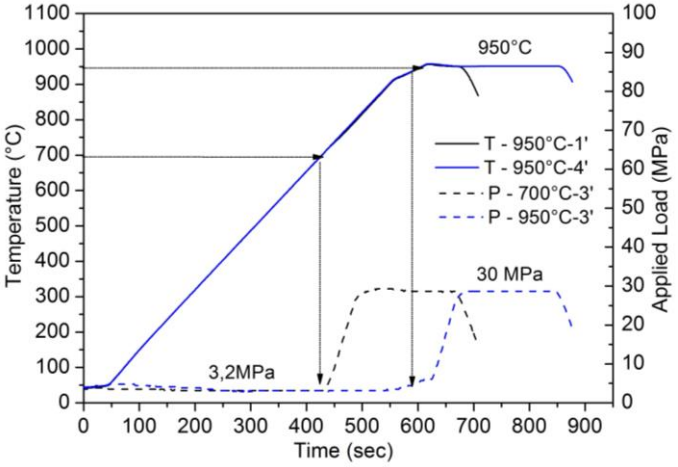

Figure V - 18: Pressure and temperature cycle of MM-720' powder.

As shown previously the densification process can be studied by the analysis of the SPS outputs. The decomposition of PCA in MM-720' is monitored by the change of the vacuum pressure inside the chamber and the densification evolution by the

displacement trend, both parameters are reported in Figure V-19 for both previous and optimized cycle, named MM-720'/P-700°C and MM-720'/P-950°C respectively (Tab. V-4). In spite the updated SPS cycle, from Figure V-19 only one peak is recorded at 500°C in vacuum trend and almost a perfect overlap of the two curves is evident. It was supposed to have a second peak at 950° in Figure V-19a corresponding to the CO_2 emission for the optimized cycle in accordance with Figure V-16b. The perfect overlapping between the vacuum trends of the two cycles confirms that any additional gas emission occurred during SPS cycle of MM-720'/P950°C. Although the improved application at 950°C of the pressure, the stearic acid did not decompose, or at least the gas emission remained entrapped in the sintered sample as in previous results (Fig.V-17). At this point an improved densification of the sintered sample is not expect. In fact the displacement of MM-720'/P950°C (blue line) shows a gradual increase associated to powder rearrangement up to 900°C, but once the pressure is applied a vertical increase is reported. The incomplete densification of MM-720'/P950°C is firstly attested by the absence of gas emission at 950°C (Fig.V-19a) and then by the lower displacement (Fig.V-19b). All the assumptions made by the analysis of the SPS outputs are confirmed by the density measurements and the LECO analysis (Tab.V-4).

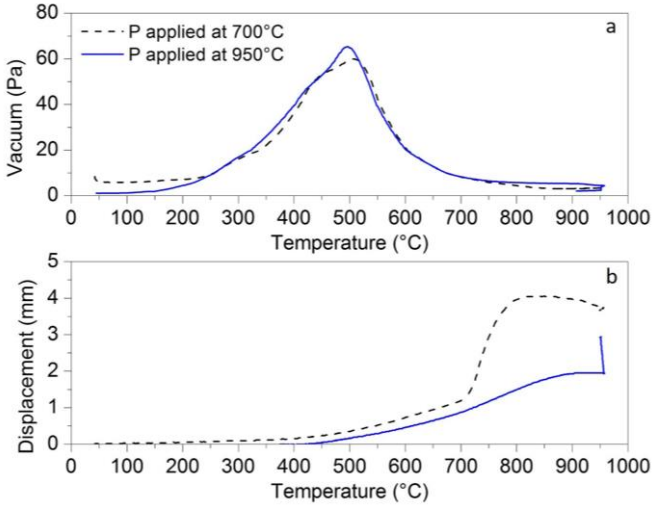

Figure V - 19. Vacuum (a) and displacement (b) curves of MM-720' milled powder sintered by two SPS cycles: initial SPS cycle (black dash line) and optimized SPS cycle (blue solid line).

A comparison of density and content of carbon before and after SPS between the two samples produced by the different sintering cycles are reported in Table V-4. The relative density of MM-720'/P950°C is even lower than the density of MM-720'/P700°C. Despite the delayed application of the pressure and the longer holding

time of the temperature, the level of carbon after SPS still high, this means that this solution is inefficient for the correct decomposition of the PCA, leading again to a high residual porosity.

Table V - 4. Properties of MM-720' sintered by two different SPS cycles.

Processing		Density	Rel. Density	C_{powder}	C_{SPS}
Milled powder	SPS cycle	(g/cm^3)	(%)	(%)	(%)
MM - 720'	P - 700°C	7.88	88	0.324	0.310
	P - 950°C	7.63	86	0.324	0.321

5.3.2 Modification of MM parameters

5.3.2.1 Evolution of powder morphology and microstructure

As stated in section 5.2.2 the decomposition of stearic acid is facilitated by a small particle size. Therefore an attempt was made to further refine the particle size. It is important to carry out MM for long time because this leads to a severe strain hardening by plastic deformation of the powders, and consequently to a fracturing process (Suryanarayana, 2001). In section 5.2.1 the use of a continuous cycle was leading to a continuous increase of the particle size. The use of a continuous milling cycle favoured the agglomeration of the powder due to the increase of temperature inside the vial. At this point to reduce particle size the milling cycle has been changed from continuous to interrupt in order to give time to the milling system to cool down during the pause of 9 minutes after 2 minutes of on. Six milling times have been studied: 20, 120, 200, 720, 3000 and 6000 minutes, named MMi-20', MMi-120', MMi-200', MMi-720', MMi-3000' and MMi-6000' respectively (Tab.IV-3). The first four milling times have been selected to compare the effects of an interrupted cycle with the previous continuous cycle on the MM behaviour of the powders. The MMi-3000' and MMi-6000' have been chosen to strongly refine the particle size according to the requirements (Suryanarayana, 2001). Particle size and morphology evolution of the powders are shown in Figure V-20.

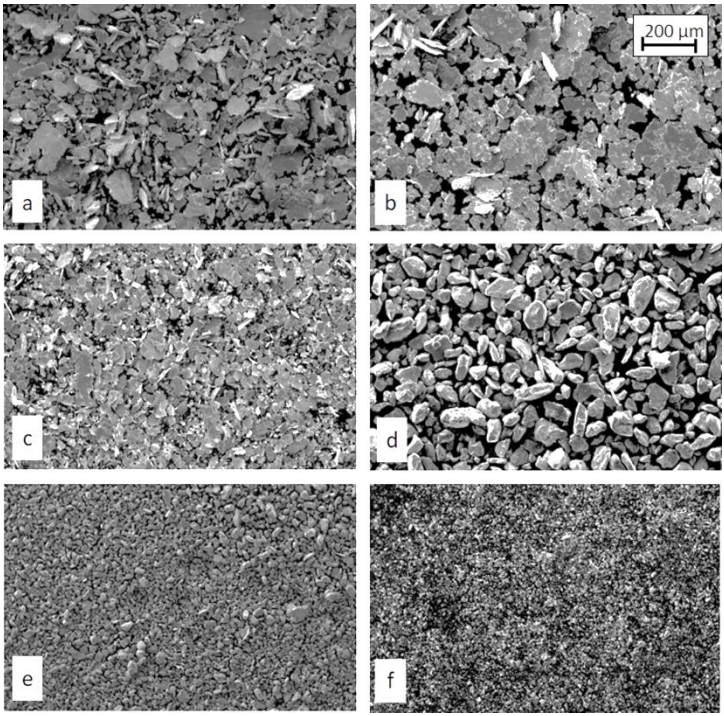

Figure V - 20. Variation of powder morphology as a function of milling time: (a) 20, (b) 120, (c) 200, (d) 720, (e) 3000 and (f) 6000 minutes conducted by interrupted cycle.

From 20 minutes to 200 minutes (Fig. V-20abc) of milling the benefit of the interrupted cycle is not very evident. Increasing the milling time to 720 minutes (Fig. V-20d) the powder becomes more homogeneous and equiaxed compared to powder milled in continuous (Fig.V-6f), in addition the particle size is sensibly decreased. On milling for 720 minutes, all the particles got compacted and more spherical because the impact action of the milling media smooth the powder and promote welding between them. Since the powder milled with an interrupted cycle experience much less heating from the impact events, their particle size is smaller than the powder milled by continuous cycle. By the way this morphology and particle size is very similar of MM-720' and still not suitable for SPS cycle. According Suryaranayana after the predominance of welding events a fragmentation of the powder, induced by the severe strain hardening promoted by prolonging milling time, occurs especially if a cooling pause during MM is used (Suryanarayana, 2001). As MM has been prolonged up to 6000 minutes, the particles started to fragment (Fig. V-20e-f). The ability of the particles to accept further deformation is diminished. Fracturing becomes significant, and leads to a decrease in particle size until equilibrium is reached between cold

welding and fracturing. The addition of the cooling pause overcomes the welding phenomena mentioned above, especially for very long milling times. Powders are subjected to a limited thermal increase and the level of strain hardening due to plastic deformation increases inducing brittle fracture. Fracturing goes on until a very fine size and regular powder particle shape is obtained as typical of every milling process (Sheibani et al., 2007; Suryanarayana 2001). This morphology and size are more suitable for sintering process because degassing of stearic acid should be promoted and a finer particle size is more suitable for SPS (Diouf et al., 2012 [1]; Pellizzari et al., 2011 [1]; Pellizzari et al., 2011 [2]). Another important contribution to the fragmentation mechanism during MM for long milling time is given by the presence of oxide in MMi-720' as confirmed by LECO analysis reported in Figure V-21. For purpose of comparison C and O content for continuous and interrupted cycles are graphed in Figure V-21.

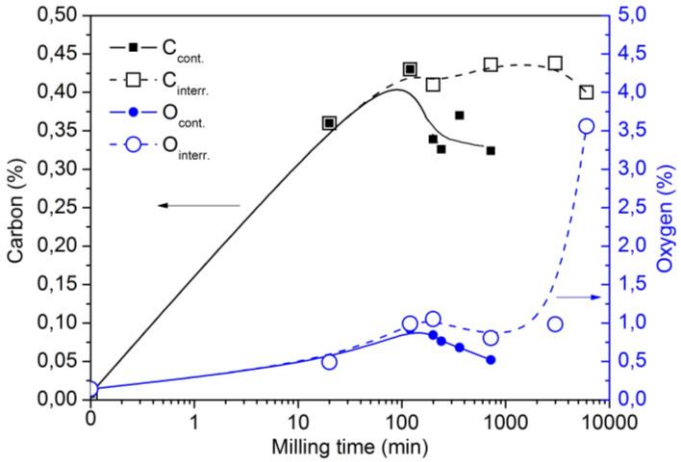

Figure V - 21. Carbon and oxygen content of powder milled with continuous and interrupted cycle.

It is clear that the oxygen level depends directly to the particle size and morphology as explained in section 5.2.1, and especially to the specific surface area of the powder. The ratio between specific surface area on volume increases during the initial and finale stages of MM, when flaking process (MMi-120' and MMi-200') and the fracturing process predominate (MMi-3000' and MMi-6000'). When particle size increases due to welding events the ratio decreases (MMi-720'). The change of the ration between specific surface area on volume according to the MM behaviour, has severe effects on the amount of oxygen absorbed by the powder during milling and during handling. A decrease of the dimension of the powder leads to a higher oxidation. For this reason the oxygen level prolonging milling time increases up to

3.5% while particle size drastically decreases. This is in accordance with the contamination level found by Madavali et al, they found an oxygen level of 4.97% after 80 hours of milling in air (Madavali et al., 2014). Also Gomez found that oxygen content increases with the milling time until 8 h up to 2% (Gomez et al., 2006). Independently of the milling time the trend of oxygen content is the same for both cycles since particle morphology and size are very similar. The higher amount of oxygen for interrupted MM in Figure V-21 is associable to the finer particle size than continuous cycle (Fig. V-6 versus Fig. V-20). The high absorption of oxygen for long milling time is associable also to the higher reactivity of the powders. The special structure (high surface area) and the energy state (high non equilibrium state) induced by MM enable the oxygen absorption on Cu powder surfaces. This is accompanied by the breakage of Cu-Cu surface bonds and the creation of new Cu-adsorbate bond (Besenbach et al., 1993; Wen et al., 2010). Moreover the high surface excess energy leads to different phenomena which promote the absorption of oxygen: disturbs of the balance and symmetry of the forces and masses, change of the interatomic distances, increase of the shear strain and influences of the atomic ordering pattern on the surface (Poluboyarov et al., 2005). Once the oxygen during milling got incorporated in to the copper powders to form oxide layers it acts as a hard second phase (Menapace et al., 2016). Oxide layer makes the particle brittle and therefore should result in finer particle. The agglomerated coarse powders get cracked and broken prolonging MM.

If, on one side, prolonging milling time leads to a smaller particle size, on the other one the use of a cooling pause limits the partial decomposition of PCA during MM. This is confirmed by the LECO analysis (Figure VI-21) showing that by increasing milling time the carbon content decreases for continuous MM (black dense square), whilst it remains constant for interrupted MM (black empty square). This means that a major amount of PCA must decompose during SPS and this may influence the correct progression of densification.

In order to study the structure of the copper powder, XRD analysis have been carried out for all the powder milled both by continuous and interrupted milling. By the analysis of the spectra of mechanical milled powder any formation of second compounds has been detect among the entire continuous cycle. Up to 720 minutes a continuous decreased of the intensity of the peaks and an increase of the full width half maximum for milled powders have been revealed, confirming the reduction in the particle/crystallite size (Prasad et al., 2004; Wen et al., 2010). Similar behaviour was shown by powder milled interruptedly up to 3000 minutes. Only the spectra of powder milled for 6000 minutes shows a change in the behaviour. The presence of copper oxide in the MMi-6000' sample is confirmed. For this reason in Figure V-22 only XRD of AT-Cu, MMi-3000' and MMi-6000' are reported.

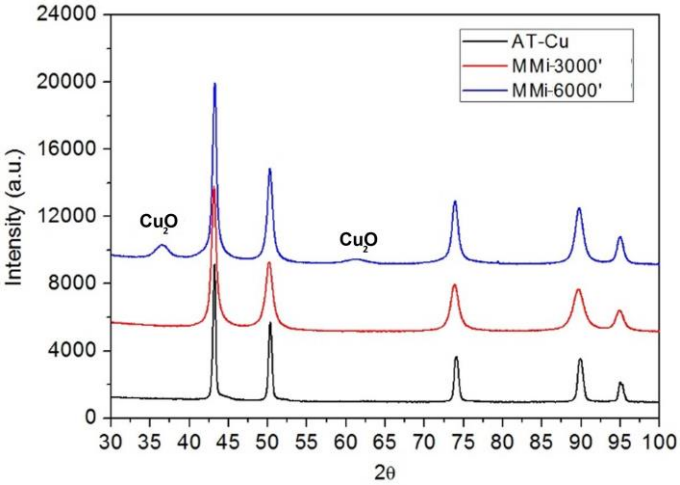

Figure V - 22. XRD spectra of AT-Cu, MMi-3000' and MMi-6000' powders.

XRD peak corresponding to phases Cu_2O was observed, suggesting that the synthesized copper powder was reasonably pure and that it did not pick up excessive amounts of impurities to form new phases till that milling time (Xiao et al., 2008). The presence of the (111), (200) and (220) peaks confirms that the face-centred cubic structure of the copper powder is also retained after milling (Xiao et al., 2008). There have been instances in the literature where the mechanically alloyed powders exhibit changes in crystal structure due to phase transformations by increasing milling time (Suryanarayana, 2001; Suryanarayana et al., 2011). These include pure metals, which may exhibit polymorphic changes or intermetallics, where either the high-temperature or high-pressure phases are stabilized. This may happen due to an increase in the free energy of the system due to a reduction in particle size and the consequent increase in surface energy. In present case, are no polymorphic transformations and therefore no change in crystal structure were observed. The formation of oxide is associated with the oxygen that is absorbed at the powder surface when exposed to air after ball milling (Azabou et al., 2012; Khitouni et al., 2009). Possible mechano-chemical reactions can be:

$2Cu + ½O_2 \rightarrow Cu_2O$

$Cu + ½\ O_2 \rightarrow CuO$

Prolonging milling the formation of copper oxide is enhanced by the reduction in particle size and consequent increase in surface energy and oxidation of the powder (Azabou et al., 2012; Khayati et al., 2013; Marques et al., 2007). Khayati et al.

estimated an incubation time for the solid state reaction between copper and oxygen of approximately 25 hours milling after which the oxidation kinetics exhibited an enhanced rate. In the current study it should be noted that owing to the little amount of Cu_2O and the restriction of the XRD resolution, the actual incubation time is longer and between 3000 and 6000 minutes. Under these conditions, high amount of fine activated Cu milled powder are available to be in contact with oxygen, leading to a relatively high reaction rate and a fraction of copper oxide was produced. The presence of Cu_2O enhances the fracturing process of the powders because it acts as hard phase during mechanical milling (Menapace et al., 2016).

Vasil'ev and Lomaeva proposed a model for the formation of nanocrystalline structures during MM consisting in the formation of a thin amorphous-like layer, which captures oxygen atoms from the particle surface or gas phase, leading to the formation of metastable copper–oxygen phases (Valiev et al., 2004). It is, therefore, reasonable to assume that the energy delivered to the powder during milling is accumulated in energy-rich copper–oxygen compounds on the particle surface. Moreover the reduced particle size shortens the diffusion path required for the reaction of copper oxide to proceed (Sheibani et al., 2007; Sheibani et al., 2008). The extension of MM leads both to the particle size refinement with the associate oxide formation and to the microstructural evolution with the achievement of a nanostructure. By strain induced grain refinement several process are involved: lattice distortion, crystallite refinement, formation and evolution of sub-boundaries and creation of defects such as dislocation, vacancies, twins etc. (Wang et al., 2006). By the XRD analysis is possible to evaluate each single microstructural parameter. In Figure V-23 the evolution of crystallite size and lattice strain for all the milled copper powder have been calculated both for continuous and interrupted cycle.

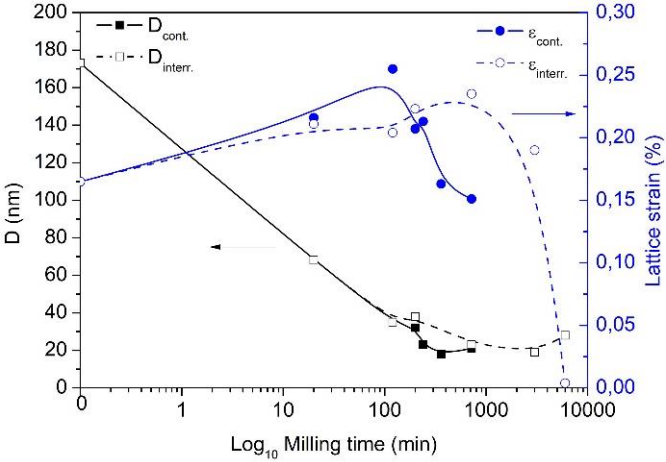

Figure V - 23. Evolution of crystallite size and lattice strain as function of milling time for powder milled by continuous and interrupted cycle.

Over all, the variation of crystallite size and strain with milling time of the interrupted and continuous cycle follows a similar trend for both the cycles. A prolonged MM leads to a drastic decrease of crystalline size down to 20 nm independently of the type of cycle. The decreasing crystallite size is due to formation of new defects such as dislocations that can appear in different ways: formation of highly dense regions of dislocations inside the parent grains, pile up at the grain boundaries or untidy clusters into the grain. All these phenomena lead to the formation of sub-grain structures, therefore decreasing the effective crystallite size (Khayati et al., 2013). At the same time an initial increase of lattice strain followed by a drastically decrease has been attested for both type of milling cycle. This is unusual for milled powder, which usually show a continuous increase of lattice strain (Suryanarayana, 2001; Xiao et al., 2008). Both type of cycle show a decrease of lattice strain prolonging milling time. The interrupted cycle seems to show some delay of the microstructure evolution because the lattice strain curve is shifted at longer milling time. The addition of a cooling pause plausibly slows down the milling kinetic and therefore the microstructural evolution as well. By the value of crystallite size and lattice strain it was possible to calculate the dislocation density introduced by MM according to equation 4.2 as well as the value of the cell parameter by the software MAUD (Fig.V-24).

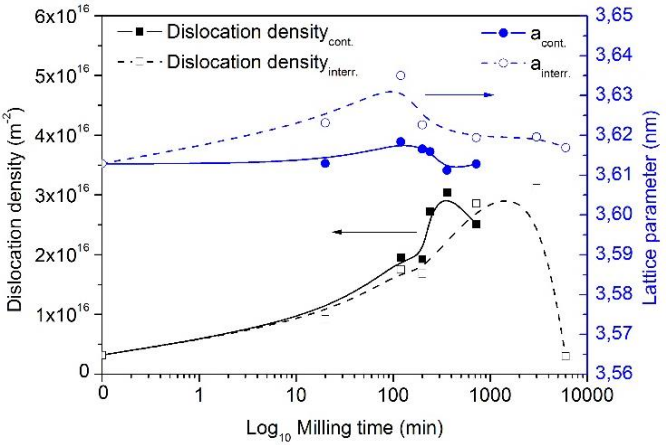

Figure V - 24. Dislocation density and lattice parameter as function of milling time for powder milled by continuous and interrupted cycle.

As the energy is continuously input into the powder the dislocation density increases with the milling time and then decrease in correspondence of the longest milling times (MM-720' and MMi-6000'), independently of the type of cycle. By the way the higher drop of dislocation density is measured for MMi-6000'. During the milling process, part of the mechanical energy transforms into enthalpy in the form of dislocation, defect, etc. stored in the milled powders. The increasing dislocation

density may cause the dislocation–dislocation, dislocation–twin interaction, which can result into formation of highly dense immobile dislocation and blocked dislocation in local region, such as grain and twin boundaries. The internal strain in these regions is higher than in the surrounding environment, where crack can easily form and grow, consequently causes particles to be broken into debris. After 6000 minutes a drop of dislocation density is reported. It has been suggested that the final grain size achievable by MM of pure metals is determined by the minimum grain size that can sustain a dislocation pile-up within a grain and by the rate of recovery during MM process (Marques et al., 2007; Khoshkhoo et al., 2014). The latter one can be partially responsible for the drop of dislocation density by increasing milling time (Khoshkhoo et al., 2014).

In addition to dynamic recovery an important role is played by the dissolved oxygen which can be present in the copper matrix as interstitial and as substitutional element (Botcharova et al., 2003). Unfortunately the oxygen content measured by LECO is affected by the amount of oxygen present on the powder surface, so actual oxygen dissolved in the copper matrix is unknown. By the way in literature it has been proved that oxygen content dissolved in the matrix increases prolonging milling time (Botcharova et al., 2003; Gomez et al., 2006; Raghu et al., 2001). The effect of the increasing oxygen in the powder is demonstrable analysing other parameters which are affected by it. Botcharova et al. demonstrated the dependence of copper lattice parameter on milling time and consequently on the oxygen content (Botcharova et al., 2003). In this sense the curve of lattice parameter vs. milling time in Figure V-24 is in accordance with what expected (Botcharova et al., 2003).

At the beginning of milling, lattice parameter increases to a maximum of 3.636nm, on further milling a decrease of it is observed. The dependence of the lattice parameter can be explained by the dissolution of oxygen, which can be assumed to take place by interstitial mechanism firstly and by a substitutional mechanism finally (Botcharova et al., 2003; Khitouni et al., 2009). Since lattice parameter increases only a limited amount of oxygen atoms may be dissolved on interstitial site of copper lattice because of their limited number. By the way as mentioned by Prasad et al., the interstitial oxygen atoms have a strong binding to both screw and edge dislocations in view of their asymmetric elastic distortions which cause a strong Cottrell locking (Prasad et al., 2004). Oxygen atoms take positions along the core of dislocations and clog the migration of vacancies along the dislocation pipe. It is sufficient that interstitials migrate to dislocation jogs and lock them to prevent dislocation core diffusion. For this reason dislocation density increases with milling time. Further oxygen atoms have to occupy lattice sites according to the substitutional mechanism no more interstitial ones. This would lead to a strong decrease of lattice parameter due to the larger difference in the atomic radii (atomic radius of oxygen being substantially smaller than that of copper). By the way dislocation density continues to increase due to the strong strain hardening. When the grain size reaches a saturation value, further

milling will not produce more dislocations due to the difficulty of generating dislocations at small grain sizes, and in fact the slope of dislocation density slightly decreases between MMi-720' and MMi-3000' (Fig. V-24). After 6000 minutes of milling once oxygen level exceeds the solubility limit the formation of copper oxide cluster occurs (Fig. V-22). This leads to a further decrease of lattice parameter. The interstitial oxygen atoms diffuse out from the face-centred cubic lattice to form copper oxide and their Cottrell locking action terms. At this point the dislocation density decreases drastically and existing dislocations will be rearranged and some will be annihilated. This microstructural evolution is very interesting because rarely reported in literature and deserves further detailed study.

Among all the powder milled by interrupted cycle the most suitable for sintering is MMi-6000' according to the dimensional and morphological requirements. In the next section a comparison between MM-720' and MMi-6000' during SPS has been developed.

5.3.2.2 Effect of nanoparticle size and oxide during SPS

From a thermodynamics perspective, nanocrystalline constituents have to be thought of as bulk grains with a significant fraction of grain boundaries. The grain boundaries, being non-equilibrium entities, provide a large driving force for grain coarsening during sintering, owing to their mobility (Sharma et al., 2011). Therefore MMi-6000', due to its nanostructure should be more favourable for sintering in comparison with coarse MM-720'. Moreover MMi-6000' is characterized by a very fine particle size which is supposed to enhance densification (Diouf et al. 2012 [1]; Pellizzari et al., 2011 [1]). In order to evaluate the effects of particle size and of oxide on the sintering behaviour, MM-720' and MMi-6000' have been compared. In Figure V-25 the displacement and its derivative for both powders are reported. As SPS cycle has been kept the initial cycle with the application of sintering pressure at 700°C (Fig. V-10) since MMi-6000' particle size is supposed to be more suitable for the decomposition of stearic acid.

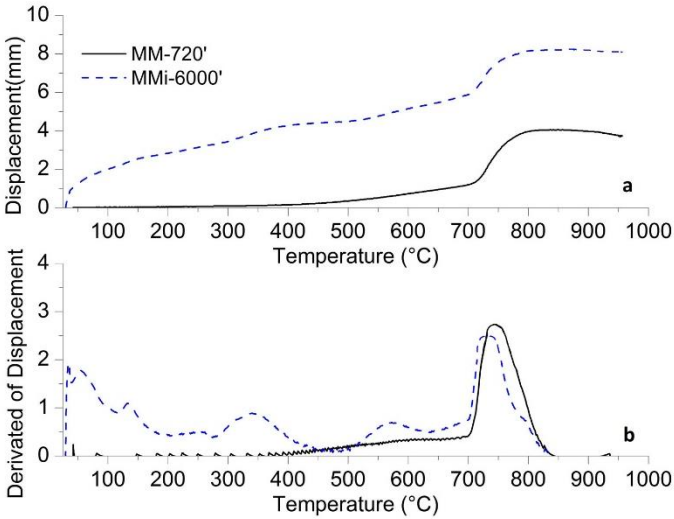

Figure V - 25. Displacement and displacement rate of MM-720' and MMi-6000'.

Figure V-25 highlights the different sintering behaviour of MM-720' and MMi-6000'. MMi-6000' shows a higher displacement since the beginning of SPS cycle, due to the intense powder rearrangement (Fig.V-25a). In general, rearrangement occurs through the relative movements of the particles and it is negatively affected by the interparticle friction at the contact point, which increases by decreasing particle size (Diouf et al., 2013). Even if MMi-6000' is characterized by a smaller particle size and therefore to a higher number of contact points, the displacement curve is higher than MM-720' (Fig.V-25a). A possible explanation can be found looking at the displacement rate curves (Fig.V-25b). The displacement rate shows different peaks, due to the fact that powder rearrangement is not continuous, but it sensibly depends on the powder agglomeration and instantaneous movement of the batch of powder along the punch stroke. Nanoparticles create easy agglomerates that initially prevent the rearrangement by a high friction at the contact points, but by the application of a limited pressure (3MPa) the agglomerates can be destructed and rearrangement occurs. On the other side the large particle size of MM-720 should lead to a higher rearrangement due to the lesser number of contact points. By the way the low intrinsic packing density of coarse particles prevents their rearrangement and displacement is limited (Fig.V-25a). Once the load is applied at 700°C the bulk densification begins and finishes with the attainment of a constant displacement and a displacement rate equal to zero for both powders. This confirms the complete densification of the powders.

The microstructure of MMi-6000' looks very fine, homogeneous without any evident porosity (Fig.V-26). In comparison with MM-720 (Fig.V-14) no copper recrystallized areas are visible, meaning that overheating did not occur as

consequence of the small particle size (Diouf et al., 2012 [1]). Therefore the densification is not aided by the presence of skin melted Cu particles leading to faster diffusion of atoms to neck region, (Sharma et al., 2011). By the way it is known that a nanocrystalline particles have a significant volume fraction of grain boundaries, which provide faster diffusion paths for mass transport.

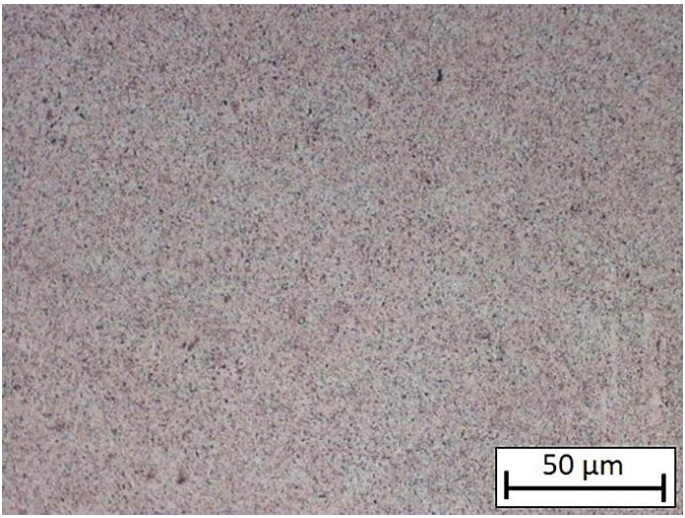

Figure V - 26. OM micrograph of MMi-6000' microstructure.

The retention of the finer crystallite size of Cu will also cause an improved sintering kinetics due to the higher sintering force. According to Herring's scaling law, the sintering time follows a direct power law relationship with particle size. The finer the particle size, the faster the grain boundary diffusion induced mass transport to neck region. An additional contribution to enhance mass transport can be ascribed to short circuit diffusion, due to the presence of a large number of line defects, (Sharma et al., 2011). At this point a higher density of MMi-6000' was expected, by the way as reported in Table V-5 relative density is very low (~80%).

Table V - 5. Properties of MMi-6000'.

Sample	Rel.Density	C_{powder}	C_{SPS}	O_{powder}	O_{SPS}	HB5
	%					
MMi-6000'	80.3	0.401	0.346	3.561	0.609	40

This result seems incomprehensible, especially looking at the microstructure, but by further analyses two main causes have been found to be responsible of the poor densification of MMi-6000': the first one is the significant presence of oxide in the milled powder, and the second one is the powder morphology.

The sintering mechanism occurring during SPS of ultrafine-grained copper have been described by Zhaohui et al. (2008) who has proposed a sequence of four stages: (1) activation and refining of the powder; (2) formation of the sintering neck; (3) growth of the sintering neck and (4) plastic deformation. The first two stages are promoted by the spark discharge; the growth of the neck and plastic deformation are promoted by the Joule effect and the mechanical load. Joule heating is related to materials electrical resistance, which is closely associated to the particle–particle contacts. Electrical resistance is also affected by the presence of an oxide layer on the powder surfaces, particularly in the early stages of sintering when the formation of necks is occurring. To explain the sintering mechanisms during the early stages of sintering, the behaviour of oxide layers under the influence of temperature and electric field must be considered. For this purpose the resistance versus temperature curve of MM-720' and MMi-6000' during SPS are reported in Figure V-27.

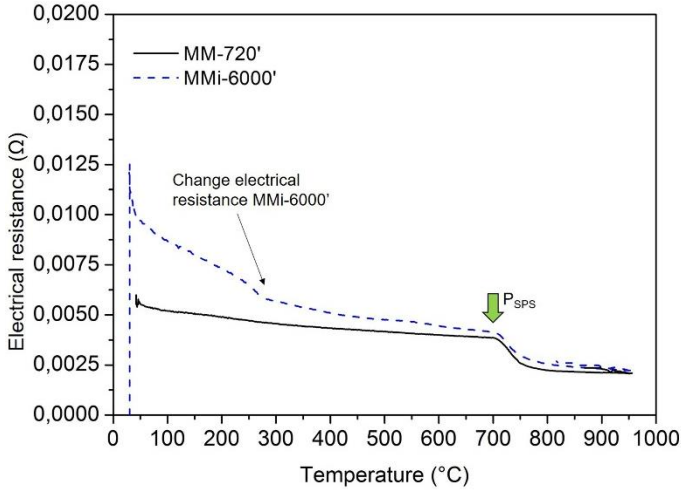

Figure V - 27. Electrical resistance versus Temperature curves of MM-720' and MMi-6000' during SPS.

From Figure V-27 the different behaviour of the two materials during SPS is evident, by the way in both cases the electrical resistance decreases increasing the temperature. Before the application of the sintering load at 700°C, MMi-6000' shows a higher electrical resistance than MM-720'. Then the electrical resistance of MMi-6000' sharply decrease and it is almost the same value for both the materials once the

pressure is applied. The different value of electrical resistance at the beginning of SPS is associable to the particle size of the milled powders and to the presence of copper oxide. It has been demonstrated that comparing powders having different diameters, the contact points between the powders increase decreasing particle size and on contrary the total contact area decreases (Diouf et al., 2012 [1], Diouf et al., 2012 [2]). By the relation between contact area and resistance (R=ρh/S), a decrease of particle size leads to an increase of resistance. Therefore a higher resistance value is expected for nanocrystalline MMi-6000' particles; since resistance is inversely proportional to the contact area (Diouf et al., 2012; Sharma et al., 2011). The results shown in Figure V.27 are in perfect accordance with what expected. At the same time the continuous decrease of electrical resistance for both materials is associate to the increase of the contact area between the particles. When the load is applied, it further promotes the contact between the particle, and a drastic decrease of electrical resistance is evident (Fig. V-27). MM-720 shows a linear trend of the electrical resistance till the application of the load at 700°C, instead the electrical resistance of MMi-6000' shows a change of the slope at around 250°C. This phenomenon is strictly related to the presence of oxide which affects the electrical properties of the material during SPS. The electrical conductivity transition in granular materials depends on the statistical distribution of the shape and size of the particles, the applied force, and the local properties at the contacting zone between particles, i.e. degree of oxidization, surface state and roughness. By the representation of current-voltage and temperature-current curves (Fig.V-28a-b) it is possible to highlight the three main phenomena occurring during SPS: i) Ohmic linear behaviour, ii) non Ohmic behaviour and iii) destabilization of the current/voltage curve once the pressure is applied. The first phenomenon is an Ohmic linear behaviour without any significant change in temperature (Fig. V-28b). This insulating behaviour is attributed to the presence of copper oxide. Up to this point, the current was also flowing through the oxide-oxide path, other than through the die walls. The copper oxide has much higher resistivity (20Ohm m) as compared to copper (1.58×10^{-8} Ohm m), and this obstructs the flow of current (Sharma et al., 2011). The different current values observed up to the breakdown point into the compact MMi-6000' and MM-720' are in line with the different oxidation states of the two powders. The current measured in sample MMi-6000' is lower than that in MM-720, confirming a much higher surface oxidation in the first powder. This is in agreement with the X-ray analysis, which showed 21vol% of copper oxide in MMi-6000', while no oxides (or at least higher than the sensitivity of XRD apparatus ~3%) were detected in powder MM-720'. Moreover up to the breakdown it is evident that the current increase in the MM-720' specimen is more pronounced than in MMi-6000'. Probably also the severe and prolonged strain hardening induce by MM in MMi-6000' negatively affect the electrical resistance increasing the gap between the electrical resistance of the two materials.

Going forward SPS cycle, an instability of the current-voltage curve is observed at around 2V in Figure V-28a and a change in the temperature-current curve is observed both for MM-720' and MMi-6000' (Fig.V-28b).

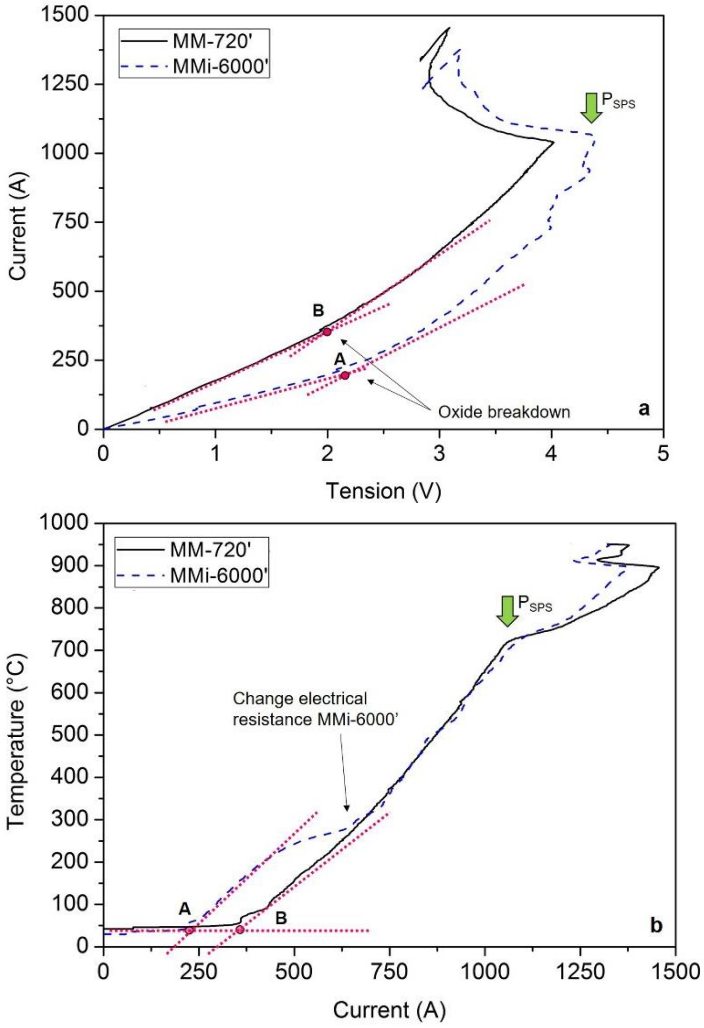

Figure V - 28. (a) Current-voltage curves, (b) Temperature-current curves of MM-720' and MMi-6000' during SPS.

The change of slope of current curve indicates the breakdown of the oxide, since the electrical resistance depends on the material properties (resistivity and

thickness) at the contact location. After this breakdown current flows more through the metallic particles, heating up the material, as confirmed by the temperature jump in Figure V-28b. Above this threshold, temperature increases and MM-720' curves (current-voltage and temperature-current) have a stable behaviour. MMi-6000' shows a more unstable behaviour up to 300°C, temperature at which a drastic change of the electrical resistance occurs (Fig. V-27).

The third effect consisting in the destabilization of the current/voltage curve occurs at 700°C, when the pressure is applied. This event causes a destabilization in the voltage/current curve and decreases the heating efficiency confirmed by the decrease of the slope of the temperature-current curve. By the application of the pressure a sharp increase of the contacting area occurs and electrical resistance decreases as highlighted in Figure V-27. At this point it can be deduced that the poor densification of MMi-6000' is obstructed by the high electrical resistance due to the mutual contribution of the small particle size and the presence of copper oxide acting as a surface diffusion barrier. In addition the fine particle size hinder the favourable occurrence of overheating, in fact no recrystallized regions are visible at the contact region in MMi-6000' microstructure (Fig. V-26).

Another reason for the poor densification of MMi-6000' is the incomplete decomposition of stearic acid during SPS although the finer particle size in comparison with MM-720'. Even if the smaller particle size was supposed to facilitate the decomposition of stearic acid during SPS, the amount of carbon after SPS still high in MMi-6000', only 13.5% has been decomposed (Tab V-5). The QMS analysis of MMi-6000' powder is reported in Figure V-29.

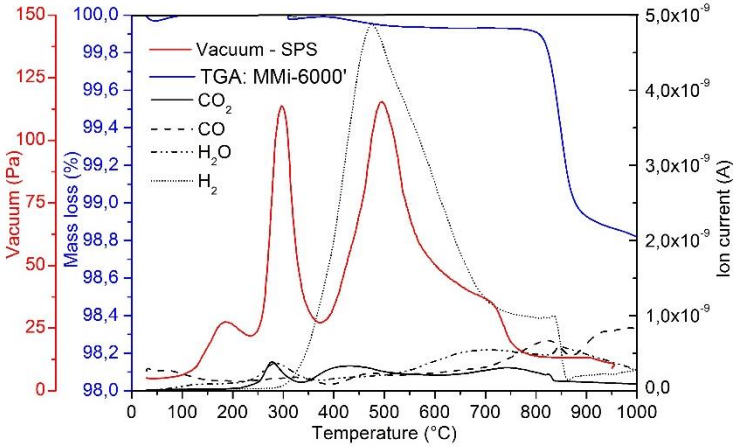

Figure V - 29. TGA and QMS of MMi-6000' powder and vacuum trend during SPS.

The decomposition of PCA occurs in two steps: firstly by the emission of CO_2 and H_2 at 350°C and 500°C respectively, then at 800 and 950°C two peaks of CO have been recorded with a drastic mass loss in TGA curve (blue solid line). The latter ones are responsible of the residual porosity in the sintered material as in the case of MM-720' (Fig.V-16b). This affects considerably the densification process, and as confirmed by the vacuum trend (red solid line) no change in pressure is recorded at 950°C, since the SPS pressure has been applied at 700°C vanishing any possible gas emission. By these results is clear that also MMi-6000' powder is not suitable for sintering leading to a high residual porosity (TabV-5). The SEM micrographs reported in Figure V-30b shows a quite irregular particles morphology for MMi-6000. Although this sample was looking as uniform and regular particles (Fig.V-30a), actually these consists in very small and compact agglomerations of very thin flake like particles.

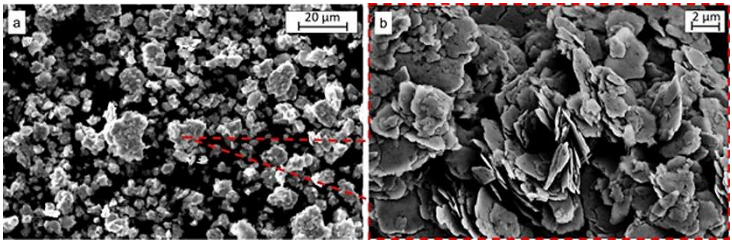

Figure V - 30. SEM micrographs of MMi-6000' powder at high resolution.

This powder morphology complicates the densification of the powders during sintering leading to a higher residual porosity. Moreover stearic acid is entrapped in the agglomerated particle delaying its decomposition process and increasing the internal porosity. In addition it may be easily appreciated that it is very difficult to pack irregular particle in a dense manner, and the presence of agglomerates makes the sintering process even more difficult (Bouvard et el., 2000; Shukla et al., 2013). Finally the oxygen absorption at powder surface leads to the formation of thermally unstable compounds. Whose decomposition during SPS releases gaseous species that cause the formation of pores (Wen et al., 2010). Although the invisible large porosity in Figure V-26 a residual nano-porosity could be confirmed by TEM (Fig.V-31a-b). The micrographs evidence a consistent amount of nano pores, located mainly at the grain boundaries. Also clearly evident it is the pinning effect exerted by these pores, as the grain size is much lower in the area where pores are visible at the grain boundaries (Diouf et al., 2013; Zhang Z.H. et al., 2008). Generally, these pores are very fine (< 100 nm), but some larger ones (> 100 nm) were also observed. A similar effect was observed by Zhang et al., (Zhang Z.H. et al., 2008).

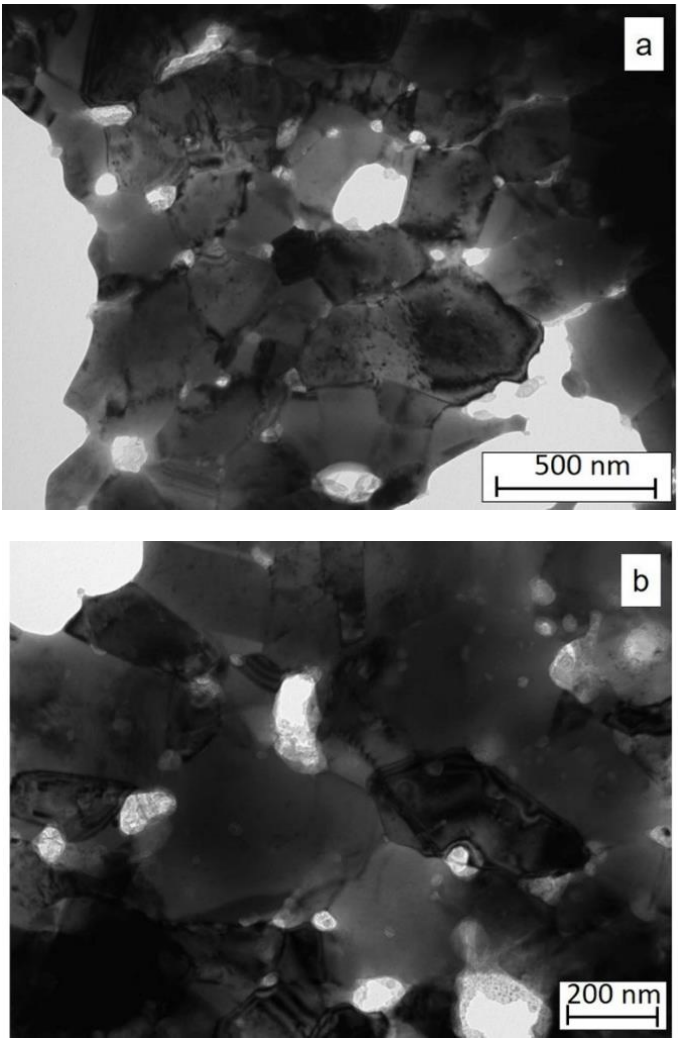

Figure VI-31. TEM micrographs of MMi-6000' sintered sample.

The average grain size measured for sintered MMi-6000' samples by XRD is in the range of 80nm. The XRD analysis confirms the limitation of grain coarsening by SPS. It is widely recognized that a major difficulty in synthesis of nanostructured materials is the grain growth during sintering. The use of ''activated'' sintering, involving a combination of lower temperature and shorter time, makes it possible to obtain a bulk nanocomposite; in particular, the advent of field assisted sintering

techniques, e.g. , SPS has the advantage in fabrication of bulk nanocomposite. As indicated earlier, SPS involves the application of pulsed electrical direct current in combination with resistance heating to achieve a high heating rate, so that grain coarsening can be minimized. Because of the high heating rate, the final sintering temperatures can be reached in less time. This has the advantageous implication of suppressing the low-temperature densifying mechanism (such as surface diffusion); hence, grain coarsening/growth can be limited within the nano-crystalline regime, (Sharma et al., 2011). If on one side the limited grain grow leads to improved mechanical properties on the other side residual porosity could be detrimental. Obviously the presence of high residual porosity affects the mechanical properties of the sintered material, as will be explain and shown in chapter VII. Meanwhile in Table V-5 the value of Brinell hardness of MMi-6000' is reported and is equal to 40HB. Although the prolonged milling process the mechanical strengthening of the powder is ineffective leading to a very low hardness. This result is in conflict with what expected because an intense and prolonged MM usually leads to a severe plastic deformation, an intense introduction of defects and therefore to a strain hardening of the final product. Moreover also the density decrease prolonging milling time and this could be very detrimental for the mechanical properties of the components (Fig-V-32). At this point is clear how prolonging milling time is worthless both for enhancing mechanical properties and for the densification behaviour during SPS process. By this results the improvement of mechanical hardening of copper has been promoted by the addition of a second phase during MM, as will be explain and analysed in the next chapter.

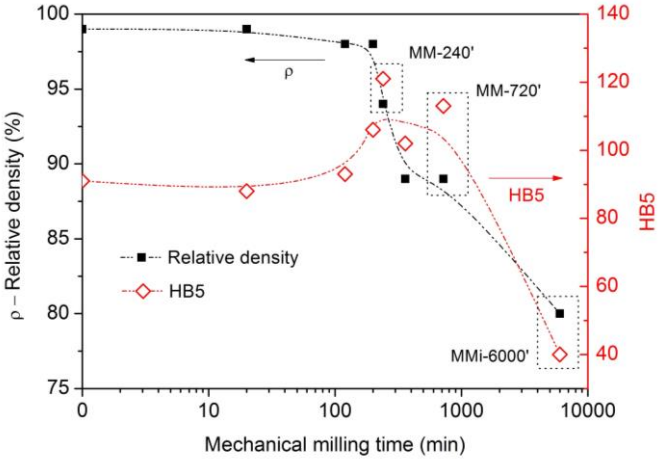

Figure V – 32. Relative density and hardness as function of the mechanical milling time.

5.3.3 Modification of MM parameters and SPS cycle

Before describe the MA cycle an ultimate development and understanding of the SPS cycle of MM copper has been carried out in the last part of my PhD program, and the promising results are reported in this section. By previous sections is clear how the two solutions (5.3.1 and 5.3.2) are not beneficial for the densification of milled copper powder. In this section the densification of copper powder is enhanced coupling the optimized particle size of interrupted cycle, i.e. MMi-6000' (5.3.2) and the optimized SPS cycle with the application of the pressure at 950°C instead 700°C (5.3.1). An advanced improvement has been made looking at Figure V-16 and V-29, in which the vacuum peaks are shifted toward higher temperature if compared to the QMS peaks. This is related to the different heating rate, 100°C/min during SPS and 20°C/min during QMS. Therefore in order to have the peaks detected by QMS between 800 and 950C° during SPS, the heating rate must be decreased. For this reason the heating rate has been maintained 100°C/min up to 700°C and then decreased down to 20°C/min up to the sintering and loading temperature of 950°C. The vacuum trend during SPS and the QMS curves are reported in Figure V-33. Very interesting and satisfying results have been obtained, the expected peaks at 800°C and 900°C have been detect by the vacuum trend during SPS. This means that the correct decomposition of stearic acid finally occurred as confirmed by the relative density measurements and the level of carbon before and after SPS, reported in Table V-6.

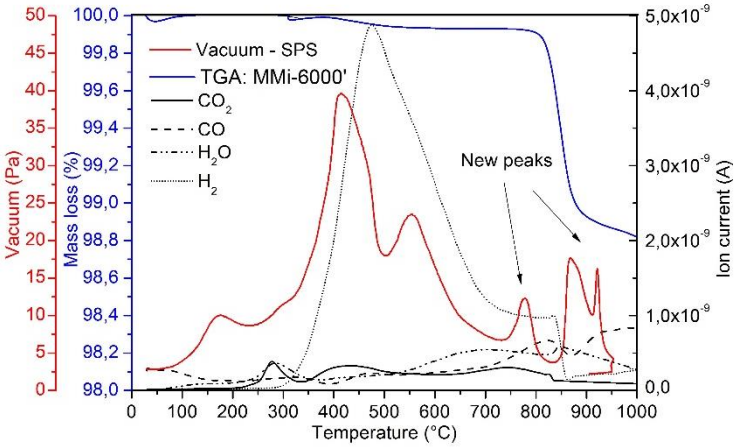

Figure V - 33. TGA and QMS of MMi-6000' powder and vacuum trend during SPS with a heating rate of 20°C/min.

Table V - 6. Properties of MMi-6000' sintered with a heating rate of 20°C/min.

Sample	Rel.Density	C_{powder}	C_{SPS}
	%		
MMi-6000'_100°C/min	80	0.40	**0.35**
MMi-6000'_20°C/min	90	0.40	**0.06**

The level of carbon is drastically decreased from 0.4% to 0.06% after SPS, and a 10% of relative density has been gained. The increase of density may be attributed to two mutual effects: the correct decomposition of the PCA attested by the presence of the peak between 800 and 900°C, and the prolonged sintering time due to the lower heating rate. It is widely diffuse to carry out an annealing treatment at around 500°C on the powder before sintering in order to allow the proper decomposition of PCA. By the way sometime the annealing leads to an unwanted grain growth. Moreover in this specific case, where the decomposition of PCA is complete at higher temperature than 500°C, the use of an annealing treatment could be useless and in some case even detrimental. The proper optimization of the SPS carried out in this section could be considered a suitable alternative. By the way before to affirm the complete success of this solution, XRD analysis must be carried out in order to evaluate the effect of a prolonged SPS cycle on the grain size. Unfortunately this promising result leads the last part of the PhD period, therefore a proper characterization of the sintered sample has not been possible to carry out. For this reason in chapter VII the characterization of the mechanical properties and of the wear behaviour have been conducted on MMi-6000' sintered in section 5.3.2.

5.4 Conclusions

In this chapter MM of copper powder has been deeply analysed.

- Firstly the best MM parameters have been found to limit the contamination level arising from the grinding media, than the effect of milling time has been studied by the evolution of the particle size, morphology and microstructure of the milled powder. In the case of continuous cycle a predominance of welding events has been demonstrate prolonging milling time, instead by the use of a interrupted cycle the powder undergoes to the typical MM behaviour of ductile materials: flattening, welding and finally fracturing.
- The particle size and morphology affect significantly the densification behaviour during SPS. On one side large particle size limits the correct decomposition of PCA during SPS even by the application of the pressure at high temperature. On the other side fine particle size leads to the presence of oxide which hinders the densification due to its high electrical resistance. Moreover, even in the case of a

finer particle size, the densification can be limited if the decomposition of PCA is not properly designed.

- Several attempts have been made in order to increase the final density and successful results have been obtained by the application of the SPS pressure at 950°C instead 700°C and by the use of a slower heating rate, 20°C/min instead 100°C/min. This allows the proper decomposition of PCA during SPS and limits the residual porosity.
- Despite the complete understanding of the processes occurring during MM and SPS of copper powder, materials show a sharp decrease of hardness and density increasing milling time. At this point is clear how prolonging milling time is worthless both for enhancing mechanical properties and for the densification behaviour during SPS process.

From this chapter three main milling times have been selected according to the size and morphology of the powders after MM: MM-240' (flaking), MM-720' (welding) and MMi-6000' (fracturing). The selection has been made in order to evaluate the thermal conductivity, the wear behaviour and the mechanical properties as function of the level of strain hardened induced by MM and compare them with the mechanical alloyed sample produced in next chapter.

Chapter VI

Mechanical Alloying of Copper and TiB_2

Part of this chapter has been published in:

G. Cipolloni, M. Pellizzari, A. Molinari
"Tribological behavior of TiB_2 reinforced Cu-matrix composites produced by mechanical alloying and spark plasma sintering"
Proc. Of the 2015 European Powder Metallurgy Congress & Exhibition
4-7 October, Reims, France

G.Cipolloni, M.Pellizzari, A.Molinari, B.T.Cao
"Produzione e caratterizzazione di compositi a matrice in Cu rinforzati con particelle di TiB_2"
Proc. Del 35° Convegno Nazionale della Associazione Metallurgia Italiana
5-7 November 2014, Roma, Italia

6.1 Effect of milling time on MA behavior

6.1.1 Selection of the MMC as function of milling time

The first requirement for a composite material to fully exploit its superior performance is the homogeneous distribution of the reinforcement. High energy ball milling has been successfully used to improve particle distribution throughout the matrix and for this reason MA process of Cu and 0.5wt%TiB_2 have been deeply studied in this chapter.

Figure VI-1 shows the variation of MMC's powder morphologies as a function of milling duration, ranging from 5 to 240 minutes. MA was conducted using the milling parameters in chapter V: 0.5wt% of stearic acid as PCA, a BPR equal to 10:1 and milling cycle conducted in continuous. During milling, the powder mixtures are subjected to high-energy collisions, which would result in the occurrence of micro-forging, fracture or agglomeration phenomena in composite powders. The specific

morphology is dependent on the dominant mechanism. For short milling time (5 to 20 minutes), micro-forging is evident, leading to changes in particle shape without significant cold welding. After 5 and 10 minutes of milling some intact as-atomized powder particles are still present. The particle morphology appears mainly equiaxed up to 10 minutes even if some flake particles are present. A very evident flattening occurs after 20 minutes, when the plastic deformation of the Cu powder governs the alloying process (Fig. VI-1a-c).

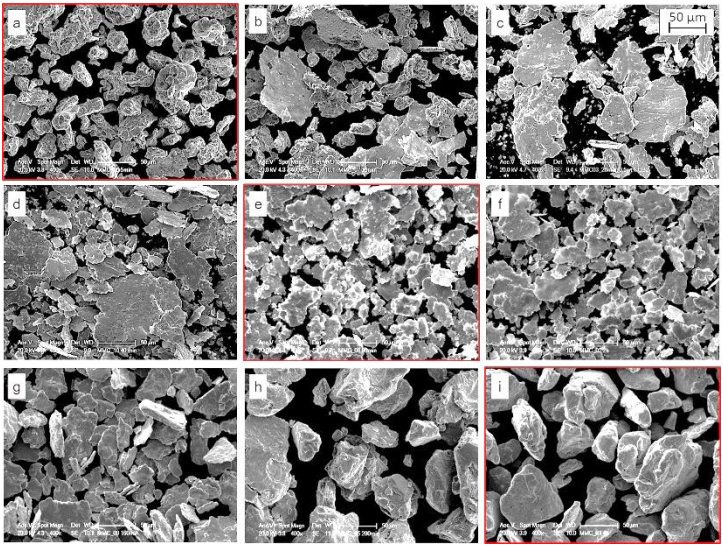

Figure VI - 1. SEM micrographs of MMC powders as function of milling time: a) MMC-5', b) MMC-10', c) MMC-20', d) MMC-40', e) MMC-80', f) MMC-120', g) MMC-160', h) MMC-200' and i) MMC-240'.

These morphologies derive from the high ductility of Cu under repeated collisions caused either by milling medium or the reinforcement. By increasing milling duration, from 20 up to 120 minutes, the powders are progressively plastically deformed and their morphology turns gradually into thinner flakes (Fig.VI-1c-f) (Sahani et al., 2011, Maurice et al., 1994). In addition, since powder particles undergo increasing strain hardening, their fracture is activated resulting in a finer particle size (Fig. VI-1e-f). After prolonged milling (160 to 240 minutes), as a result of cold welding, the particles show a marked increase in size and their morphology became again more equiaxed (Shukla et al., 2013). Cross sectional views reported in Figure VI-2 clearly show that flake-like particles pile-up, according to a well-known mechanism reported by several authors and also shown in the previous chapter (Fogagnolo et al., 2003; Suryanarayana, 2001, Maurice et al., 1994). The use of a continuous cycle leads to a

drastic increase of the temperature inside the vial inducing the predominance of welding events over fracture ones. From Figure VI-2h and Figure VI-2i it is evident how during MA the edges of the particle become smoother increasing milling time due to the intense compacting action of the milling medium.

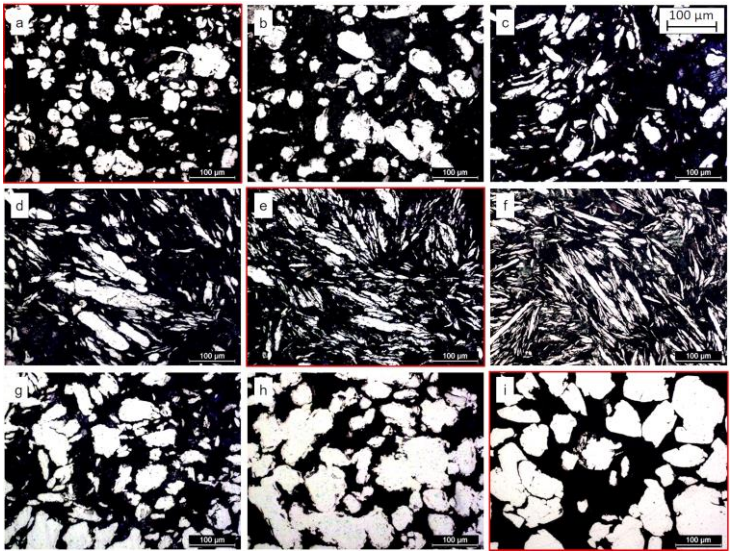

Figure VI - 2. OM micrographs of MMC powders as function of milling time: a) MMC-5', b) MMC-10', c) MMC-20', d) MMC-40', e) MMC-80', f) MMC-120', g) MMC-160', h) MMC-200' and i) MMC-240'.

The particle size distributions and the cumulative distribution curves of powders milled for different times are reported in Figure VI-3a-b. It should be noticed that the sieving experiments could not always carried out in the most proper way, owing to a small portion of fine particles sticking on the walls of the sieving equipment. This explains why, in some cases, the cumulative curves did not reach 100% of the analyzed powders (Fig.VI-3a).

From Figure VI-3a it is evident that MA causes a general increase of particle size compared to AT-Cu (dash black line). The mean particle size value (D_{50}) increases by increasing milling time, at a markedly higher rate after 120 minutes. This can be plausibly explained by the higher temperature achieved by the system during prolonged continuous milling, due to frictional heating (Rajkovic et al., 2006). Generally, almost all milled powders exhibit the largest particle size fraction in the range 45-90µm. The two only exceptions are MMC-5' and MMC-10', which also showed a relatively higher fraction of particles in the range 25-45µm. The distribution changed by varying the milling time. After short milling duration, namely up to 120

minutes, the powders show a narrow distribution. This suggests that for short milling duration, since plastic deformation and fracturing actions are predominant over cold welding, the milled powders did not show any significant change in size.

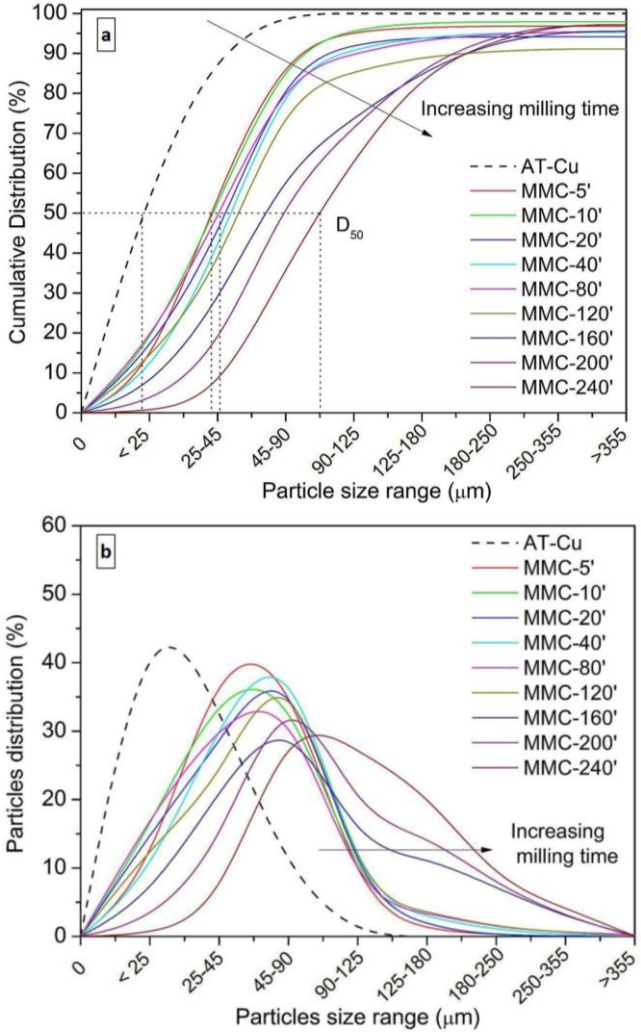

Figure VI - 3. Cumulative distribution (a) and particles distribution (b) of MMC powder as function of milling time.

For longer milling duration (160, 200 and 240 minutes), the powders show two distinct effects: firstly a broadening of size distribution highlighting a bimodal distribution, then a clear shift of the curves towards larger particle size. The largest particles fraction (90-125 μm), which gives rise to the main distribution peak, shifts towards bigger sizes, if compared to the powders milled for shorter time (45-90μm). Moreover, for the last three milling time more than 10% of particles, having sizes bigger than 180μm, give rise to a second peak. In this chapter in order to give a clear and complete explanation of the different phenomena occurring during MA and sintering three representative samples have been selected according to the particle size and morphology, namely MMC-5', MMC-80' and MMC-240' (micrographs highlighted by red borders in Figure VI-1 and Figure VI-2). In Figure VI-4 the three selected milled powders of MMC-5', MMC-80' and MMC-240' are reported and their particles size distribution as well.

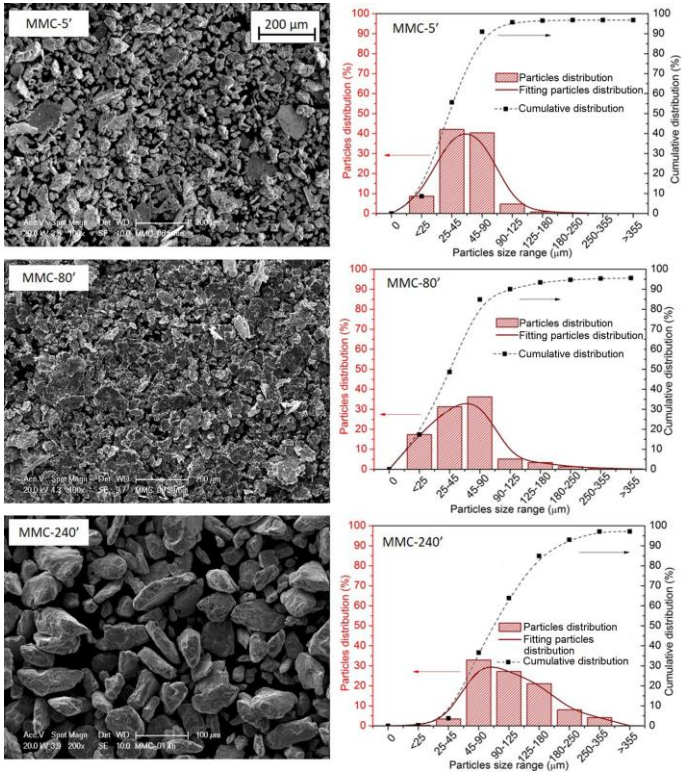

Figure VI - 4. Selected MMCs powders with their cumulative and fraction particles distribution as function of milling time.

The distribution of TiB_2 particles in MMC-5', MMC-80' and MMC-240' can be evaluated by Figures VI-5-6-7, respectively. After short milling durations (MMC-5'), TiB_2 particles are not homogeneously dispersed within Cu particles, as confirmed by a large fraction of free TiB_2 particles between Cu particles. At the milling stage, collisions with milling medium promote deformation of Cu powders, but modest refinement only of TiB_2 and poor alloying with Cu matrix. Moreover the adhesion between reinforcement and matrix is not adequate as demonstrated by the presence of voids between the two constituents (Fig. VI-5).

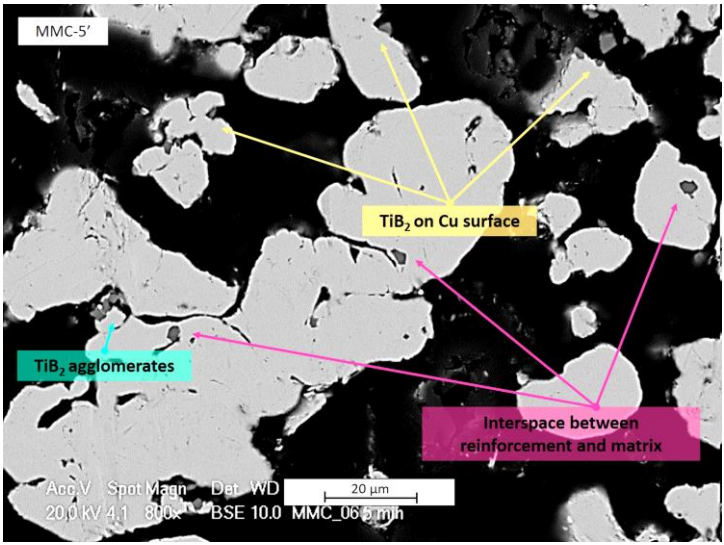

Figure VI - 5. SEM micrograph of powder cross section of MMC-5'.

When longer milling durations are employed (MMC-80'), the larger plastic deformation led to the formation of layered structures. The proceeding of MA process is clear, a continuous overlapping of flake like particle is enhanced by the impact events with the grinding medium (Fogagnolo et al., 2003; Rajkovic et al., 2006 [1]). This aids the dispersion of TiB_2 within the matrix especially at particle boundaries or few microns below the surface. From Figure VI-6 is clear that the welding of flakes promotes the formation of agglomerates. Some particles area look already compact due to accelerate welding phenomena and a severe plastic deformation of the particle core which proceeds toward the surface prolonging MA (Maurice et al., 1994). Moreover not only welding events occur between singular flakes, but also between already formed MMC aggregates, as highlighted by red arrows in Figure VI-6 leading to a larger particle size. The high and prolonged energy impact enhances the formation

of bigger agglomerates by aggregation of small particles. TiB_2 looks better dispersed than in MMC-5' being not only found at particle surface but also in subsurface area. Although a higher amount of reinforcement becomes better incorporated in the Cu matrix in comparison with MMC-5', the alloy powders was still inhomogeneous and for this reason MA has been prolonged up to 240 minutes (Fig.VI-7).

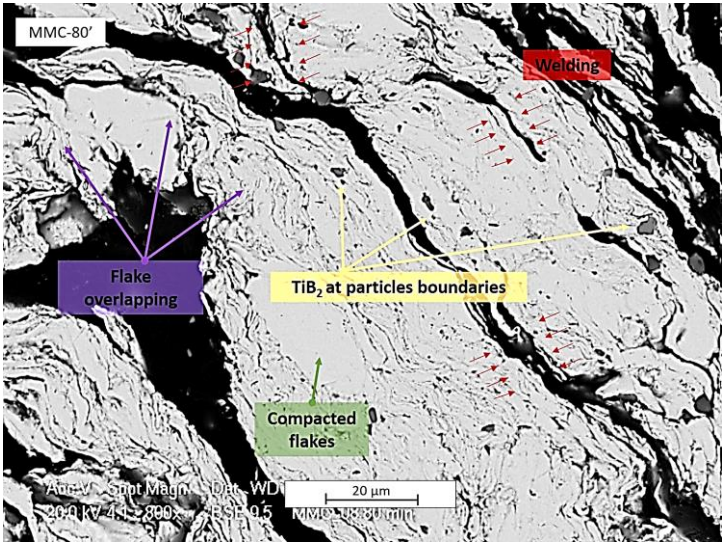

Figure VI - 6. SEM micrograph of powder cross section of MMC-80'.

By further increasing milling time up to 240 minutes, very few individual TiB_2 particles which have not been alloyed with Cu are presented, while most hard particles are incorporated within the Cu matrix giving very homogeneous composite powders (Fig.VI-7) (Fogagnolo et al., 2003). Although the large particles size of copper powder, a refinement of TiB_2 is evident and this guarantees a more uniform and homogenous microstructure. The microstructure of particles after milling for 240 minutes evidences a well distribution of TiB_2. The good bonding between matrix and reinforcement is now evident and MA can be considered completed. In this regard, welding traces between flakes almost disappear and just few visible crack are detected after 240 minutes. As demonstrated by Maurice et al. prolonging MA different types of crack are generated leading to different type of fracture: forging fracture, shear fracture and dynamic fracture. Cracks formed by forging fracture grow radially along the major axes of the particles. Cracks formed by shear fracture run perpendicular to the particle's minor axis. Meanwhile dynamic fracture with randomly oriented cracks occurs in high energy

mill during impacts with high collision velocity (Maurice et al., 1994). In Figure VI-7 typical cracks by shear and dynamic fracture are visible.

Comparing MM and MA it is evident that particle size and morphology of MMC-240' is similar to MM-720'. This means that milling process of MA is accelerated and welding events are anticipated. The welding process that occurs during MA is driven by cold deformation. There is a critical deformation at which higher deformation will produce welding while lower deformation will not. The presence of reinforcement particles between the particles during welding increases local deformation in the vicinity of the reinforcement. Reinforcement particles can be seen trapped in the interfacial boundaries, thus high deformation surrounds the reinforcement particle. An increase in the local deformation improves the particle welding process. The occurrence of welding events at 240 minutes for MMC-240' instead of 720 minutes for MM-720' demonstrates that MA process is completed in a shorter time, and this can be attributed to the presence of TiB_2 particles. Another possible explanation for the acceleration of MA process is that hard particles act as small milling agents, thus reducing the milling time. If the presence of reinforcement results in a higher deformation of the metallic matrix and advances the MA process, a higher reinforcement fraction will result in a still greater deformation of the metallic particles and will accelerate the process even more (Fogagnolo et al., 2003).

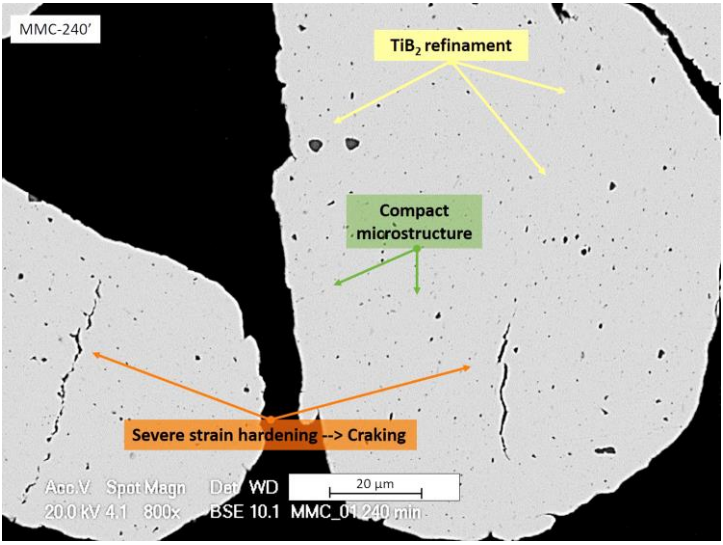

Figure VI - 7. SEM micrograph of powder cross section of MMC-240'.

By examining the effects of milling duration on morphology, size, and alloying efficiency of milled particles as well as the correlation between them, it can be

concluded that the optimum milling conditions are achieved for MMC-240'. This statement is proved in view of: (i) the equi-axed particles morphology showing high tendency towards isotropic sintered material, (ii) large-size particles exhibiting less inter-particle friction which promote the rearrangement stage of sintering, (iii) bimodal particle size distribution showing a possible achievement of high compacted density which may assist consolidation, and (iv) high mechanical alloying efficiency along with well dispersion of fine reinforcement particles. On the other side, the relatively big particle size and the intense strain hardening increasing milling time may hinder sintering, in view of the conclusion of chapter V. For this reason, in spite of the above considerations, it was decided to sinter all the nine powder batches, but in this chapter the sintering behavior of the three main milling times will be described: MMC-5' (small nodular particles), MMC-80' (flake-like particles), and MMC-240' (big nodular particles). The SPS cycle has been kept the same of paragraph 5.2.2. (Fig. V-10).

6.2 Spark plasma sintering of MMC

The influence of MA on the sintering process has been evaluated following the densification of the samples. The displacement curves of MMC-5', MMC-80' and MMC-240' and their derivate are displayed in Figure VI-8. In order to evaluate the effect of MA, AT-Cu displacement curve is reported as reference. Despite of the presence of 0.5wt%TiB_2 the trend of displacement curves during SPS of mechanical milled copper and mechanical alloyed powders is almost the same (Fig. V-11 and Fig. VI-8). As in the case of MM the explanation of the sintering process can be divided into two stages: before and after the application of the load at 700°C Figure VI-8.

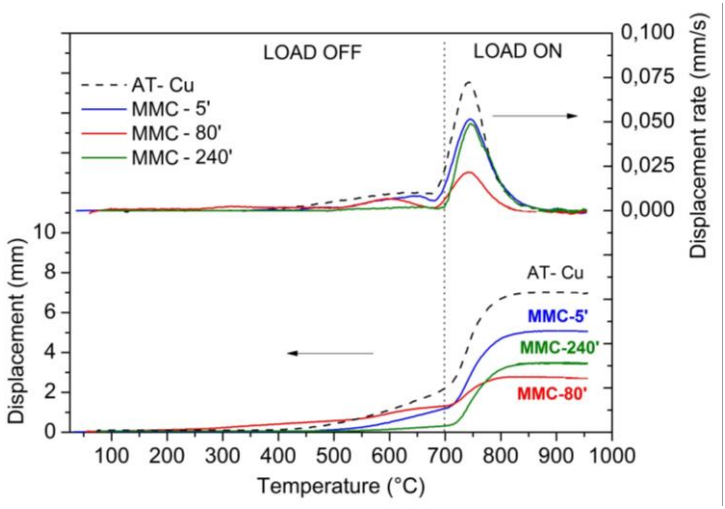

Figure VI - 8. Displacement and displacement rate curves of AT-Cu, MMC-5', MMC80' and MMC-240'.

The pressure-free regime of curves will be firstly described. Densification shows an increasing tendency with rising temperature. For AT-Cu, MMC-5' and MMC-80' powders, densification starts much before the application of pressure (700°C) and gradually increased up to the loading temperature. According to previous statement this behavior is due to particles rearrangement and it is ruled by their compressibility during the early stage of sintering. Moreover, as reported in literature, bulk deformation at about 600°C (before load application) is quite important for AT-Cu, because of its low hardness (Diouf et al., 2012 [1]). The situation is very similar for MMC-5', where the poor alloying with TiB_2, does not significantly modify the densification behavior. However, the presence of hard particles between those of Cu and on Cu particles' surfaces clearly reduces densification with respect to AT-Cu. This is evidenced by the lower displacement before and after loading. In the case of MMC-80', the displacement curve shows a gradual and progressive densification already above 200°C, i.e., at a much lower temperature than AT-Cu and MMC-5' due to mutual powder rearrangement and local deformation. Although the earlier begin of densification of MMC-80', the softest powder, i.e. AT-Cu, achieves the highest displacement in view of the highest densification rate. Increasing milling time the presence of hard TiB_2 particles in mechanical alloyed copper decreases the compressibility of the powder reducing densification rate. This effect is even more evident in MMC-240' where the finer dispersion of TiB_2 particle further impairs densification (Bouvard et al., 2000). In the case of MMC-240', densification proceeds to a very low extent only before the application of pressure, suggesting that both re-arrangement and localized deformation do not play a significant role. Rearrangement is very low, in view of the relatively high apparent density of large equi-axed composite powders compared to the flake-like ones (German, 1992). Furthermore a lower deformation is expected due to the higher strain hardening to which particles are subjected after longer milling time and due to the more efficient dispersion hardening of reinforcement particles.

The behavior in the loading regime is rather different. Once the compacting force is applied (700°C), a fast shrinkage could be observed for AT-Cu, explained by the strong bulk deformation of equi-axed soft metal particles. A slightly lower displacement is shown by MMC-5', in view of the reinforcing TiB_2 particles. A comparable displacement is shown by MMC-240', in spite of the lower compressibility of this powder. In this material the loading pressure permits the local deformation which couldn't occur under free load conditions. For this reason the displacement curve and the displacement rate curve are higher than MMC-80'. On the other side very low densification is observed for MMC-80', since it has already occurred during the load free regime. Figure VI-8 shows the displacement rate of all samples as a function of temperature. A general important observation is that in all cases the densification rate falls to zero at about 900°C, confirming that sintering temperatures higher than this value are suited to get the maximum possible density.

Relative density data of MMCs are reported in Table VI-1 as function of milling time.

Table VI – 1. MMC powder characteristics.

Sample	O_{powder}	O_{SPS}	C_{powder}	C_{SPS}	ρ	HV 0.05
	(%)					
MMC-5'	0.41	0.17	0.33	0.04	99.6	99
MMC-10'	0.83	0.18	0.35	0.18	97.9	97
MMC-20'	0.88	0.17	0.30	0.09	98.7	121
MMC-40'	1.02	0.3	0.38	0.11	98.8	133
MMC-80'	1.29	0.19	0.40	0.14	98.1	145
MMC-120'	1.19	0.36	0.39	0.24	97.8	151
MMC-160'	0.79	0.38	0.42	0.33	96.1	200
MMC-200'	0.80	0.42	0.40	0.35	96.9	217
MMC-240'	0.78	0.38	0.40	0.38	96.5	228

Considering displacement curves it is possible to see that the relative density is not proportional to the final displacement. This is because the four powders are characterized by very different values of tap density, which is the apparent density of the starting powder when poured into the SPS die. Therefore the starting height of the lower punch, i.e. the zero point of displacement, is not the same for all the samples. The relative densities as in the case of MM decreases prolonging milling time due to the severe strain hardening subjected by the powder during milling (Fig. VI-9d). Moreover by the change from MM to MA a more drastic decrease of density is expected in MMC due to the addition of a hard second phase. By the way, from Figure VI-9d relative density of MMCs are acceptable in comparison with mechanical milled copper (Table V-3). For example MM-240' has a density equal to 94% instead MMC-240' equal to 96%, this is in contrast with what expected. This result confirms that TiB_2 is not significantly detrimental for the densification of MMC which achieves very high relative density in comparison with MM sample. MA induces an even dispersion of fine hard TiB_2 fragments into the copper powder avoiding the formation of agglomerates assuring the achievement of high relative density. By the way a residual porosity in the sintered sample still present even in MMCs (Table VI-1). This can be associated to the incomplete decomposition of stearic acid, as in the case of MM. As reported in Figure VI-9a-b the particle size and morphology control the oxidation level of the powder and decomposition kinetic of PCA.

As stated in chapter V, the oxygen content increases increasing the specific surface area of the powder as in the case of flake like powder (MMC-80'), instead when particle size increases reducing the specific surface area the oxidation is limited (MMC-240'). After the SPS cycle the oxygen level has been reduced (Fig.VI-9a). From Figure VI-9b the carbon content in the powder is almost constant in the MMC's powders independently of the milling time. By the way as in the case of MM, after SPS

the level of carbon decomposed decreases increasing milling time. Since particle size is small and flake like, the decomposition of PCA is facilitated (Table VI-1). It is evident how for MMC-160', MMC-200' and MMC-240' the level of carbon before and after SPS is almost the same, confirming that the decomposition of PCA during SPS did not occur. The larger and more compacted powders hinder the correct and free decomposition of stearic acid.

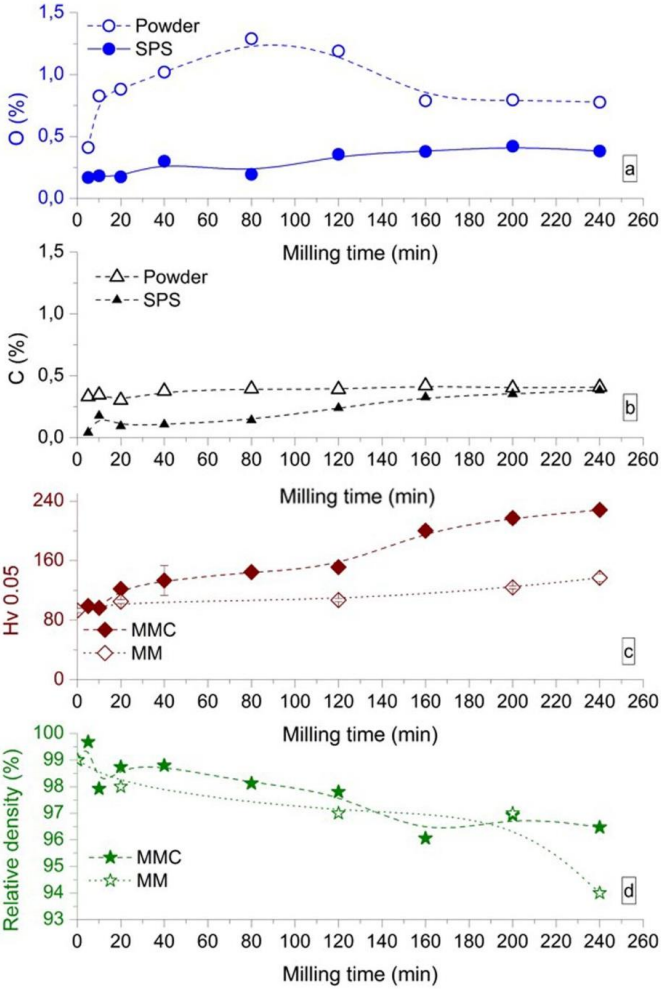

Figure VI - 9. Oxygen and carbon content before and after SPS, hardness and relative density of sintered MMC samples as function of milling time.

In fact TGA analysis of MMC-240' (solid green line) shows a decrease at 900°C as in the case of MM-720', corresponding to the emission of CO-CO_2 during QMS (Fig.V-16b). This is related to the more packed and larger particle size of MMC-240' which delays considerably the decomposition of PCA in comparison with MMC-5' and MMC-80' (solid blue line and solid red line respectively). The application of the load at 700°C hinders any gas release and is responsible for the lower relative density of MMC-240'. Since particle size and morphology of MMC-5' and MMC-80' are more suitable for degassing, the decomposition of stearic acid during heating in the TGA analysis occurs up to 500°C by three different events explained in chapter V. Any other mass loss at higher temperature has been detected by TGA, this means that the decomposition of PCA in MMC-5' and MMC-80' finishes at 600°C. In the case of MMC-5' and MMC-80' the application of the load at 700°C does not limit the decomposition of PCA during SPS.

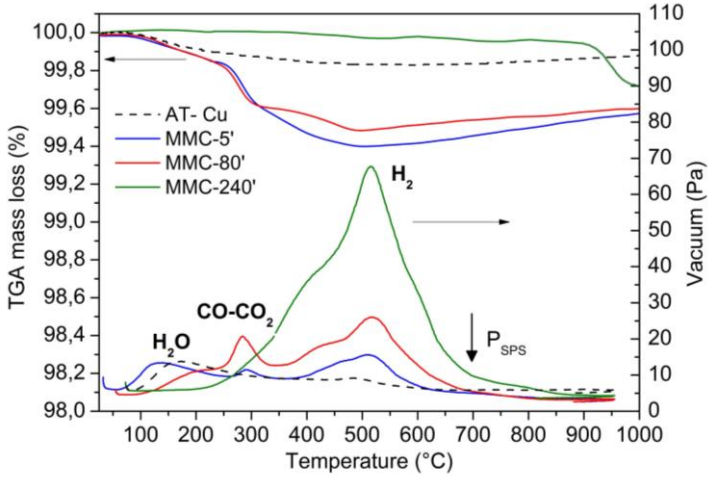

Figure VI - 10. TGA analysis and vacuum trend during SPS for AT-Cu, MMC-5', MMC-80' and MMC-240'.

The micro-structures of etched MMC sintered from powders milled for different durations are shown in Figure VI-11. By considering these micrographs, interesting information regarding porosity, reinforcement distribution, grain size and interface bonding between TiB_2 and copper matrix can be illustrated. In each micrograph, light areas correspond to the Cu matrix, blue regions are TiB_2 and black dots could be either visible pores, copper oxide particles or even selectively etched interfaces of very fine TiB_2 particles. From Figure VI-11 it is clear how the microstructures of sintered samples keep memory of the particle size and morphology of the milled powder (Rajkovic et al., 2008). For short milling time, the Cu area and reinforcement are clearly recognizable, this demonstrates the incomplete alloying between the two phases

(Fig.VI-11a-c). When MA leads to a severe plastic deformation and all particles turn into a flake morphology, microstructure of sintered sample show a clear anisotropy, as in the case of MMC-80' (Fig.VI-11e). By increasing milling time, the dispersion of TiB_2 is gradually improved and the two phases look more homogenized. In MMC-120' (Fig. VI-11f) flake like particles are still evident, but their rearrangement is not perpendicular anymore to the loading direction as in the case of MMC-40' and MMC-80' (Fig.VI-11d-e). In MMC-120' flakes look thinner and some of them are randomly pressed and deformed. Increasing milling time microstructure and TiB_2 dispersion are more uniform and homogeneous, and TiB_2 refinement actually occurs (Fig.VI-11g-i).

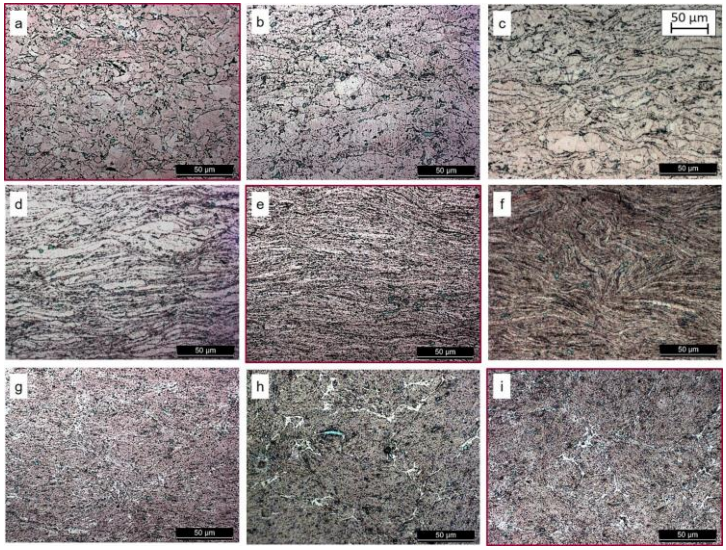

Figure VI - 11. Microstructures of MMCs as function of milling time: a) MMC-5', b) MMC-10', c) MMC-20', d) MMC-40', e) MMC-80', f) MMC-120', g) MMC-160', h) MMC-200' and i) MMC-240'.

As mentioned above clear differences can be highlighted between MMCs, in Figure VI-12-13-14 microstructures of the three main milling times (MMC-5', MMC-80' and MMC-240') are reported. In the case of MMC-5', it is clear that after short milling duration, due to the insufficient collisions with milling media, TiB_2 particles are not much refined and in-homogeneously dispersed inside the matrix (Fig.VI-12). As a consequence, presence of large TiB_2 particles associated with interconnected porosity at interfacial boundaries indicating discontinuous bonding between the reinforcement and Cu, are detected. The nature of the interface between the constituents of the MMCs determines the ability of the matrix phase to hold the reinforcing particle and prevent its pull out during the service life. Additionally, due to the largely in-completed alloying generated by 5 minutes of MA, MMC-5' shows an ineffective contacts at

interfaces between the large reinforced particles and the matrix, leading to the formation of interconnected pores upon on completion of sintering process.

By increasing milling time, the dispersion of TiB_2 inside sintered products was gradually improved. Micrographs of the sintered MMC-80' show visible pores and reinforced particles tend to be distributed along the flake direction (Fig.VI-13). This is firstly supported by the fact that both porosity and reinforcement tend to locate at former particles boundary regions. Once milling process is completed, the powders possessed flake-like forms which keep the memory of its shape even after applying the compacting pressure. As a result, upon on the completion of sintering, majority amount of those thin flakes would align in the direction perpendicular to that of punch stroke leading to the distribution of porosity and reinforced particles following the direction. Nevertheless, large TiB_2 particles are still present and some longitudinal pores could not be completely eliminated. The inhomogeneous distribution of TiB_2 leaves unreinforced Cu areas inside the composite material, which is expected to affect its properties. By the way the adhesion between matrix and TiB_2 in MMC-80' is improved with respect to MMC-5'.

MMC-240' exhibits the best microstructure after sintering in which porosity is very fine and evenly distributed and the distribution of TiB_2 is quite homogeneous,. Visible porosity is still observed, however, it also became much finer in size and dispersed quite well in the matrix. Another remarkable feature that should be pointed out is the white region located at particles' boundaries. As in the case of MM, they are portions of the Cu matrix undergoing re-crystallization during sintering (Rajkovic et al., 2008). This was explained in view of local temperature's increment due to Joule effect, which either promoted the Cu matrix re-melting or re-crystallization, as reported in chapter V (Diouf et al., 2012 [2]). Only for the products sintered from powders undergoing sufficiently long milling time, such as MMC-160', MMC-200' and MMC-240'; or the as-milled MM-360' and MM-720' Cu powders re-crystallized regions are detected (Fig. VI-11g-h-i; Fig. V-13e-f).

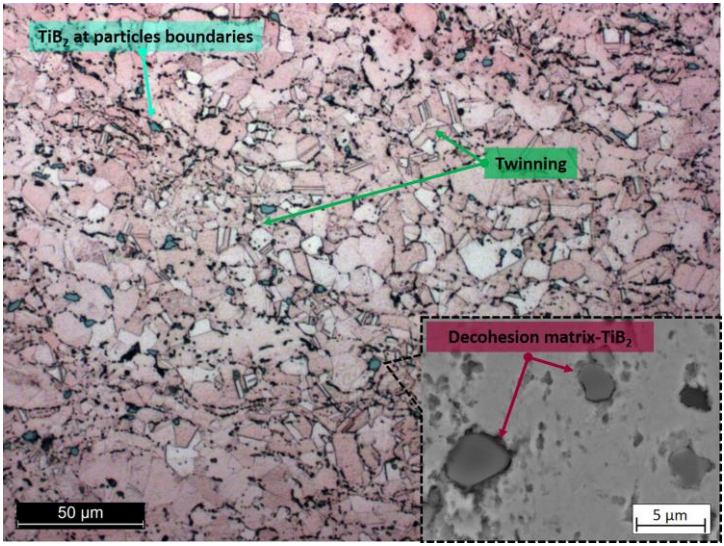

Figure VI - 12. Microstructures of MMC-5'.

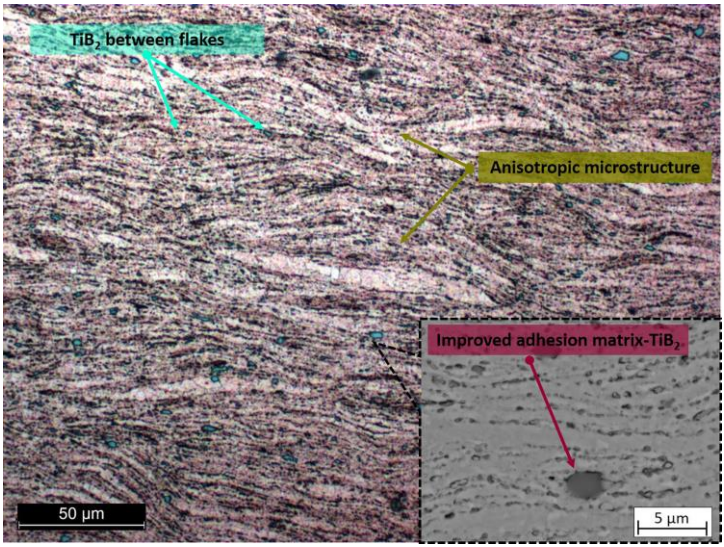

Figure VI - 13. Microstructures of MMC-80'.

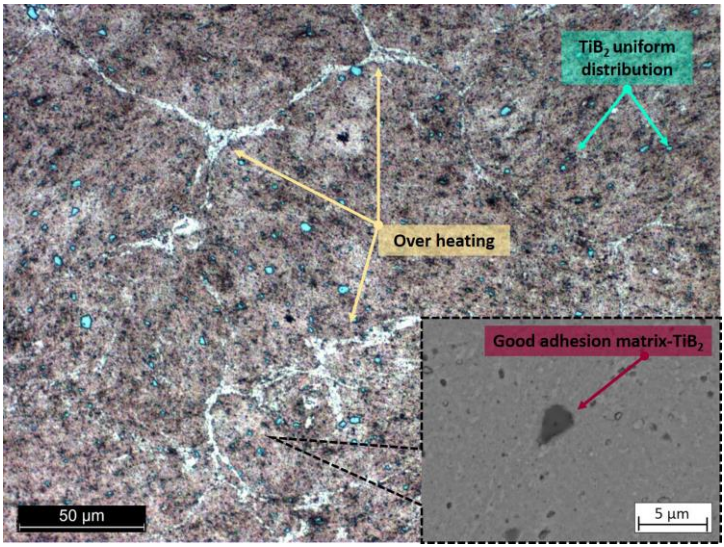

Figure VI - 14. Microstructures of MMC-240'.

The hardness of sintered samples as a function of milling time is reported in Table VI-1. It can be observed that the hardness is directly proportional to the milling duration, showing an opposite tendency with respect to density. This can be partly explained in view of strain-hardening effect induced by high energy collisions between powder particles and milling media. The longer the milling process, the higher the strain hardening, and therefore the higher the hardness of as-milled powders. This is finally reflected in a higher hardness of the sintered material, since the relatively short sintering time and temperature used in present work, do not allow complete recovery and re-crystallization. It can be observed that the increasing porosity by increasing milling time is expected to reduce the hardness of the sintered samples. From this viewpoint the increasing hardness confirms that strain hardening abundantly compensates the negative effect of porosity.

A comparison of hardness between MMC and MM-Cu samples is reported in Figure VI-15. The presence of TiB_2 in the matrix, promotes dispersion strengthening which explains the higher hardness of MMC than MM-Cu (Fig.VI-15). As a result, the hardness of MMC's powder is increased due to the well-known Orowan mechanism (Anderson et al., 1993; Wang et al., 2014). This seems to be confirmed also by the step increase of hardness for milling times longer than 120 minutes. Figure VI-11g-h-i clearly highlight that a uniform dispersion of reinforcement is obtained only in this time range: no more unreinforced Cu particles are present. A comparison with MM-Cu (Fig.VI-15), which does not show a similar stepwise trend, supports the above interpretation.

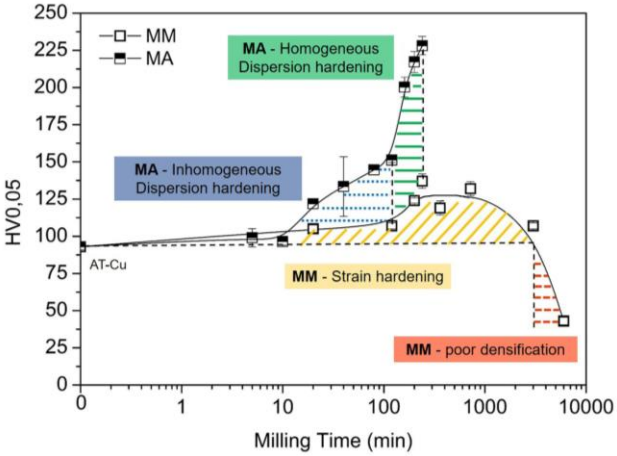

Figure VI - 15. Hardness comparison between MMCs and MM-Cu samples.

6.3 Conclusions

In this chapter the MA process of Cu and TiB_2 was investigated.

- Up to 120 minutes the predominance of particle plastic deformation allows a uniform flake-like powder morphology accompanied by a slight size increase (D50 ≈ 30μm). For longer milling times (up to 240min) the occurrence of welding promotes the formation of equi-axed particles and a marked particle size increase (D50 ≈ 110μm). The milled powder highlights a bimodal particle size distribution and a very uniform dispersion of TiB_2 for long milling time.
- MMC materials exhibit density values between 99 and 96%, which are acceptable in comparison with mechanical milled copper samples. The final density generally decreases by increasing milling time, in view of the higher particles' hardness. By MA the hardness of the sintered MMC is enhanced by TiB_2 dispersion hardening. Increasing milling time the refinement of TiB_2 and its more uniform distribution lead to a sharp increase of hardness. The hardness of MMC-240' is three time higher than the starting hardness of AT-Cu. At this point it can be concluded that the choice to switch from MM to MA has been beneficial.

From this chapter two main milling times have been selected according to the size and morphology of the powders after MA: MMC-80' (flaking) and MMC-240' (welding). The selection has been made in order to evaluate the thermal conductivity, the wear behaviour and the mechanical properties as function of the level of strain and dispersion hardening induced by MA and compare them with the mechanical milled samples produced in previous chapter.

Chapter VII

Material characterization of MM-Cu and MA-Cu+TiB_2

Part of this chapter has been published in:

G.Cipolloni, M.Pellizzari, A.Molinari
"Tribological behavior of TiB_2 reinforced Cu-matrix composites produced by mechanical alloying and spark plasma sintering"
Proc. Of the 2015 European Powder Metallurgy Congress & Exhibition
4-7 October, Reims, France

7.1 Thermal conductivity

Some representative materials produced by both, MM and MA were selected for the characterization: AT-Cu, MM-240', MM-720', MMi-6000', MMC-80' and MMC-240'. MM-240', MM-720' and MMi-6000' have been chosen to evaluate the effect of strain hardening by MM. MMC-80' and MMC-240' have been selected to evaluate the combined effect of strain and TiB_2 dispersion hardening. Moreover each sample is representative of a certain powder morphology and size which can severely affect the behaviours of the sintered material. In addition Cu-Be alloy (Cu-2%Be-0.5%(Co + Ni)) has been tested in order to compare the materials produced by MM and MA with a commercial alloy widely used in thermal and electric applications. For the production of the samples the pressure during SPS has been changed from 30MPa to 60MPa to improve the densification. The pressure has been applied at 700°C and the holding time of pressure and temperature were 3 and 1 minutes respectively. The density and hardness value of the new sintered samples are reported in Table VII-1. Despite a slight increase of density (~1%) for all the samples, the trend still the same of chapter V and VI, thus increasing milling time the density decreases both for MM and MA.

Table VII – 1. Hardness and density values of the tested material.

Sample	HV 0.1	Density (%)
AT-Cu	103 ± 2.1	99
MM-240'	150 ± 1.2	94
MM-720'	110 ± 2.3	90
MMi-6000'	45 ± 1.8	81
MMC-80'	130 ± 1.9	98
MMC-240'	207 ± 2.0	97
Cu-Be	400 ± 1.2	100

The most negative and in some case inevitable drawback of mechanical strain hardening by MM and of particles dispersion by MA in a copper matrix is the decrease of thermal conductivity due to the formation of defects among the matrix and the presence of a reinforcement particles acting as a barrier to the thermal flow (Sule et al., 2014). In the specific of this PhD thesis, on one side the use of MM and MA enhances the hardness, on the other side a decrease of the thermal conductivity is expected. In order to evaluate the effect of MM and MA on thermal properties, conductivity measurements have been carried out and results are reported in Figure VII-1. Thermal conductivity have been evaluated in a range of temperature between 400 and 500°C. The effects of MM and MA on thermal conductivity are totally different: on one side a detrimental effect of MM has been attested especially for long milling time, on the other side MA shows some interesting and promising results in contrast with what expected. AT-Cu shows a thermal conductivity equal to 300W/mK. Once MM is carried out, MM-240' exhibits an unexpected increase of thermal conductivity up to 320W/mK which needs further investigation, meanwhile MM-720' and MMi-6000' show a drastic decrease of thermal conductivity down to 270W/mK and 200W/mK respectively. The decrease of thermal conductivity as function of milling time is more related to the intense increase of the residual porosity than to the presence of crystallite defects (Ondracek et al., 1972). Although the lower amount of defects, i.e. dislocations, and lattice strain exhibited by MMi-6000' by the XRD analysis in chapter V, a lower thermal conductivity than MM-720' has been revealed due to the higher porosity, 19% of MMi-6000' against 10% of MM-720'.

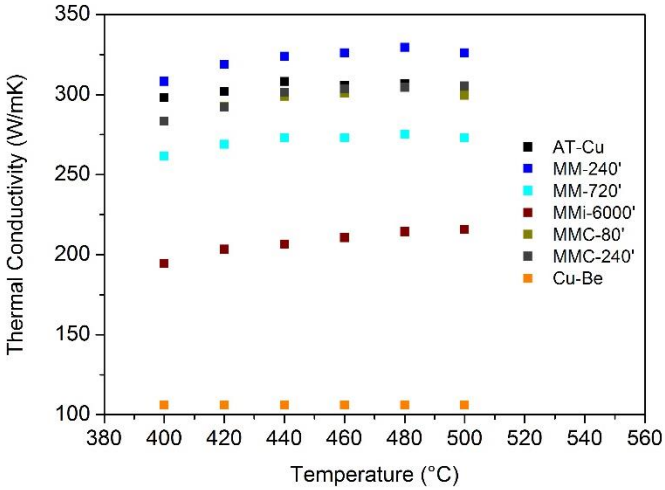

Figure VII – 1. Thermal conductivity between 400 and 500°C for all the materials.

The thermal conductivity of MMC-80' and MMC-240' is equal to 298 and 297W/mK respectively, very similar to the value of AT-Cu. Although the mechanical strain hardening and the addition of TiB_2 the thermal conductivity of MMC has not been severely affected, and this results is very positive. Probably the small amount of reinforcement (0.5wt%) and the good dispersion especially for long milling time have been able on one side to increase the hardness and on the other side to guarantee a very good thermal conductivity in comparison with AT-Cu. These results broadens horizons of the research because since any decrease of thermal conductivity will be revealed, an increase of TiB_2 content can be favoured in order to increase the hardness and the wear resistance, but this is aim of further researches. A very important observation is that all the materials produced by MM and MA show a higher thermal conductivity than commercial Cu-Be alloy, characterized by a thermal conductivity equal to 106W/mK. Finally it can be noticed that all the materials exhibit a stable thermal conductivity within the temperature range analysed (400-500°C), which is typical of the service temperature range during injection moulding of plastic materials.

As mentioned above, a close relation between thermal conductivity and residual porosity exists, as demonstrated by Ondracek and Schulz (Khaleghi et al., 2012; Ondracek et al., 1972). In Figure VII-2 the theoretical trend of thermal conductivity as function of porosity calculated for all the samples according equation 7.1 is reported.

$$K = K_0 \frac{1-P}{1+\beta P} \qquad (7.1)$$

Where K_0 is the thermal conductivity of nonporous material (~400W/mK), P is the porosity and β is the geometrical factor pf pores.

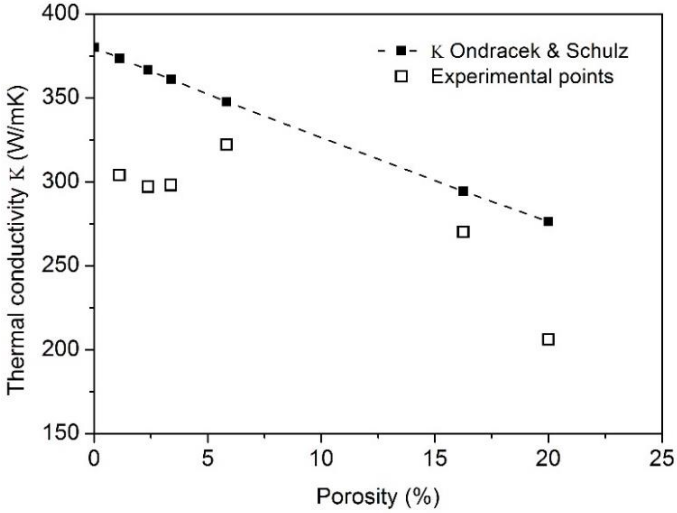

Figure VII - 2. Theoretical trend of thermal conductivity and experimental values as function of residual porosity.

It must be considered that β represents the factor shape of pores in equation 7.1, and for calculation a round shape porosity has been consider, thus β equal to 0.5. A clear linear relation exists between the two values, increasing porosity the thermal conductivity accordingly decreases. In Figure VII-2 experimental points have been reported with purpose of comparison with the theoretical trend. All the empirical points stand below the theoretical ones for three reasons: firstly the approximation of shape of pores to a round shape is roughness, secondary the Ondracek equation does not consider the defects induced by MM and the presence of a second phase by MA, and finally the presence of oxides is neglected (Kaczmar et al., 2014). Copper oxide which is characterized by a lower thermal conductivity affects considerably the thermal behaviour of the powder especially for MMi-6000'. Equation 7.1, neglecting all these parameters, overrates the thermal conductivity of all the samples. In Figure VII-3 a map of thermal conductivity values versus porosity of copper based material is graphed, in particular experimental points of this Ph.D research (black square) and data collected by literature review (blue square) are reported (Gelbstein et al., 2015).

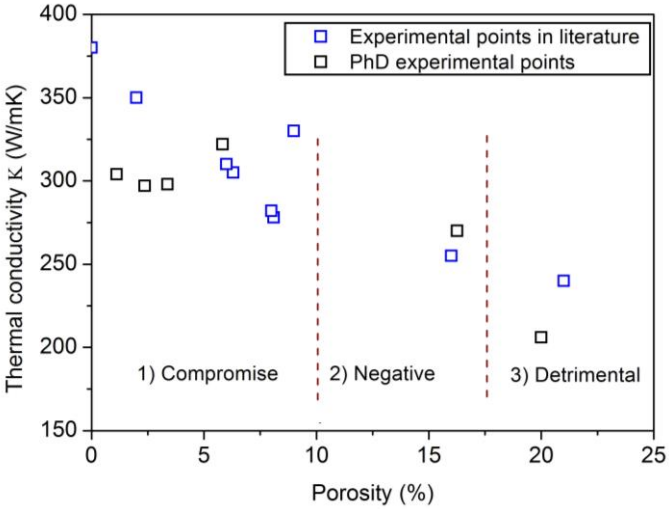

Figure VII - 3. Thermal conductivity of experimental values as function of residaul porosity (Gelbstein et al., 2015).

It is clear that the relation between porosity and thermal conductivity remains valid and three ranges of thermal conductivity can be detected according to the entity of the effect of porosity. Since porosity is limited the thermal conductivity slightly decreases but still acceptable if compared to the thermal conductivity of pure full dense copper (~400W/mK). It must be considered that in the specific case of this PhD even the AT-Cu shows a relative low thermal conductivity in comparison with the theoretical value. This is due to the presence of oxide even in the starting powder. When porosity increases up to 10%, the thermal conductivity is almost halved, and the effect is even more detrimental for higher value of porosity. It can be conclude that the MMC-240' still showing the best properties among the material produced: hardness has doubled and thermal conductivity has been kept constant.

7.2 Tribological Behaviour

7.2.1 Sliding wear behaviour

The wear behaviour of a material depends on the testing conditions, but also on the interrelation generated with the counterface. For this purpose in Figure VII- 4 the microstructure of AISI M3:2 (65HRC) is reported. It is important to notice that the microstructure of the counterface is uniform, and a homogeneous dispersion of the precipitated carbide is evident. The average dimension of the precipitates is ~3μm and this data is important to compare it with the width of the scratch on the worn surface.

Moreover in Figure VII-5 the microstructure of the Cu-Be alloy is reported in order to compare it with the microstructure of the over material produced in chapters V and VI.

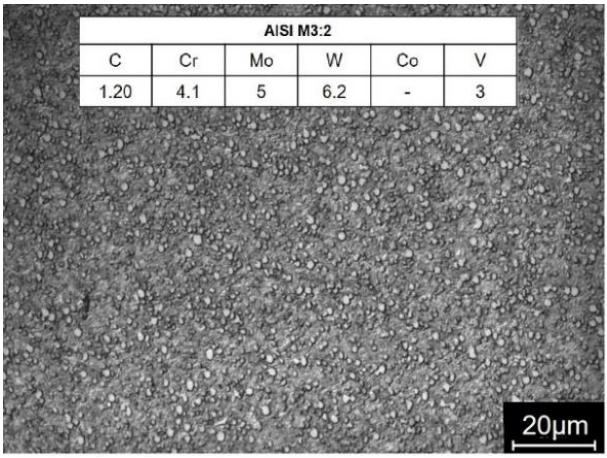

Figure VII – 4. AISI M3:2 microstructure.

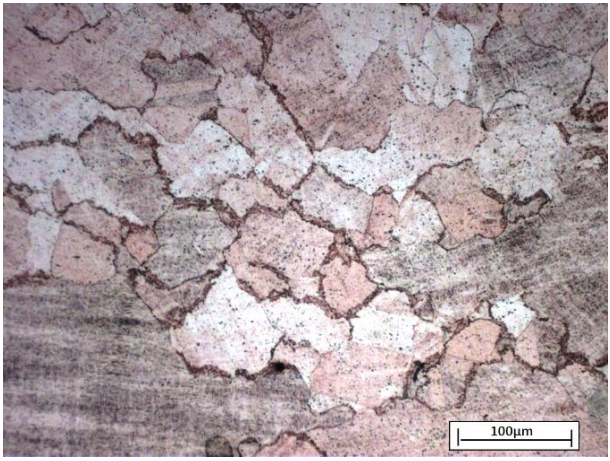

Figure VII – 5. Cu-Be alloy microstructure.

Initially the wear tests were carried out for 15, 30 and 240 minutes under a load of 50N with a sliding speed of 0,63m/s and a Hertzian pressure of 85MPa. In order to highlight the wear mechanisms a typical record of the friction coefficient is displayed in Figure VII-6, as representative of those of all samples listed above for a sliding test of 240 minutes, since all the materials show a similar macroscopic tribology behaviour.

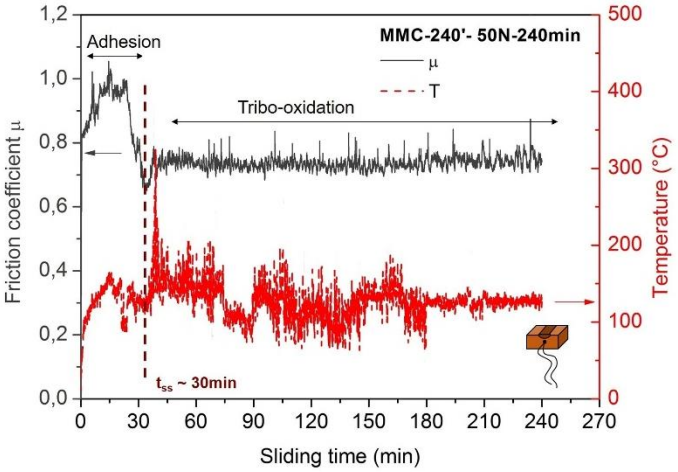

Figure VII – 6. Friction coefficient and Temperature evolution for 240min of dry sliding test of MMC-240'.

In Figure VII-6 also the record of the temperature during the sliding test is reported, and a clear relation with the trend of the friction coefficient is evident. Two distinct friction regimes can be observed. The first one, occurring at an early stage of the wear process (typically within the first 30 minutes), is characterized by the presence of a high friction coefficient (~1). During this first stage the temperature increases then slightly decreases approaching 30 minutes of test. The second one is characterized by the attainment of a steady-state (ss) friction (~0.7) and is achieved after a time (t_{ss}) in accordance with other studies (Akhtar et al., 2009; Straffelini et al., 2005). The high initial value of friction is typical of an adhesive metal-metal contact. The oscillations of friction coefficient observed during this period remark the occurrence of stick-slip phenomena. On the other side the low friction coefficient during the second period recalls a milder condition characterized by metal-oxide, oxide-oxide contact (Straffelini et al., 2004; Straffelini et al., 2005). Despite the oscillation due to the instability of the thermocouple, temperature shows an average value of 130°C during regime in the case of MMC-240'. Further the effect of temperature will be analysed and compared.

By carrying out the sliding tests for 15, 30 and 240 minutes it was possible to characterize the evolution of the wear mechanism (Fig. VII-7). After 15 minutes only, the wear surface evidences a quite rough aspect, with clear traces of metallic Cu (red regions) and Cu oxide (grey-blue regions) as well. A clear accumulation of material is evident in the wear track. The inlet area is characterized by severe abrasion scratches which aids the formation of the track during the initial stage of test. By the formation of the track the contact changes from not conformal to conformal reaching a more stable

wear regime. The outlet area is characterized instead by an intense accumulation of wear debris. The high friction coefficient typical of copper-copper contact (μ~1) suggests the occurrence of an adhesive contact between the specimen and the counterpart.

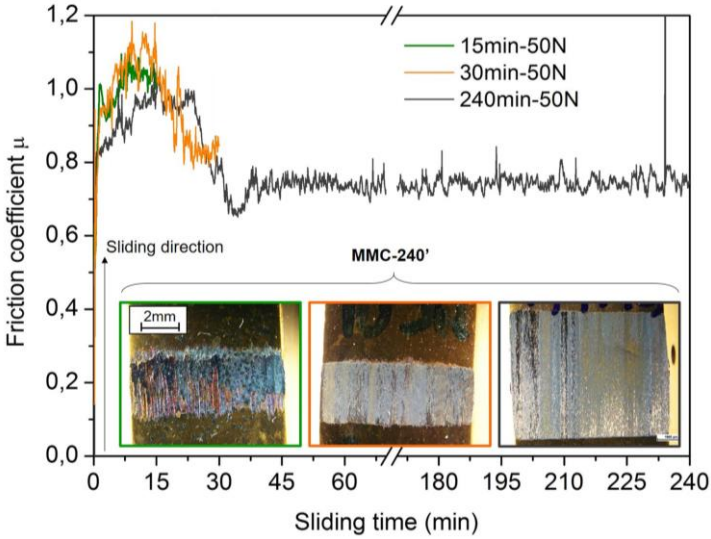

Figure VII – 7. Friction coefficient evolution for 15, 30 and 240 minutes of dry sliding test with their wear tracks.

After 30 minutes the friction coefficient starts to decrease and a definitely different wear surface is observed (Fig VII-7). Any massive accumulation of material is detected in the outlet area and scratches due to the abrasion action are vanished in the inlet region (Fig. VII-7). The material accumulated during the running in is either transferred on the disc or compacted and pressed in the track to form a protective oxide layer. After 240 minutes, with the attainment of a lower friction regime (μ~0.7), the tracks is larger and clean. At this point a homogenous protective oxide layer cover the wear track and wear behaviour is governed by a tribo-oxidative mechanism. In Figure VII-8a-b all the discs used for all the sliding times at 50N and for all the materials are reported, except for MMi6000' that will be shown in the next pages due to its peculiar behaviour. As reference also an undamaged disc of AISI M3:2 is reported in Figure VII-8a. Looking at the discs a perfect correspondence is evident with the information obtained by the evolution of the friction coefficient about the wear behaviour. Independently of the type of material tested the morphology of the disc after 15 and 30 minutes is almost the same, showing three different areas: a bright one typical of the starting surface morphology of the reference disc, some red stripes confirming the adhesive wear between the two surfaces and a more darker oxidized

area. Increasing sliding time up to 240 a totally different morphology is highlight by Figure VII-8b; the surfaces of all the discs are completely and homogeneously covered by an oxide layer. Only Cu-Be shows a different behaviour, even after 240 minutes the disc looks more shiny and only few narrow stripes of transferred material are evident, this lead to the different microstructure, hardness and composition in comparison with the material produced by MM and MA.

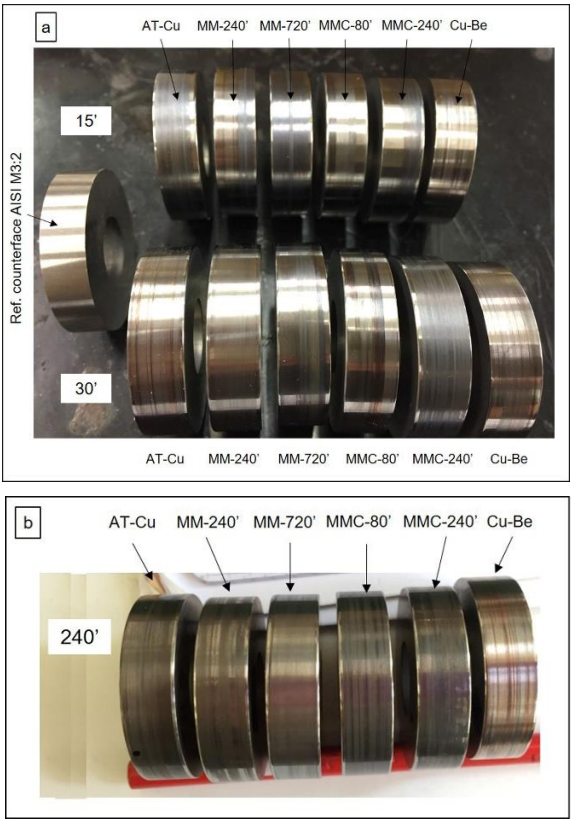

Figure VII – 8. (a) AISI M3:2 discs after 15 and 30 minutes of sliding time, (b) AISI M3:2 disc after 240 minutes of sliding time

At this point a deep characterization of the discs have been carried out, OM and SEM micrographs after 15 and 240 minutes of sliding test are reported in Figure VII-9 and Figure VII-10. The occurrence of an adhesive contact between the specimen and the counterpart is evident in Figure VII-9, a strong materials transfer from the Cu block to the steel surface after the first 15 minutes test is highlighted. Patches of copper are evident on the surface of the disc, and they are deformed and smeared along the

sliding direction, favoured by the high ductility of the Cu matrix (Eyre et al., 1981). Even if the colour of the OM micrograph can be affected by the setting parameters, copper layer looks clean and not completely oxidized.

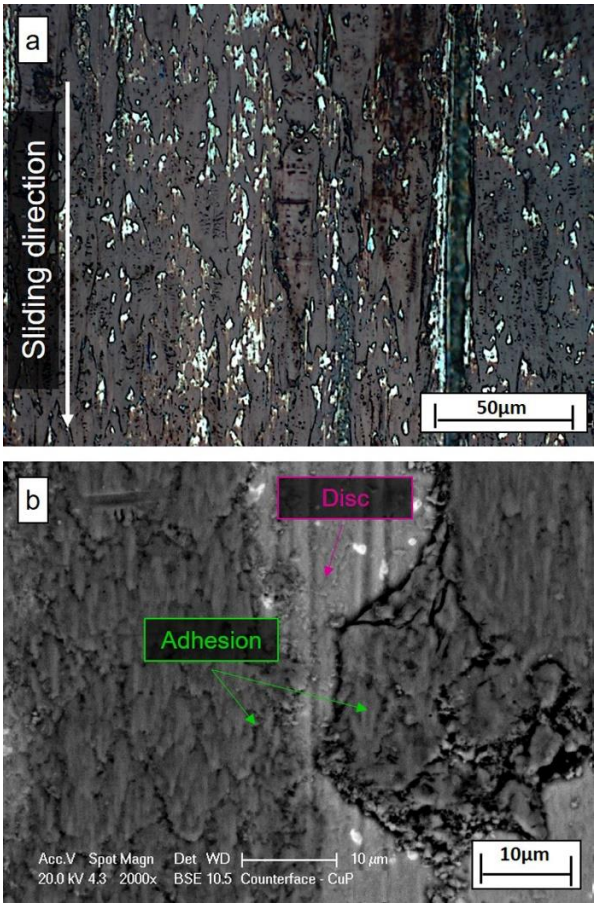

Figure VII – 9. Top view of the surface of the disc after 15mins of sliding (a) OM (b) SEM.

During the running in stage the contact nature changes from not conformal to a conformal, and the creation of the wear tracks leads to a severe wear. The production of wear debris leads to the accumulation of material inside the track which promotes two events: on one side the transfer of material on the disc, i.e. adhesion, on the other side wear debris can either be packed inside the track or pulled out of the wear system. Prolonging the sliding time the material transferred on the disc oxidizes due to the severe conditions as high contact pressure and temperature. At this point the contact

change from metal-metal to oxide-oxide, leading to a milder wear. When a tribo-oxidative behaviours governs the wear mechanism adhesion phenomena are more difficult. When the oxide layer reaches a critical thickness it breaks producing wear debris. Once oxide debris are removed from the wear system, the substrate material could oxidize again. The continuous formation and fragmentation of oxide layer during sliding wear consists in a dynamic phenomenon. At this point the surface of the disc drastically changes, a sever oxidation is evident in Figure VII-10 (Straffelini et al., 2004; Straffelini et al., 2005).

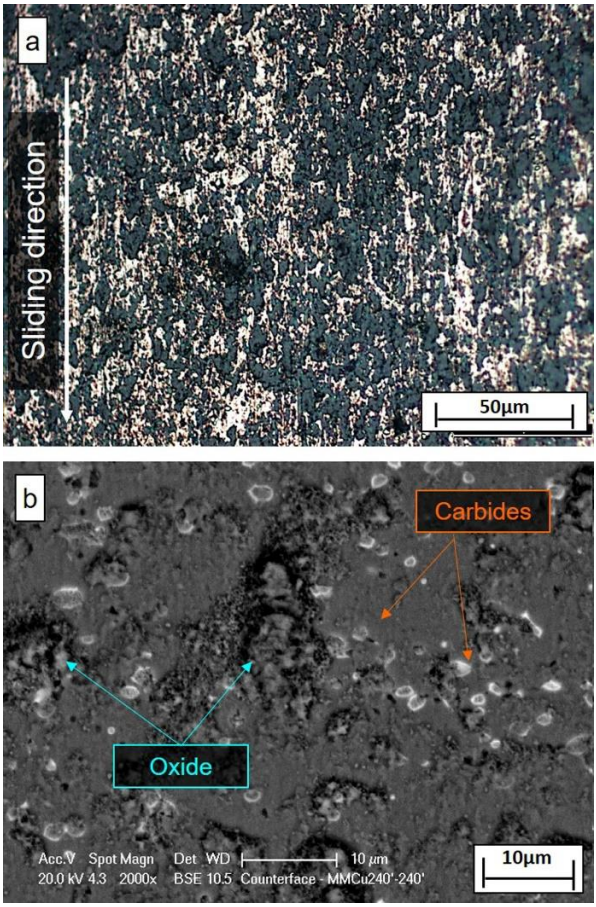

Figure VII - 10. Top view of the surface of the disc after 240mins of sliding (a) OM (b) SEM

The severe shear stress during the test enhances the strain hardening and the micro fragmentation of the oxide. Oxide is removed from the track or from the disc by

spalling and dark spots are evident on the surface on the counter face (Fig VII-10b).The occurrence of triboxidation is also confirmed by the SEM and EDXS analysis of the worn surface of the block. Figure VII-11 shows the presence of protective copper oxide patches responsible for the lower friction coefficient (Fig VII-6). The analysis of the tracks and wear debris clearly highlights that after the transition wear becomes tribo-oxidative, and the reduction in friction coefficient is, therefore, due to the lubricating action exerted by the surface oxides. The protective surface oxide layer is made by the compaction and sintering of the oxide particles (Gao et al., 2015; Straffelini et al., 2004; Zhang Y.S. et al., 2008).

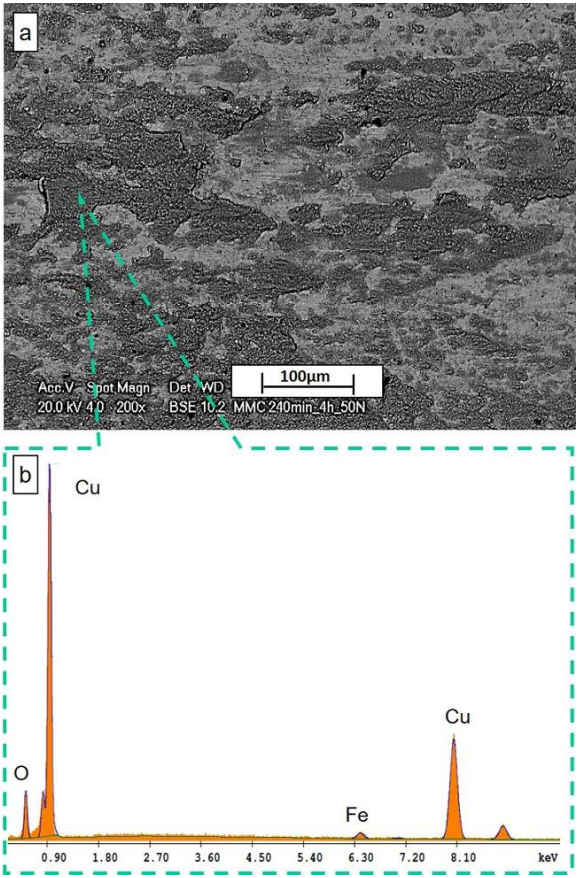

Figure VII – 11. The morphology of the worn surface of MMC-240' minutes after 240 minutes of sliding (a); EDAX spectrum of the darker areas (b).

Prolonging sliding time part of the copper layer previously transferred on the disc is either compacted in the track or removed from the wear system by the production of wear debris (Zhang Y.S et al., 2007: Zhang Y.S et al., 2008). In Figure VII-12 the morphology of debris of MMC-240' after 240 minutes of sliding test are reported.

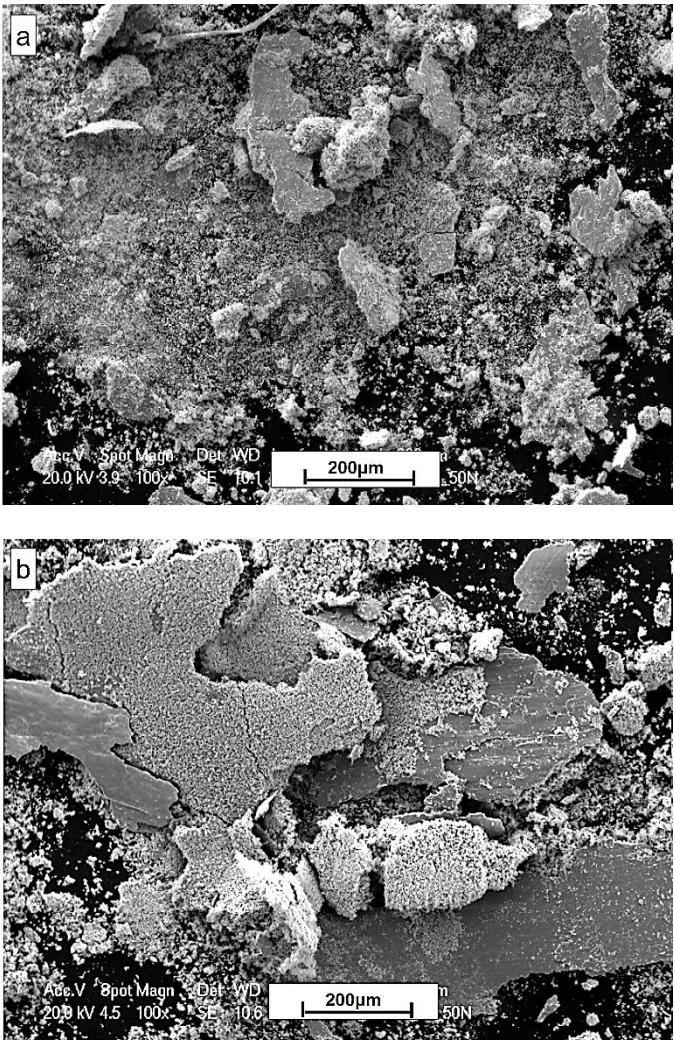

Figure VII – 12. The morphology of the wear debris of MMC-240' after 240 minutes of sliding

The dimension of the debris is variable and most of them are covered by oxides. All the analysed materials show similar size and morphology of debris. The debris are mainly composed by two different size and morphology: large plate like debris and a fine white dusty oxide powder. The first one usually shows a shiny surfaces due to the intrinsic metallic nature which in some area is covered by the fine particles of oxide, as very evident in Figure VII-12b (Straffelini et al., 2004; Straffelini et al., 2005). It must be considered that the more the material is hard the more the debris will be hard, leading to a more severe abrasion contribution in addition to the abrasion action of the AISI M3:2 carbides.

Since the wear mechanisms governing the sliding wear behaviour have been deeply investigate and explained, the PhD thesis continuous with the comparison of the different materials in order to evaluate the effect of MM and MA and interesting information can be deduced. In Figure VII-13 the friction coefficient of AT-Cu, MM-240' and MMi-6000' are reported in order to evaluate exclusivity the effect of MM.

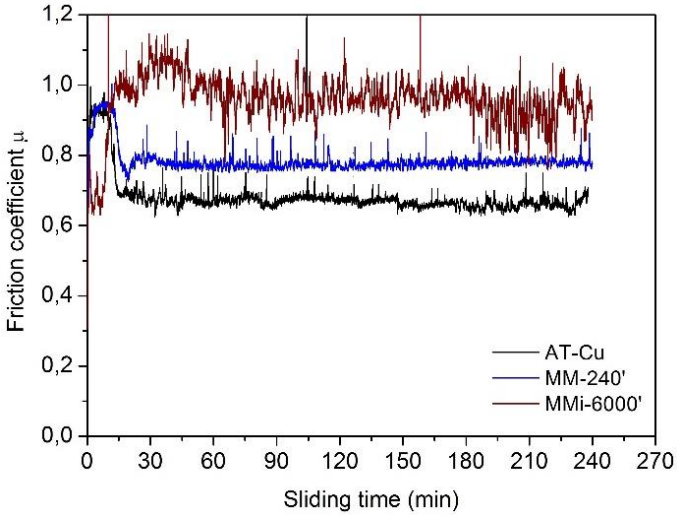

Figure VII - 13: Comparison of the friction coefficient evolution for 240 minutes of dry sliding test for: AT-Cu, MM-240' and MMi-6000'.

AT-Cu and MM-240 show the same friction coefficient evolution, instead MMi-6000' is characterized by a higher friction coefficient close to 1 which is maintained almost constant for the entire sliding test. The more intense oscillations of the friction coefficient attest the more frequent occurrence of stick and slip phenomena in MMi-6000'. The absence of a complete and stable transition from the adhesion mechanism to the tribo-oxidative regime is confirmed also by the analysis of the disc reported in Figure VII-14. The discs, especially for 240 minutes of sliding time, look shiny and less oxidized than in Figure VII- 8b. Despite the high friction coefficient which suggest the

occurrence of a severe adhesion phenomenon even for MMi-6000' some oxidized area on the counterface has been revealed by the OM micrograph (Fig.VII-14). This is also confirmed by a slight decrease of the friction coefficient in Figure VII-13.

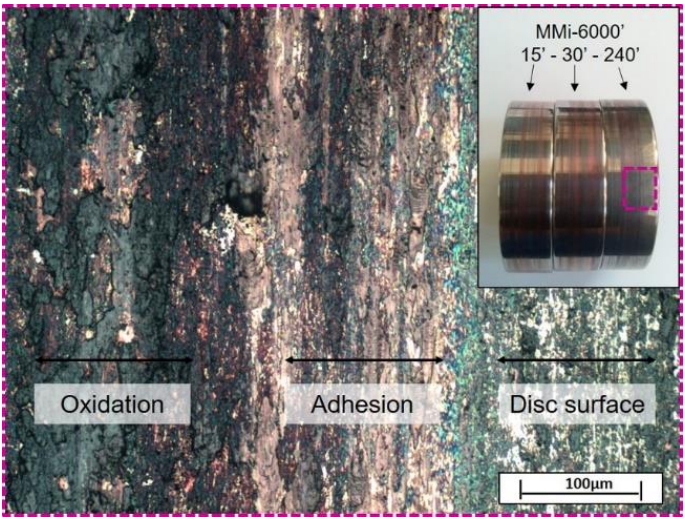

Figure VII - 14. Discs of AISI used for MMi-6000' and highlight of the surface of the disc after 240 minutes of sliding test.

Concerning MM-240' it can be noticed that increasing the hardness of the material the transition time required to achieve the steady-state (t_{ss}) shifts toward longer time (black line versus blue line) (Fig VII-13). For harder material it is more difficult to change from not conformal to conformal contact because the high hardness obstructs the formation of the wear track due to the higher wear resistance. This means that harder material takes more time to create the oxide layer (Straffelini et al., 2004; Straffelini et al., 2005). In addition MM-240' material shows a higher friction coefficient compared to AT-Cu because an addition abrasion contribution to the carbides of AISI M3:2 is given by the harder wear debris produced. Similar behaviour of the friction coefficient is shown by the MMC as reported in Figure VII-15.

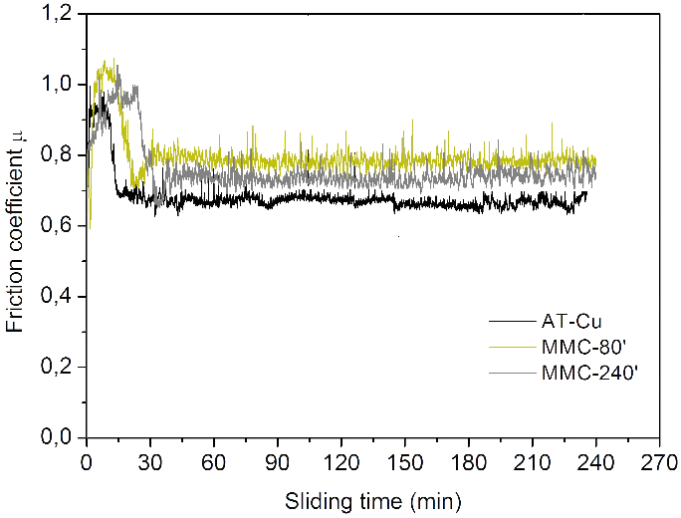

Figure VII – 15. Comparison of the friction coefficient evolution for 240 minutes of dry sliding test for: AT-Cu, MMC-80' and MMC-240'.

Also for MMC increasing the hardness the transition time required to achieve the steady-state (t_{ss}) shifts toward longer time. The t_{ss} increases adding TiB_2 and prolonging milling time. In addition composite materials have a higher friction coefficient compared to AT-Cu because a more intense abrasion contribution is given by the harder wear debris. Moreover for MMC the TiB_2 particles give a third-body abrasion contribution in addition to the carbides of AISI M3:2 counterface and to the wear debris. From Figure VII-15 also the contribution of the dispersion of reinforcement can be evaluated, MMC-240' which is characterized by a more uniform and more homogenous dispersion shows a lower friction coefficient than MMC-80'. In MMC-80', which is characterized by a lamellar microstructure and by a not uniform dispersion of TiB_2, the abrasion contribution is more significant than in MMC-240' and friction coefficient is slightly higher. Despite the similar wear behaviour the wear coefficients of the materials differ. In Figure VII-16 the wear coefficients calculated by Archard's equation (Chapter IV) for all the samples tested under dry sliding conditions for 30 and 240minutes at 50N are reported.

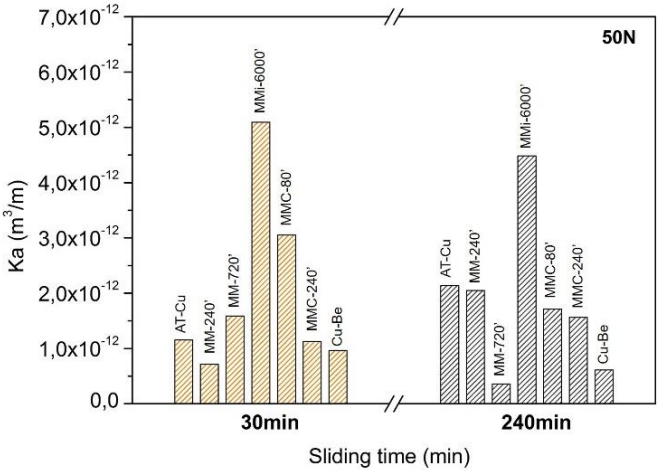

Figure VII – 16. Wear coefficient for all the samples tested under dry sliding conditions for 30 and 240 minutes at 50N.

In general the different wear coefficient shown in Figure VII-16 can be explained by the different ability to create and to maintain in place the surface oxide layer during sliding, considering that hardness severely affects this capability. Only if the oxide is firmly attached to the sliding surface it can get compacted protecting the underlying base alloy (Straffelini et al., 2005). On one side during the running in regime a low hardness facilitates the formation of the track in which the debris can be compacted generating rapidly the oxide protective layers. In this case a thick oxide layer can be easily formed and wear change rapidly from adhesive to tribo oxidative as confirmed by the shorter t_{ss} of the softer material than for MMC (Fig. VII-13 and Fig. VII-15). For this reason the wear rate for short sliding time of AT-Cu and mechanical milled samples are comparable and even lower in some case than that of MMC-240' which produce lower amount of debris and take more time to reach the tribo-oxidative protective wear mechanism. In fact during the running in state a hard material creates less debris consequently the wear track is smaller and less deeper, leading to a more difficult accumulation and formation of the oxide layer. By the way prolonging sliding time it must be considered that a higher hardness leads to the formation of harder debris, consequently the protective oxide layer will be harder providing a lower wear coefficient. Moreover a harder material is characterized by a high load bearing capability to keep the protective layer attached to the worn surface as shown by the OM micrographs of the worn surface of MMC-240' (Fig. VII-17a). On contrary softer material with a low load bearing capability usually highlights spalling of the softer oxide patches, and wear resistance is consequently reduced (Fig VII-17b).

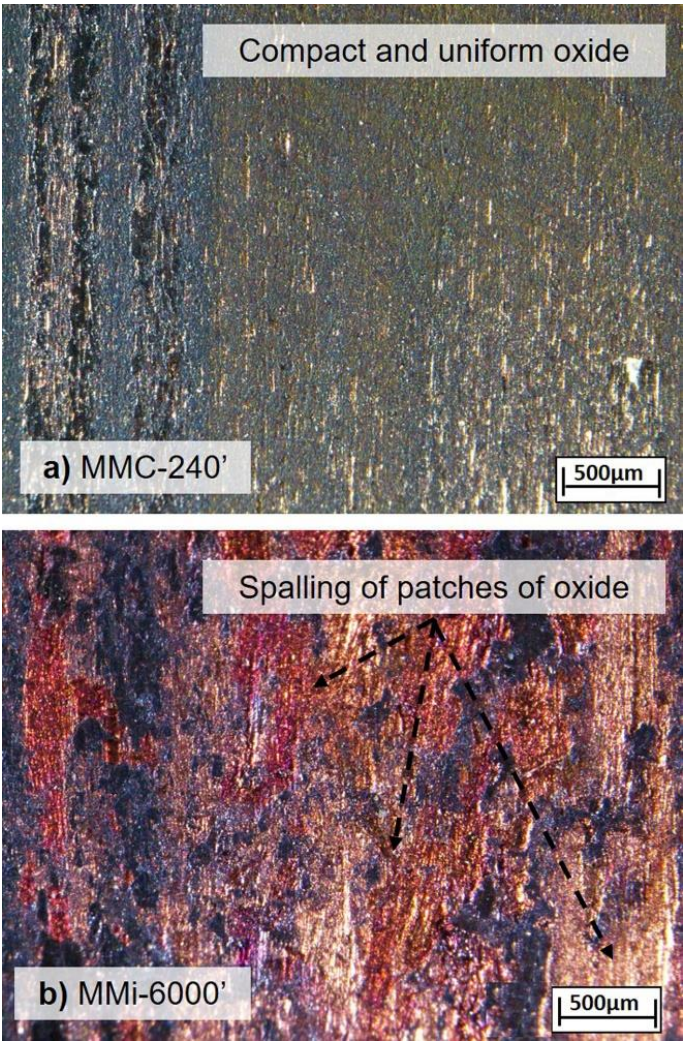

Figure VII – 17. Worn surface of MMC-240 and MMi-6000' after 240 minutes of sliding time.

The dependence of wear coefficient on hardness is very clear especially for long sliding time, increasing hardness the wear coefficient decreases, as reported in Figure VII-18. By increasing sliding time the benefits of prolonging milling time and adding TiB_2 become more evident.

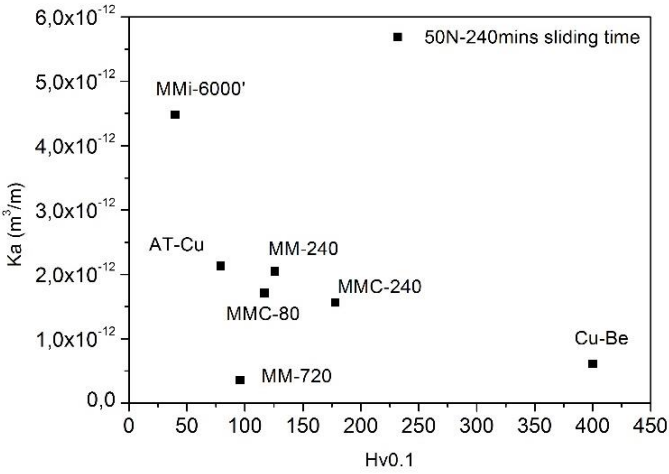

Figure VII – 18. Dependence of wear coefficient on hardness for long sliding time.

It can be noticed that MMi-6000' shows the highest wear coefficient because its oxide layer is softer and it can be easily damaged and removed during sliding leading to a lower wear resistance (Fig. VII-17b). As explained above the formation and creation of oxide layer is a dynamic phenomenon, once oxide is removed the new surface undergoes to adhesion again. In the case of MMi-6000' this cycle is very fast and material has not time to create a thick permanent oxide layer inside the track, but a new copper surface emerges each time that spalling occurs. For this reason the friction coefficient of Figure VII-13 is close to 1, typical of the copper-copper contact.

Beside MMi-6000' also MMC-80 shows a strange behaviour for short sliding time despite its higher hardness, a high wear coefficient has been obtained after 30 minutes of sliding test. This is associate to the unsuitable microstructure of MMC-80'. The flake like particle are aligned in the direction of the tangential force during sliding favouring the delamination of the wear surface as highlighted in Figure VII-19. A massive quantity of debris is promoted during the running in stage and the wear resistance is limited.

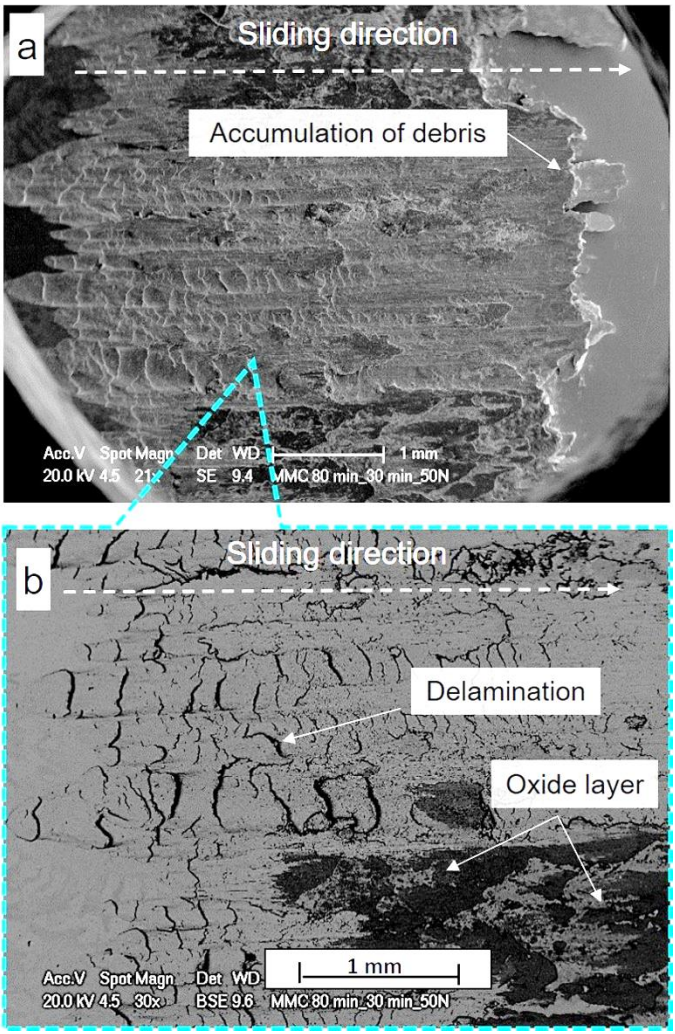

Figure VII - 19: Delamination phenomenon of MMC-80' after sliding test of 30 minutes.

It must be considered that the attainment of a tribo-oxidative wear mechanism is due to the increased contact temperature during sliding which favours the formation of oxides as demonstrate by Figure VII-6. The records of the evolution of the contact temperature with sliding time are reported in Figure VII-20 for AT-Cu, MM-240', MM-720' and MMi-6000'. It must be considered that the temperature has been acquired by a thermocouple placed below the contact surface of the disc. The distance of the hole

from the surface has been kept constant for all the sample, by the way depending on where the track has been create during the test the thermocouple could be perfectly in the middle of it or slightly decentralized. Any way the thermocouple is indicative of the massive heating of the sample during the test and not of the real contact temperature at the contact surface. Therefore the evolution of the temperature can be considered as an indirect measurement of the capability of the material to release the heats generated by the high friction and pressure service conditions.

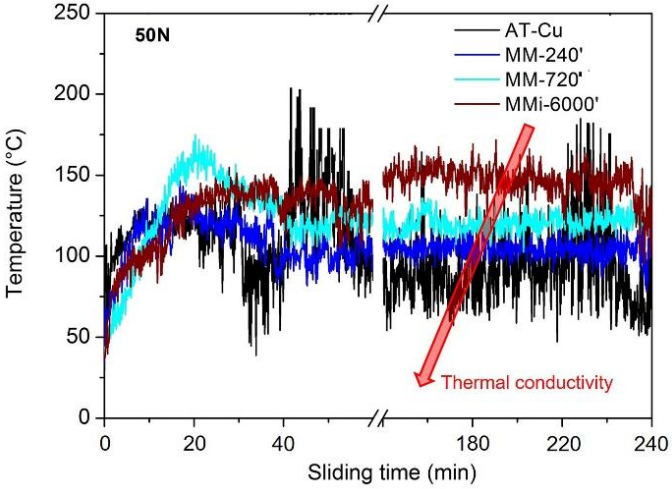

Figure VII – 20. Temperature evolution of AT-Cu, MM-240', MM-720', MMi-6000' recorded during 240 minutes of sliding test at 50N.

From Figure VII-20 the effects of MM are evident, increasing milling time the temperature increases. This is in perfect accordance with the thermal conductivity trend of Figure VII-1. MMi-6000' characterized by a low thermal conductivity (200 W/mK) shows the highest temperature close to 150°C, followed by MM-720' and MM-240' with 125°C and 110°C respectively. Despite the oscillation of the thermocouple inside the hole AT-Cu exhibits the lowest temperature close to 75°C. Temperature shows a slight increase during the running-in since a steady-state condition is reached after 30 minutes, as in the case of friction coefficient. The formation of oxide is favoured by higher temperature (Straffelini et al., 2004; Straffelini et al., 2005). Once the tribo-oxidation governs the wear mechanism the temperature remains stable because the lubricant action of oxide limits the heating caused by friction. For MMi-6000' instead any attainment is recorded, actually a slight increase of temperature between the two stage is reported in Figure VII-20. The absence of a permanent oxide induces higher friction and consequently higher contact temperature.

In Figure VII-21 the temperature evolutions of MMCs and AT-Cu are reported. In the case of MMC there is not a perfect relation between the evolution of temperature

during sliding and the thermal conductivity measurements in section 7.1. Despite the similar thermal conductivity values (300W/mK) the three materials show increasing temperatures as function of milling time in accordance with Figure VII-20.

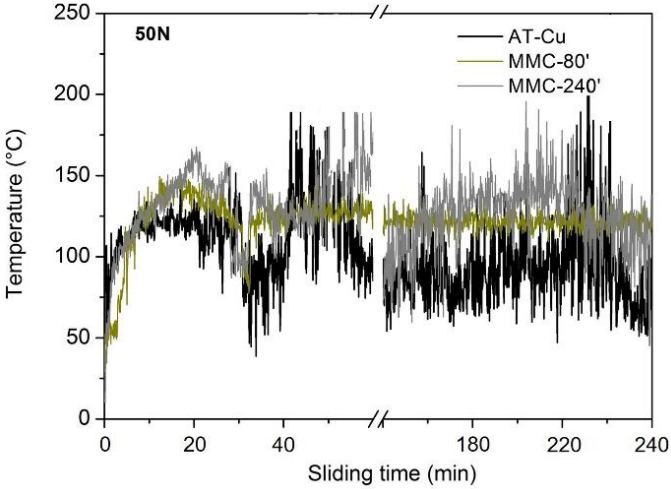

Figure VII – 21. Temperature evolution of AT-Cu, MMC-80' and MMC-240' recorded during 240 minutes of sliding test at 50N.

A schematic representation of the wear mechanisms occurring during dry sliding test are graphed in Figure VII-22.

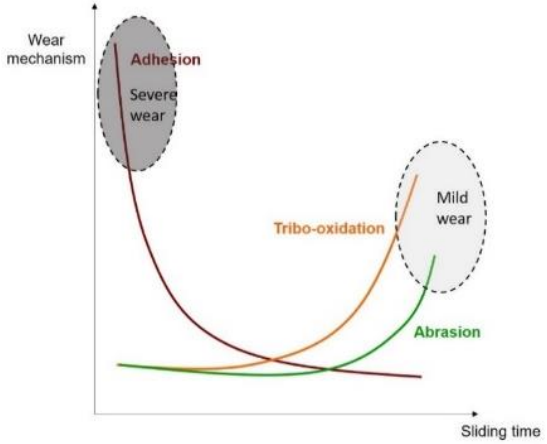

Figure VII – 22. Schematic representation of the wear mechanisms occurring during dry sliding test at 50N.

On one side harder materials (MMC) show a higher friction coefficient due to the abrasion contribution of reinforcement particles and of the harder wear debris produced during sliding (Zum Gahr, 1998). On the other one harder materials can better sustain the oxide protective layer due to the higher load bearing capability improved by the strain hardening and in the case of MMC-240 by the effective dispersion of TiB_2 particles. Moreover strain hardened materials show a higher regime temperature in comparison with AT-Cu, which induced a more intense formation of wear protective oxide. For short sliding time, when the contact switches from not conformal to conformal, MMC-80' shows some limits due its anisotropic microstructure, which enhances the delamination of the worn surface. For low load (50N), Cu-Be still the most competitive material by the way some improvements have been highlighted by MM-720' and MMC-240.

7.2.1.1 Effect of the load during dry sliding wear

In order to investigate deeply the wear mechanisms dry sliding test have been carried out also at 100N for 30 and 240 minutes for all the materials, and at 200N for MM-720, MMC-80' and MMC-240' for 240 minutes of sliding test. As in the case of 50N all the materials showed the same wear behaviour and the same phenomena. As reference the behaviour MMC-240' will be discussed in this section and all the comments and descriptions highlighted are valid for all the tested materials, as in the previous section 7.2.1. The evolution of friction coefficients as function of the applied load for MMC-240' are shown in Figure VII-23.

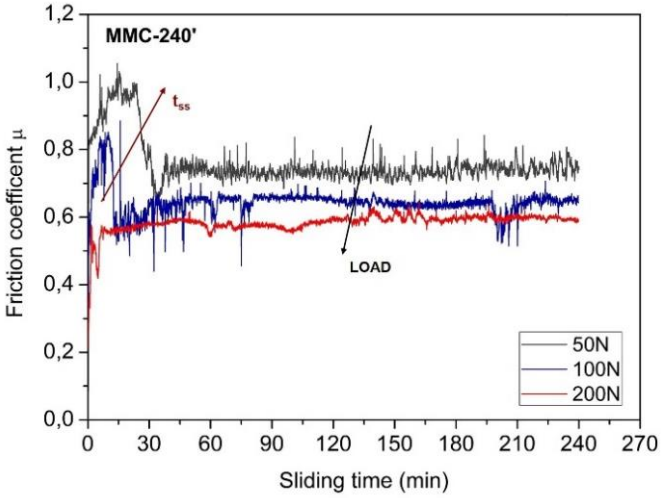

Figure VII - 23: Evolution of friction coefficient of MMC-240' as function of the applied load for 240 minutes of sliding test.

From Figure VII-23 several effects of the increase of load on the evolution of friction coefficient are evident and they are in accordance with literature results (Gao et al., 2015; Onat et al., 2010; Straffelini et al., 2004; Zhang Y.S. et al., 2007):

- μ decreases;
- μ becomes more stable → lower stick and slip phenomenon;
- t_{ss} decreases and almost disappears applying 200N.

The shift of the friction coefficient curves toward lower value increasing the applied load are associated to a change of the temperature regime during test (Fig.VII-24). It is evident that increasing the applied load a drastic increase of the temperature is promoted. As demonstrated previously, a higher contact temperature leads to a more intense formation of oxide, which acts as a lubricant in the sliding system reducing the friction coefficient (Fig.VII-23). Moreover the adhesion phenomena are drastically decreased, and for this reason oscillations of friction coefficient almost disappear (Fig VII-23).

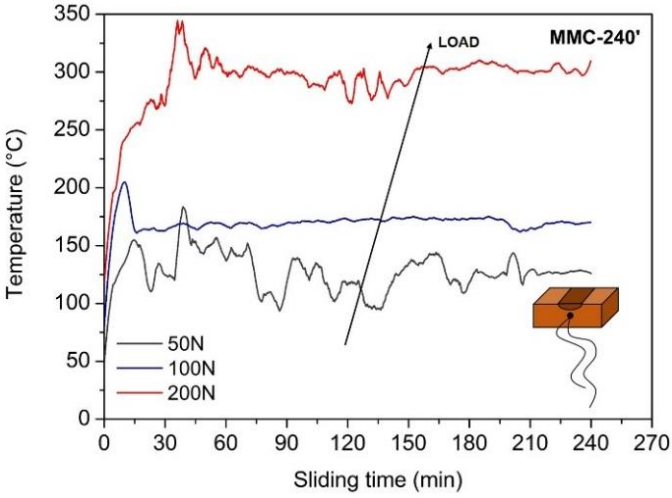

Figure VII - 24: Evolution of temperature of MMC-240' as function of the applied load for 240 minutes of sliding test.

From the value of the friction coefficient and of the temperature during steady state regime of samples MM-720', MMC-80' and MMC-240', a clear relation with the applied load has been extrapolated, Figure VII-25a-b.

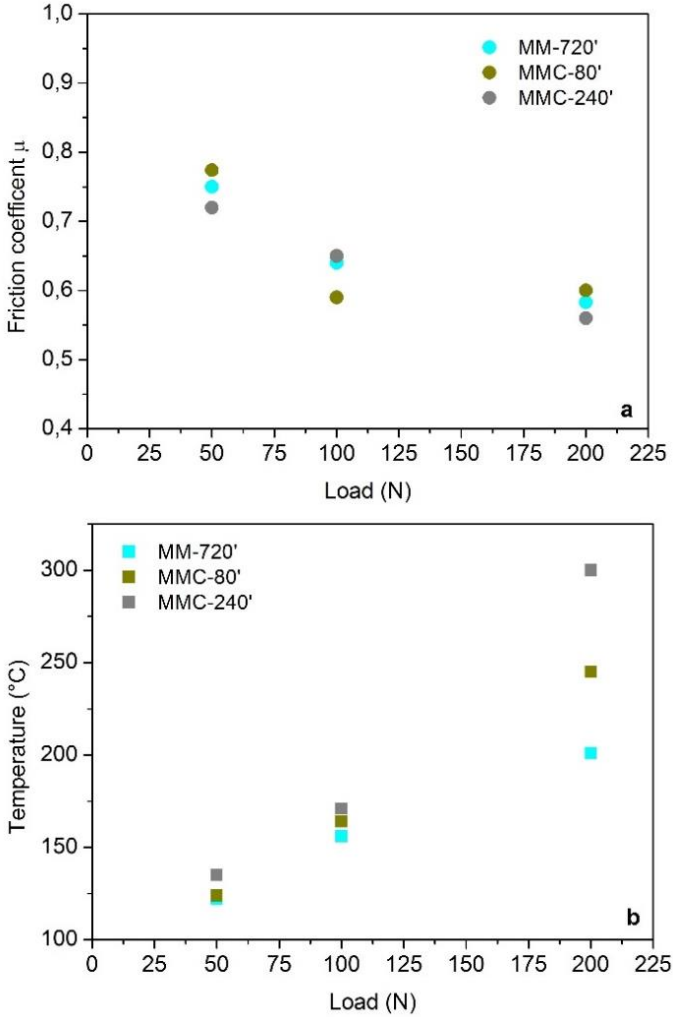

Figure VII – 25. Evolution of friction coefficent (a) and temperature (b) as function of the applied load.

All the materials show the same trend, increasing the applied load the friction coefficient decreases meanwhile the temperature increases. The wear mechanisms change accordingly to the wear conditions, a tribo-oxidation is predominant at higher load exhibiting a less intense wear especially for long sliding time. In Figure VII-26 the wear coefficient of all the material tested under 100N for 30 and 240 minutes of sliding time are reported.

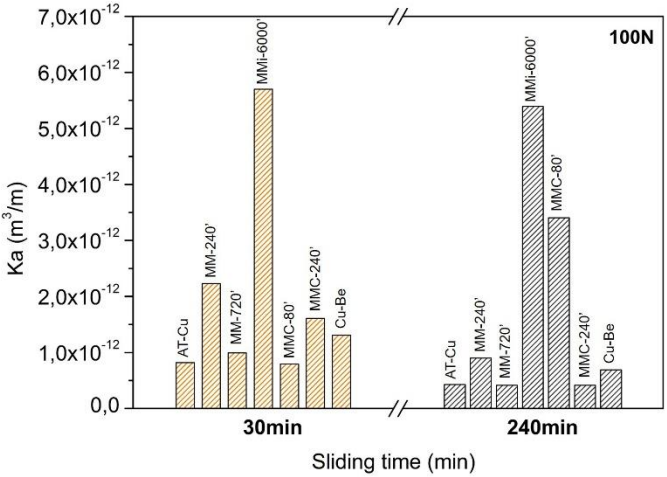

Figure VII – 26. Wear coefficient for all the samples tested under dry sliding conditions for 30 and 240 minutes at 100N.

For short sliding time (30 minutes) no significant difference of the wear coefficient between 50 and 100N is evident by the comparison of Figure VII-26 with Figure VII-16. Meanwhile for long sliding time the wear coefficient of all the samples decreases when the load is increased to 100N except for MMi-6000' and MMC-80' (Deshpande et al., 2006; Zhang Y.S. et al., 2007; Straffelini et al., 2005). The high wear coefficient of MMi-6000' and MMC-80' can be associated to the low hardness and to the anisotropic microstructure respectively, as demonstrated in the previous section. Moreover for these two materials the wear coefficient after 240 minutes is drastically increased if compared with Figure VII-16.

The lower wear coefficient of the other materials is due to the better capability to form the oxide layer thanks to the higher temperature induced by the more severe wear conditions. Also the dimension of the track in Figure VII-27b is drastically reduced in comparison with Figure VII-7, confirming a higher wear resistance. Finally it can be noticed that the wear coefficients of all the other materials are quite similar after 240 minutes of sliding time at 100N, therefore increasing the load all the materials seemed to be competitive with Cu-Be. In Figure VII-28 a map of the wear coefficient versus hardness is graphed. Neglecting MMi-6000' and MMC-80 which show peculiar wear behaviours, it is evident that increasing the applied load the effectiveness of hardness is lost. This is very particular especially for soft AT-Cu which is supposed to have a low wear resistance due to its lower hardness. By the OM observation of the worn surfaces of AT-Cu an intense accumulation of wear debris inside the wear track is evident in Figure VII-27a. The wear products are stuck and compacted inside the track, thus altered the wear loss measurement and consequently the calculation of the wear

coefficient by Archard's equation. All the others materials show a similar morphology of the wear surface, with the presence of an oxide protective layer but thinner than that in the case of AT-Cu. MMC-240' and MM-720' show wear coefficients even lower than Cu-Be, this is very promising. By the way this result deserves further investigation using different wear conditions as a change of sliding speed and higher load.

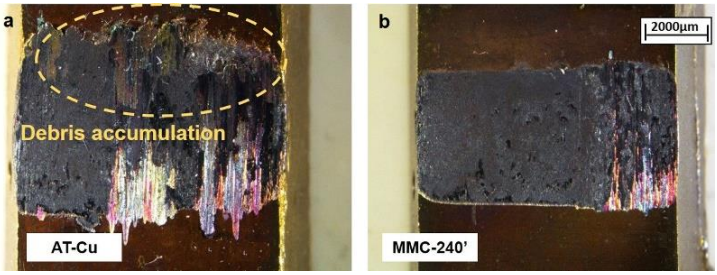

Figure VII – 27. Worn surfaces of AT-Cu and MMC-240' after 240 minutes of sliding time at 100N.

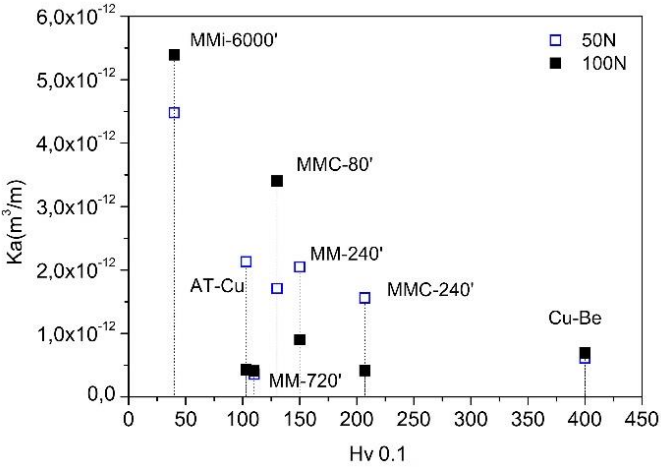

Figure VII – 28. Wear coefficient versus hardness as function of the applied load.

7.2.2 Abrasion wear behaviour

The wear resistance to abrasion has been measured by scratch test in order to have some more information about wear resistance of the produced materials. The scratch test, which is not affected by a temperature heating, by the formation of protective mechanisms and by long testing time/distance, evaluates the resistance to abrasion of a material by measuring the penetration depth of a hard indenter sliding

on the surface of the sample. The test have been carried out applying 1, 2 and 3N for a scratch length of 5mm. The penetration depth under 1N for all the materials is reported in Figure VII-29.

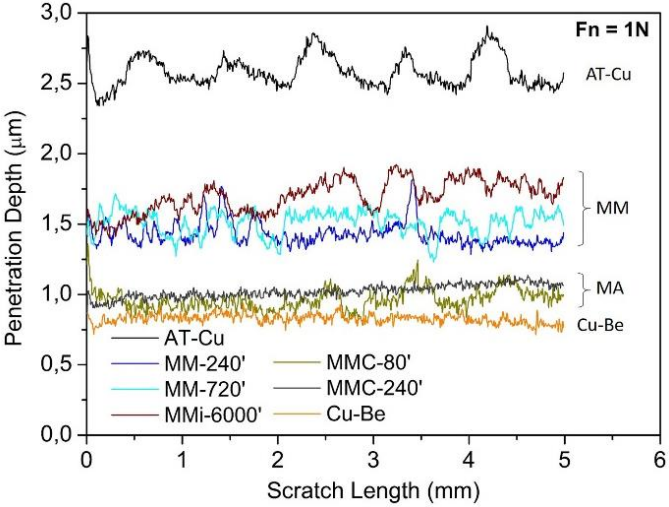

Figure VII -29. Penetration depth of scratch test of all the materials under 1N.

It can be noticed that

- AT-Cu shows the deeper penetration depth, equal to 2.5mm;
- Mechanically milled samples show a penetration depth between 1.4-2.0mm;
- Mechanically alloyed composites show the lowest penetration depth (~1mm), approaching that of the Cu-Be reference alloy.

AT-Cu exhibits very cycled up and down variations, i.e., the so-called *stick-slip sliding* (Futami et al., 2009). These events suggest that the high concentrated frictional forces induce the non-linear deformation and a micro-macro damage on the scratched contact surfaces. The penetration depth of the mechanical milled sample decreases by prolonging milling time accompanied by an increase of hardness. In fact MMi-6000' characterized by 45Hv0.1 shows the deeper penetration depth among the mechanical mille samples. By the way, despite the lower hardness than AT-Cu (103Hv0.1) MMi-6000 shows an unexpected and higher abrasion resistance.

MMCs are characterized by a lower penetration depth. For low applied load a slightly deeper penetration depth has been recorded for MMC-240' in comparison with MMC-80', although the higher hardness 207 and 130 Hv0.1 respectively. Cu-Be alloy shows the lowest penetration depth due to its higher hardness, close to 400Hv0.1. In Figure VII-30 the penetration depth as function of applied load are shown; also OM micrographs of scratch grooves at 3N for AT-Cu, MM-240' and MMC-240 has been reported as representative of each range of penetration depth.

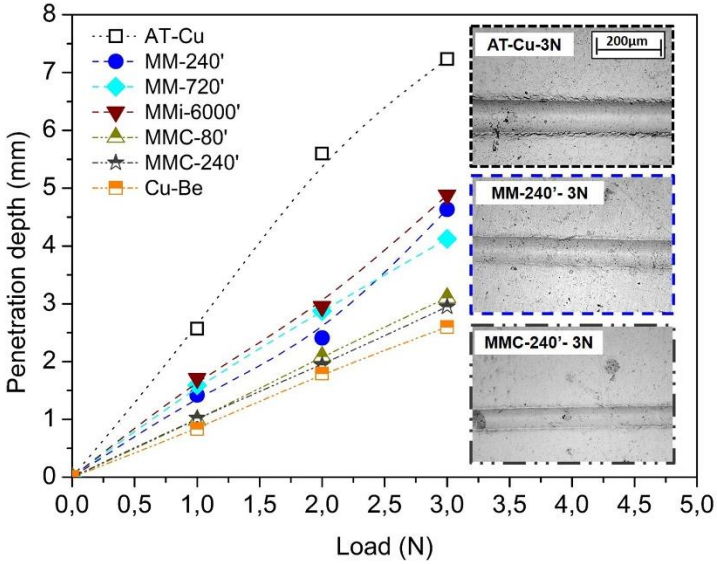

Figure VII – 30. Penetration depth of scratch test of all the materials as function of applied load; and OM micrographs of scratch grooves of AT-Cu, MM-240' and MMC-240' samples at 3N.

Increasing the load the penetration depth consequently increases (Futami et al., 2009). Although the increased load, the materials still showing the same behaviour of Figure VII-29, and the three ranges of penetration depth still evident. AT-Cu exhibits the deeper penetration depth independently of the load. Increasing the hardness the penetration depth decreases, especially changing from MM to MA, as reported in Figure VII-31. This confirms the validity and the benefits promoted by MM, and especially by MA. MMCs show a penetration depth similar to Cu-Be even at higher load, and this is very satisfying and promising.

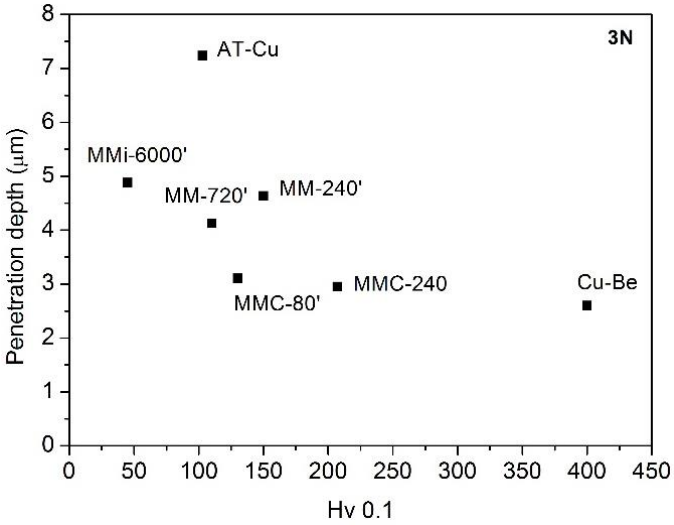

Figure VII – 31. Penetration depth of scratch test at 3N of all the materials as function of hardness.

The dependence of penetration depth with hardness is clearer for scratch test than for sliding test because this test is very short and any heating, which could severely affect the test, occurs. The formation of oxide is avoided and the performance of the material is related to its intrinsic properties. By the OM micrographs reported in Figure VII-30 it is evident how AT-Cu shows a deeper and larger scratch groove than mechanical milled and mechanical alloyed samples. The groove of AT-Cu is characterized by deformed and irregular edges attesting an elastoplastic microcracking due to its poor hardness, this result is in accordance with Futami et al. work. Usually a scratched surface shows 4 stages of damage as function of the applied load: an elastic/plastic sliding, a plastic plowing, an elastoplastic microcracking, and a fracturing and chipping of the surface scratched (Futami et al., 2009). Among the damages stated above, AT-Cu shows the first three stages, instead mechanical milled and mechanical alloyed materials exhibit only the first two.

As thermal conductivity and wear resistance point of view it can be concluded that the target of this PhD thesis has been reached by a good compromise between the two properties, especially for MMC-240', as shown by the update map of chapter III reported in Figure VII-32.

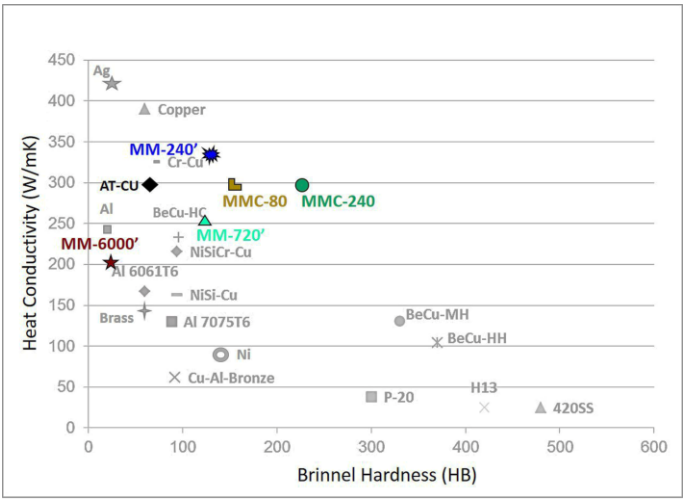

Figure VII - 32. Brinnel hardness versus heat conductivity map.

7.3 Mechanical properties

As a final step of this PhD work, a preliminary investigation on the tensile properties was carried out. Figure VII-33a and Figure VII-33b show the tensile stress-strain curves of the samples produced by MM and MA.

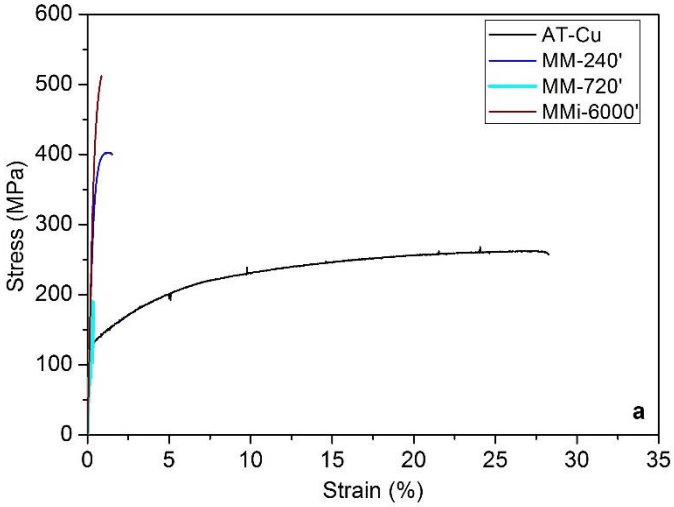

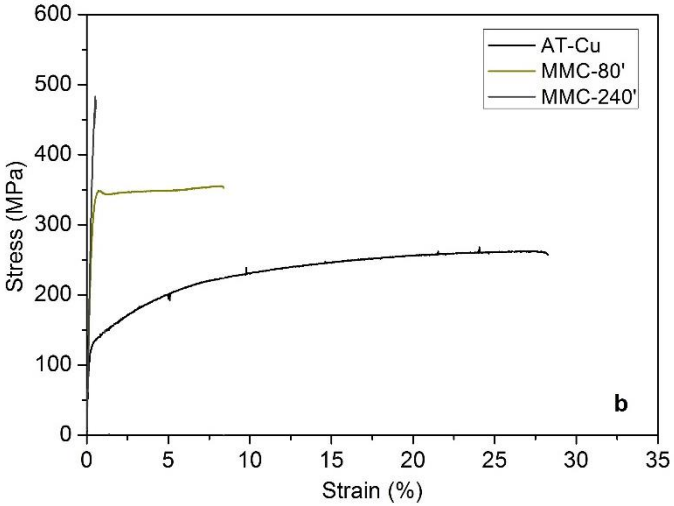

Figure VII - 33. Tensile stress-strain curves of the sintered MM (a) and MA (b) samples.

By Figure VII-33 it is evident how both MM and MA processes affect the mechanical behaviour of the sintered materials. AT-Cu is the only material showing a typical stress and strain curve of ductile material, thus exhibiting a continuous elongation up to 29% and a slight increase of the stress up to fracture. All the mechanical milled samples show a drastic decrease of the elongation but an increase of strength due to the severe strain hardening (Fig.VII-33a). MMC-240' show the same behaviour of the mechanical milled sample, meanwhile MMC-80' due to the shorter milling time highlights a different tensile stress-strain curve (Fig.VII-33b). It consists in an elastic deformation followed by yielding and a maximum stress. MMC-80 curve does not show the typical plastic instability, characterized by a continuous decrease of stress, but it shows a plastic field with almost no strain hardening and a plastic deformation reaching 8%. Table VII-2 reports the results of the tensile properties.

Table VII – 2. Tensile properties of testes samples

Sample	Yield stress (MPa)	UTS (MPa)	Elongation at fracture (%)
AT-Cu	110	276	28.8
MM-240'	209	418	1.7
MM-720'	164	226	0.3
MMi-6000'	490	510	1
MMC-80'	282	352	8.2
MMC-240'	451	489	1.2

By the characterization of the fracture surfaces using SEM, it has been possible to evaluate the mechanical behaviour of the materials and the effective consolidation of the powders. Firstly in Figure VII-34 the fracture surface of AT-Cu is shown.

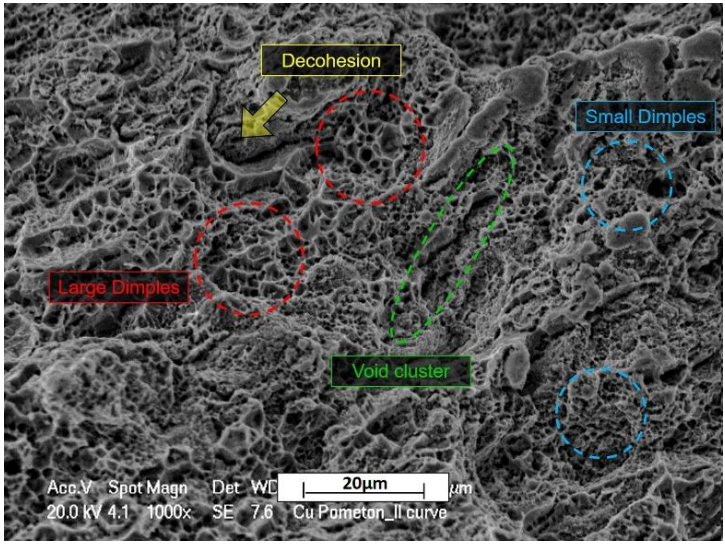

Figure VII - 34. Fracture surfaces of the sintered AT-Cu specimen.

Regarding AT-Cu, its fracture morphologies revealed clearly typical shallow dimples with different sizes, distributed throughout the fracture surfaces. Dimples are significant of a ductile fracture and, in turn, of bonding occurred between particles. As can be realized from Figure VII-34, the fracture surface seem to consist of a bimodal size distribution of dimples, large (red) and small (blue) dimples. The small dimples possess their sizes of about 1µm, the coarser ones show the 10µm in size at the largest. Another interesting feature should be mentioned here is the presence of interparticle space between some particles (yellow) which may favour the failure of the sample. The fracture could also initiates within void clusters as a result of a sequence of voids nucleation, growth and coalescence (green). After AT-Cu, MMC-80' is the only strain hardened material showing a considerable elongation during test because the loss in ductility is limited by the shorter milling time in comparison with the other materials. The fracture surface of MMC-80' also evidences both dimpled areas (blue) and areas where the flake-like morphology of the starting powder is visible (Fig.VII-35). The flake-like morphology recalls the structure of the mechanical alloyed powder and is significant of lack of bonding: fracture occurred by interparticle propagation of cracks (yellow).

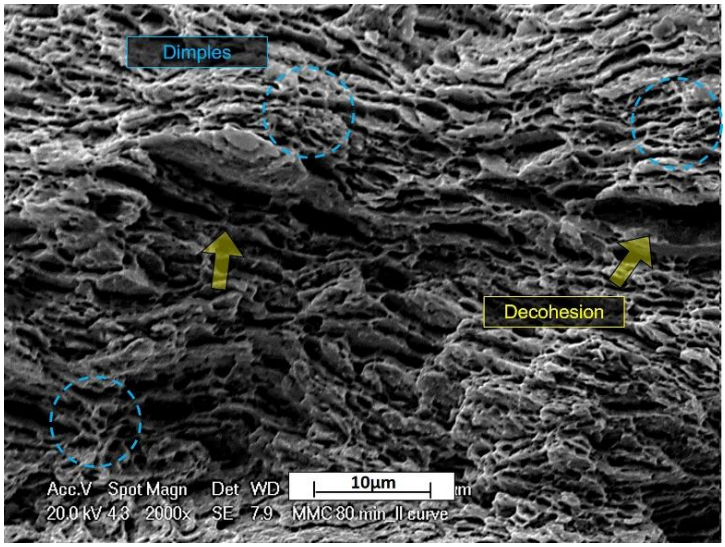

Figure VII - 35. Fracture surfaces of the sintered MMC-80' specimen.

A clear change of fracture mode is evidenced by mechanical milled and mechanical alloyed sample milled for long time (240 and 720 minutes), they show a more brittle fracture morphology. In this material trans-particle fracture is combined with clear traces of inter-particle fracture (Fig.VII-36). The generally brittle nature of fracture can be explained by the higher hardness of long-time milled sample, promoted by the stronger strain hardening and the more effective strengthening effect of TiB_2. Nevertheless, both effects reduce ductility together with porosity, which was shown to increase by increasing milling time. A quite interesting feature is the ductile nature of the inter-particle fracture of re-crystallized regions, characterized by fine dimples (blue) (Fig.VII-37). Re-crystallization is the results of the higher temperature reached during SPS at the contact area between particles, due to the local preferential current flow.

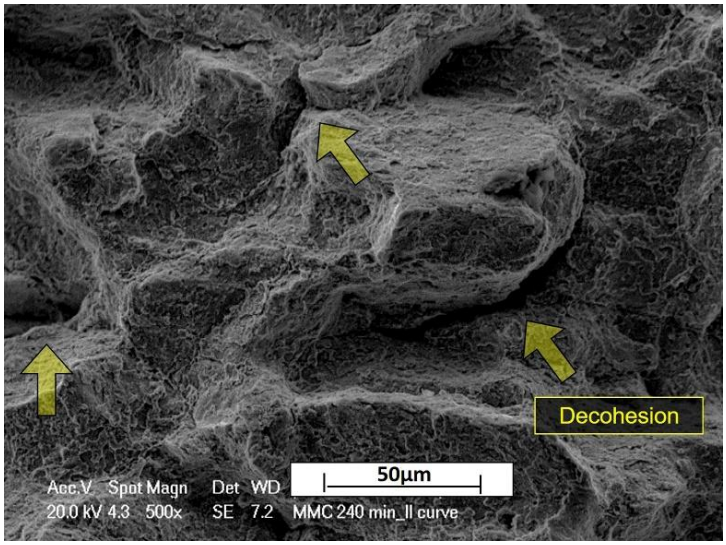

Figure VII - 36. Fracture surfaces of the sintered MMC-240' specimen.

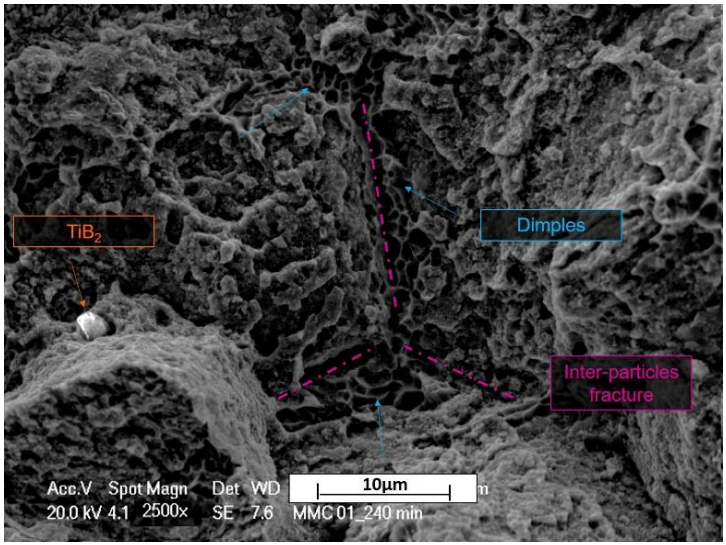

Figure VII - 37. Detail of the fracture surfaces of the sintered MMC-240' specimen.

A totally different fracture surface is shown by MMi-6000'. The specimen does not show any evidence of the typical ductile behaviour of copper, since fracture has been propagated along the prior particle boundaries, indicating a poor consolidation.

The poor consolidation is associate to the high oxidation state of the milled particles. It is important to recognize that copper oxide on particles plays an important role during SPS increasing the electrical resistance of the material and hindering the consolidation, as explained in chapter V. This effect is very clear in Figure VII-38, where each particle is recognizable and any formation of sintering neck is evident. In other words, MMi-6000' specimen is densified but not effectively sintered.

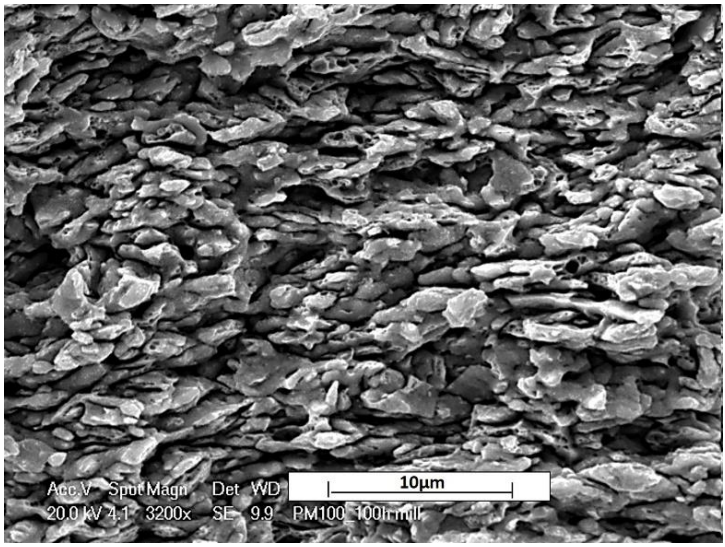

Figure VII – 38. Fracture surfaces of the sintered MMi-6000' specimen.

7.4 Conclusions

In this chapter a characterization of the materials produced by MM and MA have been carried out.

- Firstly has been demonstrate that thermal conductivity is more influenced by prolonged milling time than by the dispersion of a second hard phase. The high fraction of residual porosity increasing milling time leads to a drastic decrease of thermal conductivity. Meanwhile the MMCs show a competitive thermal conductivity in comparison with the commercial Cu-Be because they keep the same conductivity of copper despite the MA process.
- Then the sliding wear resistance and the abrasion wear resistance have been investigated. The sliding behaviour of almost all the materials except for MMi-6000' consists of two stages: a running in stage characterized by a high friction coefficient, then the attainment of a constant and lower value of friction coefficient

prolonging sliding time. During the first stage a severe adhesion phenomenon between the sample and the disc occurs by an intense transfer of material. Prolonging sliding test the high temperature promotes the transformation of the transferred layer into oxide, which acts as lubricant reducing the friction coefficient and the wear coefficient. A clear relation between hardness and wear coefficient has been found especially for long sliding time, increasing hardness the wear resistance increases. Since the oxide layer formed by a hard material is consequently harder than that of a softer material, it is more protective and less damaged during test. Moreover harder material are characterized by a higher load bearing capability to sustain and maintain in place the oxide layer. In fact in MMi-6000' which has a very low hardness an intense spalling of the oxide patches from the worn track is evident due to its low load bearing capability. By the way the hard materials show some drawbacks. Firstly due to their higher wear resistance they take more time to create the wear track and form the oxide layer, in fact they are characterized by a longer transition time from the running stage to the tribo-oxidative stage. Then the harder debris of MMC give a more intense abrasion contribution together with TiB_2 and AISI M3:2 carbides.

Furthermore the effect of the load has been analysed, and increasing the load four main events occur:

i. Friction coefficient decreases
ii. Friction coefficient stabilizes → lowers stick and slip phenomenon
iii. t_{ss} decreases and almost disappears applying 200N
iv. Regime temperature increases

Due to the more severe testing conditions the relation between hardness and wear coefficient is lost because all the material show the faster formation of the protective oxide layer leading to very low wear coefficients.

Sliding test highlights the limit of MMC-80', which has a strong microstructure anisotropy due to the flake like morphology of the milled powder. A severe delamination phenomenon occurs during sliding because flake particles are aligned to the tangential force enhancing the exfoliation process.

- AT-Cu exhibits the lower abrasion resistance followed by the mechanical milled sample and finally by the mechanical alloyed materials which have a penetration depth similar to the Cu-Be. The wear resistance to abrasion increases increasing the hardness of the material.
- Finally tensile tests show a loss of ductility and a gain of strength for all the mechanical milled and mechanical alloyed samples. Only MMC-80 keep partially the ductility of AT-Cu, its stress-strain curve consists in an elastic deformation, a yielding and a maximum stress followed by a plastic field with almost no strain hardening and a plastic deformation reaching 8%.
- The fracture surface analysis highlights a ductile fracture surface characterized by dimples for AT-Cu and partially for MMC-80'. By the way the flake-like

morphology of the fracture surface of MMC-80' recalls the structure of the mechanical alloyed. All the others material exhibit a brittle nature of fracture which can be explained by the higher hardness of long-time milled sample, promoted by the stronger strain hardening and the more effective strengthening effect of TiB_2. Nevertheless, both effects reduce ductility together with porosity, which was shown to increase by increasing milling time. The fracture consist in trans-particle fracture combined with clear traces of inter-particle fracture. A ductile nature of the inter-particle fracture of re-crystallized regions is evident. Finally in MMi-6000' fracture indicates a poor consolidation associable to the high oxidation state of the milled particles.

Chapter VIII

Conclusions

The aim of this PhD thesis was to increase the hardness and wear resistance of a copper preserving high thermal conductivity. For this purpose powder metallurgy has been employed to produce strain hardened and dispersion hardened copper matrix composites by mechanical milling (MM) and mechanical alloying (MA). Titanium diboride-TiB_2 has been selected for the production of metal matrix composites (MMC), due to the high hardness, thermal/chemical stability and the relatively high thermal conductivity compared to other ceramic materials. Spark Plasma Sintering (SPS) has been used for the consolidation. SPS allows sintering at lower temperature and in a shorter time comparing to more conventional processes like Hot Isostatic Pressing (HIP). Indeed the high heating rate peculiar of SPS preserves the fine microstructure produced by MM and MA, and reduces the interaction between the metal matrix and the reinforcing particles.

8.1 Mechanical milling

The first part of the research has been focused on the investigation of the MM process, paying special attention to the effect of milling parameters on the particle size, morphology and structure. In a second step, the effect of milling time on the sintering behaviour of the milled powders during SPS has been analysed. The main results are summarized as follows.

- Through the analysis of different process control agents (PCA) and ball to powder ratio (BPR), the best combination of particle size and particle morphology of copper milled powders have been found using 0.5wt% of stearic acid as PCA and a BPR equal to 10:1. These conditions limit the contamination level (i.e. Fe and Cr from the milling media)
- Continuous milling evidences two process stages: flaking dominates after relatively short milling time while welding prevails after longer time. Interrupted milling (2min ON-9min OFF) promotes an intense fracturing process after welding, leading to a very fine particle size.
- XRD analyses demonstrates a similar microstructure evolution during continuous and interrupted milling. Prolonging milling time causes a crystallite refinement down to nanometre range, a decrease of crystallite strain and dislocation density.

- The decomposition of PCA has been analysed in order to limit the residual porosity inside the sintered samples. The decomposition of PCA occurs in three steps: release of H_2O at 100°C, followed by emission of CO and CO_2 at 350°C, and finally H_2 at 500°C. These steps are affected by the particle size of the milled powders: by increasing particle size the decomposition of PCA is delayed towards higher temperature leading to high residual nano porosity if the SPS cycle is not properly selected. Good results have been obtained by small particle size (~10μm), by decreasing the heating rate from 100°C/min to 20°C/min up to 950°C and by applying the SPS pressure once the decomposition of PCA is completed at 950°C.
- The densification process during SPS is characterized by three main phenomena: powder rearrangement and local deformation before the application of the load followed by bulk particle deformation after loading. The entity of these phenomena depends on the particle size, morphology and on the strain hardening level accumulated during MM: the stronger strain hardening and the larger particle size due to longer milling time hinder the densification. The microstructure of sintered materials keeps memory of the original particles morphology, a severe anisotropy being observed when flaking prevails. Instead for large particle size some recrystallized area have been detected due to an intense overheating at the contact points between the powders.
- Powder milled for very long milling time (6000 minutes) shows an intense oxidation confirmed by the presence of 21vol% Cu_2O due to the very fine particle size. This severely hinders the consolidation, as well as the mechanical properties of the sintered material.
- The best combination of hardness and density has been obtained after 240 minutes of MM, with an increase of hardness from 90HB5 for atomized copper to 120HB5 for MM-240'. The decrease of hardness and density prolonging milling time up to 6000 minutes attests the limitations of MM as a processing method for strain hardened copper, and promotes the change toward MA.

8.2 Mechanical Alloying

The second part of the research has been focused on the investigation of the MA process between copper and 0.5wt% of TiB_2 powders (~3μm) as function of milling time. The following main results were obtained:

- Increasing milling time the evolution of particle size and morphology during MA is similar to continuous MM. Increasing milling time the particle size increases by the overlapping and welding events between the flakes like particles which promote also the MA of the two constituents. By increasing milling time the dispersion of the hard phase in the Cu matrix becomes more

homogeneous, refinement of TiB_2 particles is highlighted and also the adhesion between the two constituents is improved. The introduction of TiB_2 leads to a faster evolution of powder morphology and to the anticipation of the phenomena previously described for MM.

- The SPS evolution of mechanical alloyed sample is characterized by powder rearrangement, local and bulk deformation as MM process. The hardness increases with milling time due to the refinement of TiB_2 and its more uniform distribution, instead relative density decreases. The hardness shown by MMC almost doubles the value of MM sample, from 130 HB5 to 225 HB5 for the same milling time (240 minutes).

8.3 Properties of sintered MM-Cu and MA-Cu+TiB_2

The aim of the third and last part of the PhD thesis was to characterize the copper based materials produced by MM and MA. Thermal conductivity, wear behaviour under dry sliding and abrasion conditions and mechanical properties have been evaluated. The following main results have been found:

Thermal conductivity of Cu

- A detrimental effect of MM has been attested especially for long milling time. Considering the thermal conductivity of the starting copper (300W/mK) a drastic decrease of been highlighted prolonging milling time. After 720 and 6000 minutes of MM the thermal conductivity was 250 and 200W/mK respectively. The drop of thermal conductivity is related to the increase of residual porosity in the sintered samples.
- On contrary MA shows some interesting and promising results keeping the thermal conductivity of MMC comparable to atomized copper sample (300W/mK) and much higher than the commercial Cu-Be alloy (106W/mK). For mechanical alloyed material the presence of a limited fraction (0.5wt%) of TiB_2 is not detrimental, rather it is positive for strain hardening and ineffective for thermal conductivity.

Sliding wear resistance

Friction

- All the materials show the same tribological evolution under dry sliding wear conditions against an AISI M3:2 (65HRC): a severe adhesion phenomena characterized by a high friction coefficient close to 1 for short sliding time, followed by the predominance of a tribo-oxidative mechanism with the attainment of a lower friction coefficient close to 0.7 prolonging sliding time. The formation of the oxide layer is favoured by the creation of the wear track during the running-in stage, in fact the wear debris produced during this stage

can be compacted and transferred from the sample to the disc surface, especially at high temperature.

- Softer materials show a shorter transition time from high to steady state friction (t_{ss}) coefficient. Hard material due to their higher wear resistance take more time to switch for not conformal to conformal contact and the formation of oxide layer is slightly delayed and t_{ss} increases.
- MMCs show a higher friction coefficient due to the additional abrasive contribution of hard particles and of the harder wear debris produced during sliding.

Wear resistance

Low load (50N)

- Once the sliding time increase and the steady state regime is achieved, the wear resistance is governed by hardness. Harder material (MMC) can better sustain the oxide protective layer due to their high load bearing capability, improved by the strain hardening and in the case of composite milled for 240 minutes by the better dispersion of the TiB_2 particles. The wear coefficient of atomized copper has been increased from $2{,}12x10^{-12}$ m^3/m to $1.5x10^{-12}$ m^3/m for MMC milled for 240 minutes.
- Sliding test highlights the limit of MMC-80', which has a strong microstructure anisotropy due to the flake like morphology of the milled powder. A severe delamination phenomenon occurs during sliding because flake particles are aligned to the tangential force enhancing the exfoliation process.
- Material mechanically milled for 6000 minutes exhibits a poor wear resistance evidenced by a severe spalling phenomenon due to the low hardness.

Higher load (100 and 200N)

- Increasing the load following phenomena where observed:
  i. Regime temperature increases ⇨ easier formation of the oxide layer.
  ii. Friction coefficient decreases due to the predominance of tribo-oxidation;
  iii. Friction coefficient stabilizes ⇨ less intense stick and slip phenomenon;
  iv. t_{ss} decreases and almost disappears applying 200N;
  v. Wear coefficient decreases;

  Due to the more severe testing conditions the relation between hardness and wear coefficient is lost because all the material show a faster formation of the protective oxide layer leading to very low wear coefficients, $4.22X10^{-13}m^3/m$ for MMC milled for 240 minutes.

Abrasion wear resistance

- The abrasive wear behaviour, determined by the scratch test method, evidenced the positive influence of a higher hardness. For all the applied load it can be noticed that:
  i. AT-Cu shows the deeper penetration depth;

ii. Mechanically milled samples show an intermediate penetration;
iii. Mechanically alloyed composites show the lowest penetration depth, approaching that of the Cu-Be reference alloy.

The abrasion wear resistance of MMC is competitive with Cu-Be alloy thanks to the intense mechanical strain hardening combined with a uniform dispersion hardening.

Tensile test

- Tensile tests show a loss of ductility and improved strength for all the mechanical milled and mechanical alloyed samples. Only MMC milled for 80 minutes keeps partially the ductility of atomized copper (29% of elongation) reaching 8% of strain due to the shorter milling time. All the other materials show an elongation lower than 1%. Ultimate tensile strength has been increased from 276MPa of copper to 489MPa of MMC milled for 240 minutes.
- Only the fracture surface of atomized copper highlights a ductile fracture surface characterized by dimples. All the others mechanical milled material exhibit a brittle nature of fracture consisting in trans-particle fracture combined with clear traces of inter-particle fracture. The fracture of copper milled for 6000 minutes indicates a poor consolidation associable to the high oxidation state of the milled particles.
- The fracture surface analysis highlights a partial ductile fracture surface for MMC milled for 80 minutes. By the way the flake-like morphology of the fracture surface recalls the structure of the mechanical alloyed powder and is significant of lack of bonding. MMC milled for 240 minutes exhibits a brittle nature of fracture promoted by the stronger strain hardening and the more effective strengthening effect of TiB_2. Nevertheless, both effects reduce ductility together with porosity, which was shown to increase by increasing milling time.

In general MMC samples show better performance than mechanical milled samples. MMCs gain a competitive improvement of hardness and wear resistance maintaining an acceptable thermal conductivity. These results broadens horizons of the research toward MMC with a higher fraction of TiB_2. Since any decrease of thermal conductivity will be revealed in MMC, an increase of TiB_2 content can be favoured in order to increase the hardness and the wear resistance. It can be concluded that the goal of the PhD thesis has been achieved, by the way the study deserves further investigations in order to improve the performance of copper matrix composites.

List of abbreviations and acronyms

BPR	ball to powder ratio
ECAP	equal channel angular pressing
EDXS	energy-dispersive X-ray spectroscopy
HIP	hot isostatic pressing
HP	hard particle
HPT	high pressure torsion
MA	mechanical alloying
MM	mechanical milling
MMC	metal matrix composite
OM	optical microscopy
PCA	process control agent
PVD	physical vapour deposition
SEM	scanning electron microscopy
SMAT	surface mechanical attrition treatment
SPD	severe plastic deformation
SPS	spark plasma sintering
TEM	transmission electron microscopy
XRD	X-rays diffraction

References

Akhtar F., S.J. Askari, K.A. Shah, X. Du, S. Guo, *Microstructure, mechanical properties, electrical conductivity and wear behavior of high volume TiC reinforced Cu-matrix composites*. Materials characterization, **2009**. 60: p. 327-336.

Anderson K.R., J.R. Groza, *Microstructural evolution and thermal stability of precipitation-strengthened Cu-8Cr-4Nb alloy.* Material Science Engineering A, **1993**. 169: p. 167-75.

Andrews P.V., M.B. West, C.R. Robeson, *The effect of grain boundaries on the electrical resistivity of polycrystalline copper and aluminum.* Philosophical Magazine, **1969**. 19: p. 887-898.

Anselmi-Tamburini U., G. Spinolo, F. Maglia, I. Tredici, T.B. Holland, *Field Assisted Sintering Mechanisms.* Engineering Materials. **2013**. 35: p. 159-193.

Anselmi-Tamburini U., S. Gennari, J.E. Garay, Z.A. Munir, *Fundamental investigation on the spark plasma sintering/synthesis process II. Modeling of current and temperature distributions.* Material Science and Engineering A, **2005**. 394: p. 139-148.

Ashby M.F., *Materials selection in mechanical design*, Editor **2011**, Butterworth-Heinemann by Elsevier, 4th Edition.

Avelar-Batista J.C., E. Spain, M. Letch, J. Housden, R. Beechey, *Improvements on the wear resistance of high thermal conductivity Cu alloys using an electroless Ni-P coating prior to PVD deposition.* Surface & Coatings Technology, **2006**. 201: p. 4052-4057.

Azabou M., H.I. Gharsallah, L.Escoda, J.J. Sunol, A.W. Kolsi, M. Khitouni, *Mechanochemical reactions in nanocrystalline Cu-Fe system induced by mechanical alloying in air atmosphere*. Powder Technology, **2012**. 224: p. 338-344.

Bailon-Poujol I., J.P. Bailon, G. L'Esperance, *Ball-mill grinding kinetics of master alloys for steel powder metallurgy applications.* Powder Technology, **2011**. 210: p. 267-272.

Barella S., A. Gruttadauria, C. Mapelli, D. Mombelli, *Investigation of failure and dameges on continuous casting copper mould.* Engineering Failure Analysis, **2014**. 36: p. 432-438.

Benchabane G., Z. Boumerzoug, T. Gloriant, I. Thibon, *Microstructural characterization and recrystallization kinetics of cold rolled copper*. Physica B: Condensed Matter, **2011**. 406: p. 1973-1976

Benjamin J.S., *Dispersion Strengthened Speralloys by Mechanical Alloying*. Metallurgical Transaction, **1970**. 1: p. 2943-2951.

Berns H., N. von Chuong, *A new microstructure for PM tooling material*. Metallugical Physical Advanced Technology, **1996**. 6: p. 61-71.

Berns H., F.D. Sinesio, *Effect of coarse hard particles on high-temperature sliding abrasion of new metal matrix composites*. Wear, **1997**. 203-204: p. 608-614.

Berns H., S. Koch, *Influence of abrasive particle on wear mechanisms and wear resistance in sliding abrasion tests at elevated temperature*. Wear, **1999**. 233-235: p. 424-430.

Berns H., *Comparison of wear resistant MMC and white cast iron*. Wear, **2003**. 254: p. 47-54.

Besenbach F., J.K. Norskow, *Oxygen chemiasorption on metal surfaces: General trends of Cu, Ni and Al.* Process in Surface Science, **1993**. 44: p. 5-66.

Bhattacharya P., P. Bellon, R.S. Averback, S.J. Hales, *Nanocrystalline TiAl powders synthesized by high-energy ball milling: effects of milling parameters on yield and contamination.* Journal of Alloys and Compounds, **2004**. 368: p. 187-196.

Biselli C., D.G. Morris, N. Randall, *Mechanical alloying of high-strength copper alloys containing TiB_2 and Al_2O_3 dispersoid particles.* Scripta Metallurgica et Materialia, **1994**. 30: p. 1327-1332.

Boey P., W. Ho, S.J. Bull, *The effect of temperature on the abrasive wear of coating and hybrid surface treatments for injection-moulding machines.* Wear, **2005**. 258: p. 149-156.

Bonnenfant D., F. Mazerolle, P. Suquet, *Compaction of powders containing hard inclusions: experiments and micromechanical modelling*. Mechanics of Materials, **1998**. 29: p. 93-109.

Botcharova E., M. Heilmaier, J. Freudenberger, G. Drew, D. Kudashow et al., *Supersatured solid solution of niobium in copper by mechanical alloying.* Journal of Alloys and Compounds, **2003**. 351: p. 119-125.

Bouvard D., *Densification behavior of mixtures of hard and soft powders under pressure*. Powder Technology, **2000**. 111: p. 231-239.

Bull S.J., Q. Zhou, *A simulation test for wear in injection moulding machines.* Wear, **2001**. 249: p. 372-378.

Chen X.J., K.A Khor, S.H. Chan, L.G. Yu, *Overcoming the effect of contaminant in solid oxide fuel cell (SOFC) electrolyte: spark plasma sintering (SPS) of 0.5wt% silica-doped yttria-stabilized zirconia (YSZ).* Materials Science and Engineering A. **2004**. 374: p. 64–71.

Dash K., B.C. Ray, D. Chaira, *Synthesis and characterization of copper-alumina metal matrix composite by conventional and spark plasma sintering*. Journal of Alloys and Compounds, **2012**. 516: p. 78-84.

De Hoff R.T., F.N. Rhines, *Quantitative microscopy*, Editor **1968** by Mc Graw-Hill Book Co, New York.

Delie F., D. Bouvard, *Effect of inclusion morphology on the densification of powder composites.* Acta Materialia, **1998**. 46: p. 3905-3913.

Deshpande P.K., R.Y. Lin, *Wear resistance of WC particle reinforced copper matrix composites and the effect of porosity.* Materials Science & Engineering A, **2006**. 418: p. 137-145.

Diouf S., A. Molinari, *Densification mechanisms in spark plasma sintering: Effect of particle size and pressure.* Powder Technology, **2012 [1]**. 221: p. 220-227.

Diouf S., C. Menapace, A. Molinari, Study of the effect of particle size on densification of copper during s*park plasma sintering.* Powder Metallurgy, **2012 [2]**. 55: p. 3-7.

Diouf S., C. Menapace, M. D'Incau, A. Molinari, G. Ischia, *Spark plasma sintering of crymilled copper powder.* Powder Metallurgy, **2013**. 56: p. 420-426.

Elsayed A., W. Li, O. A. El Kady, W. M. Daoush, E.A. Olevsky, *Experimental investigations on the synthesis of W-Cu nanocomposite through spark plasma sintering.* Journal of Alloys and Compounds, **2015**. 639: p. 373-380.

Estrada-Guel I., C. Carreno-Gallardo, C. Leyva-Porras, R. Martinez-Sanchez, *Effect of process parameters on micro and macro-properties of an Al-based nanocomposite prepared by means of mechanical milling.* Journal of Alloys and Compounds, **2014**. 586: p. S85-S89.

Eyre T.S., *Wear mechanisms*. Powder Metallurgy, **1981**. 2: p. 57-63.

Fedrizzi A., M. Pellizzari, M. Zadra, *Influence of particle size ratio on densification behavior of AISI H13/AISI M3:2 powder mixture.* Powder Technology, **2012**. 228: p. 435-442.

Fogagnolo J.B., F. Velasco, M.H. Robert, J.M. Torralba, *Effect of mechanical alloying on the morphology, microstructure and properties of aluminum matrix composite powders.* Materials Science and Engineering, **2003**. A342: p. 131-143.

Futami T., M. Ohira, H. Muto, M. Sakai, *Contact/scratch-induced surface deformation and damage of copper-graphite particulate composites.* Carbon, **2009**. 47: p. 2742-2751.

Gan K, M. Gu, *The compressibility of Cu/SiC_p powder prepared by high-energy ball milling.* Journal of Materials Processing Technology, **2008**. 199: p. 173-177.

Gao Y., J.C. Jie, P.C. Zhang, et al., *Wear behavior of high strength and high conductivity Cu alloys under dry sliding.* Transactions of Nonferrous Metals Society of China, **2015**. 25: p. 2293-2300.

Gelbstein Y., Y. Haim, S. Kalabukhov, A. Kasiyan, *Correlation between thermal and electrical properties of spark plasma sintered porous copper*. Material Science-Sintering techniques of Materials, Editor **2015**, InTech

German R.M., *Prediction of sintered density for bimodal powder mixtures.* Metallurgical Transactions A, **1992[1]**. 23A: p. 1455-1465.

German R.M., *Sintering densification for powder mixtures of varying distribution widths*. Acta Metallurgica Materialia, **1992[2]**. 40: p. 2085-2089.

Gheisari K., S. Javadpour, *The effect of process control agent on the structure and magnetic properties of nanocrystalline mechanically alloyed Fe-45% Ni powders.* Journal of Magnetism and Magnetic Materials, **2013**. 343: p. 133-137.

Gilman P.S., J.S. Benjamin, *Mechanical alloying*. Annual Review of Materials Science, **1983**. 13: p. 279-300.

Girish B.M., B.R. Basawaraj, B.M. Satish, D.R.Somashekar, *Electrical resistivity and mechanical properties of tungsten carbide reinforced copper alloy composites.* International Journal of Composite Materials, **2012**. 2(3): p. 37-42.

Gleiter H., *Nanocrystalline Materials.* Progress in Material Science, **1968**. 33: p. 223-315.

Gomez B., E. Gordo, J.M. Torralba, *Influence of milling time on the processing of Fe-TiCN composites.* Materials Science and Engineering A, **2006**. 430: p. 59-63.

Gordo E., B. Gomez, E.M. Ruiz-Navas, J.M. Torralba, *Influence of milling parameters on the manufacturing of Fe-TiCN composite powders.* Journal of Materials Processing Technology, **2005**. 162-162: p. 59-54.

Groza J.R., J.C. Gibeling, *Principles of particle selection for dispersion-strengthened copper.* Materials Science and Engineering, **1993**. A171: p. 115-125.

Guo M.X., Wang M.P., *The relationship among microstructure evolution, mechanical property and in situ reaction mechanisms in preparing Cu-1.6wt%TiB_2 alloys.* Materials Chemistry and Physics, **2013**. 138: p. 95-101.

Harris A.M., G.B. Schaffer, N.W. Page, *The morphological evolution of hollow shells during the machanicl milling of ductile metals.* Scripta Materialia, **1996**. 34: p. 67-73.

Huang J.Y, Y.K. Wu, H.Q. Ye, *Ball milling of ductile metals.* Materials Science and Engineering A, **1995**. 199: p. 165-172.

Huang J.Y, Y.K. Wu, H.Q. Ye, *Deformation structures in ball milled copper*. Acta Materialia, **1996**. 44: p. 1211-1221.

Hulbert D.M., A. Anders, J. Andersson, E.J. Lavernia, A.K. Mukherjee, *A discussion on the absence of plasma in spark plasma sintering*. Scripta Materialia, **2009**. 60: p. 835-838.

Jaw K.S., C.K. Hsu, J.S. Lee, *The thermal decomposition behaviors of stearic acid, paraffin wax and polyvinyl butyral*. Thermochimica Acta, **2001**. 367-368: p. 165-168.

Kaczmar J.W., K. Granat, A. Kurzawa, E. Grodzka, *Physical properties of copper based MMC strengthened with alumina.* Achieves of foundry engineering, **2014**. 14: p. 85-90.

Khaleghi E., M. Torikachvili, M.A. Meyers, E.A. Olevsky, *Magnetic enhancement of thermal conductivity in copper-carbon nanotube composites produced by electroless plating, freeze drying, and spark plasma sintering.* Materials Letter, **2012**. 79: p. 256-258.

Khayati G.R., K. Janghorban, *An investigation on the application of process control agents in the preparation and consolidation behavior of nanocrystalline silver by mechanochemical method*. Advanced Powder Technology, **2012**. 23: p. 808-813.

Khayati G.R., E. Nourafkan, G. Karimi, J. Moradgholi, *Synthesis of cuprous oxide nanoparticles by mechanochemical oxidation of copper in high planetary energy ball mill.* Advanced Powder Technology, **2013**. 24: p. 301-305.

Khitouni M., R. Daly, M. Mhadhbi, A. Kolsi, *Structural evolution in nanocrystalline Cu obtained by high-energy mechanical milling: Phases formation of copper oxides.* Journal of Alloys and compounds, **2009**. 475: p. 581-586.

Khoshkhoo M.S, S. Sudino, J. Bednarcik, A. Kauffmann, *Mechanism of nanostructure formation in ball-milled Cu and Cu-3wt%Zn studied by X-ray diffraction line profile analysis*, Journal of Alloys and Compounds, **2014**. 588: p. 138-143.

Kleiner S., F Bertocco, F.A. Khalid, O. Beffort, *Decomposition of process control agent during mechanical milling and its influence on displacement reactions in the Al.TiO_2 system.* Materials Chemestry and Physics, **2005**. 89: p. 362-366.

Kwon D.H., J.W. Kum, T.D. Nguyen, D. Dudina, P.P. Choi, et al., *Production of dispersion-strengthened Cu-TiB_2 alloys by ball-milling and spark-plasma sintering.* Materials Science Forum, **2007**. 534-536: p. 1489-1492.

Kwon D.H., T.D. Nguyen, K.X. Huynh, et al., *Mechanical, electrical and wear properties of Cu-TiB_2 nanocomposites fabricated by MA-SHS and SPS.* Journal of Ceramic Processing Research, **2006**. 7: p. 275-279.

Landauer R., *The electrical resistance of binary metallic mixtures. Journal of Applied Physics*, **1952**. 23: p. 779-784.

Long B.D, H. Zuhailawati, M. Umemoto, Y. Todaka, R. Othman, *Effect of ethanol on the formation and properties of a Cu-NbC composite*. Journal of Alloys and Compounds. **2010[1]**. 503: p. 228-232.

Long B.D., R. Othman, M. Umemoto, H. Zuhailawati, *Spark plasma sintering of mechanically alloyed in situ copper-niobium carbide composite*. Journal of Alloys and Compounds, **2010[2]**. 505: p. 510-515.

Lu J., S. Shu, F. Qiu, Y. Wang, Q. Jiang, *Compression properties and abrasive wear behavior of high volume fraction TiC_x-TiB_2/Cu composites fabricated by combustion synthesis and hot press consolidation.* Materials and Design, **2012**. 40: p. 157-162.

Luo W.T., C.J. Li, G.J. Yang, *Correlation between milling conditions and iron contamination, microstructure and hardness of mechanically alloyed cubic BN particle reinforced NiCrAl matrix composite powders.* Journal of Alloys and Compounds, **2013**. 548: p. 180-187.

Luo X.T., G.J. Yang, C.J. Li, *Preparation of cBNp/NiCrAl nanostructured composite powders by a step-fashion mechanical alloying process*. Powder Technology, **2012**. 217: p. 591-598.

Lutterotti L., *Materials Analysis Using Diffraction (MAUD)*, **1997**. http://www.ing.unitn.it/~maud/

Ma Z.Y., S.C. Tjong, *High temperature creep behavior of in-situ TiB_2 particulate reinforced copper-based composite.* Materials Science and Engineering A, **2000**. 284: p. 70-76.

Madavali B., J.H. Lee, J.K. Lee, K.Y. Cho, C. Suryanarayana, S.J. Hong, *Effects of atmosphere and milling time on coursing of copper powders during mechanical milling*. Powder Technology, **2014**. 256: p. 251-256.

Marques M.T., V. Livramento, J.B. Correia, A. Almeida, R. Vilar, *Study of early stages of Cu-NbC nanocomposite synthesis.* Journal of Alloys and Compounds, **2007**. 434-435: p. 481-484.

Maurice D., T.H. Courtney, *The physics of mechanical alloying: A first report.* Metallurgical Transactions A, **1990**. 21A:p. 289-303.

Maurice D., T.H. Courtney, Modeling of mechanical alloying: Part I. *Deformation, Coalescence, and Fragmentation Mechanisms.* Metallurgical and Materials Transactions A, **1994**. 25A: p. 147-158.

Maurice D., T.H. Courtney, *Modeling of mechanical alloying: Part III. Applications of computational programs.* Metallurgical and Materials Transactions A, **1995**. 26A:p. 2437-2444.

Menapace C., G. Cipolloni, M. Hebda, G. Ischia, *Spark plasma sintering behavior of copper powder having different particle size and oxygen contents.* Powder Technology, **2016**. 291: p. 170-177.

Mishra A., V. Richard, F. Gregori, R.J. Asaro, *Microstructural evolution in copper processed by severe plastic deformation.* Material Science Engineeering A, **2005**. 410-411: p. 290-298.

Munir Z.A., U. Anselmi-Tamburini, M. Ohyanagi, *The effect of electric field and pressure on the synthesis and consolidation of materials: A review of the spark plasma sintering method.* J. Mater. Sci. **2006**. 41: p. 763-777.

Nakamichi I., *Electrical resistivity and grain boundaries in metals*. Material Science Forum, **1996**. 207-209: p. 47-58.

Nefedova E., E. Aleksandrova, E. Grigoryev, E.A. Olevsky, *Research high-temperature consolidation of nanostructured bimodal materials.* Physics Procedia, **2015**. 72: p. 390-393.

Nikzad L., R. Licheri, T. Ebadzadeh, R. Orrù, G. Cao, *Effect of ball milling on reactive spark plasma sintering of B_4C-TiB_2 composite*. Ceramics International, **2012**. 38: p. 6469-6480.

Olevsky E.A., L. Froyen, *Constitutive modelling of spark plasma sintering of conductive materials,* Scripta Materialia, **2006**. 55: p. 1175-1178.

Olevsky E.A., S. Kndukuri, L. Froyen, *Consolidation enhancement in spark-plasma sintering: Impact of high heating rates.* Journal of Applied Physics, **2007**. 102: p. 1149131-12.

Onat A., *Mechanical and dry sliding wear properties of silicon carbide particulate reinforced aluminum-copper alloy matrix composites produced by direct squeeze casting method*. Journal of Alloys and Compounds, **2010**. 489: p. 119-124.

Ondracek G., B. Shulz, *The porosity dependence of the thermal conductivity for nuclear fuels.* Journal of Nuclear Materials, **1973**. 46: p. 253-258.

Orlov D., H. Fujiwara, K. Ameyama, *Obtaining copper with harmonic structure for the optical balance of structure-performance relationship.* Materials Transictions, **2013**. 54: p. 1549-1553.

Pellizzari M., A. Fedrizzi, M. Zadra, *Influence of processing parameters and particle size on the properties of hot work and high speed tool steels by spark plasma sintering*. Materials and Design, **2011 [1]**. 32: p.1796-1805.

Pellizzari M., A. Fedrizzi, M. Zadra, *Spark Plasma co-Sintering of hot work and high speed steel powders for fabrication of a novel tool steel with composite microstructure*. Powder technology, **2011[2]**. 214: p. 292-299.

Petzow G., *Metallographic Etching*, Editor **1999** by ASM International.

Pietrak K., T.S. Wisniewski, *A Review of models for effective thermal conductivity of composite materials.* Journal of Powder Technologies, **2015**. 95: p. 14-24.

Poluboyarov V.A., A.E. Lapin, Z.A. Korotaeva, I.P. Prosvirin, V.I. Bukhtiyarov et al., *Effect of mechanical activation on the reactivity of powder copper.* Inorganic Materials, **2005**. 41: p. 110-119.

Pramanik A., L.C. Zhang, J.A. Arsecularatne, *Deformation mechanisms of MMCs under indentation*. Composite Science and Technology, **2008**. 68: p. 1304-1312.

Prasad Y.V.R.K., K.P. Rao, *Influence of oxygen on rate-controlling mechanisms in hot deformation of polycrystalline copper: oxygen-free versus electrolytic grades.* Materials Letter, **2004**. 58: p. 2061-2066.

Raghu T., R. Sundaresan, P. Ramakrishnan, T.R. Rama Mohan, *Synthesis of nanocrystalline copper-tungsten alloys by mechanical alloying*. Materials Science and Engineering A, **2001**. 304-306: p. 438-441.

Rajkovic V., D. Bozic, M.T. Jovanovic, *Characterization of prealloyed copper powders treated in high energy ball mill*. Materials Characterization, **2006**. 57: p. 94-99.

Rajkovic V., D. Bozic, M.T. Jovanovic, *Properties of copper matrix reinforced with various size and amount of Al_2O_3 particles.* Journal of materials processing technology, **2008**. 200: p. 106-114.

Richardson R.C.D., *The wear of metals by relatively soft abrasives*. Wear, **1968**. 11: p. 245-275.

Rietveld H.M., *A profile refinement method for nuclear and magnetic structures*. Journal of Applied Crystallography, **1969**. 2: p. 65-71.

Risbud S.H., J.R. Groza, M.J. Kim**,** *Clean grain boundaries in aluminium nitride ceramics densified without additives by a plasma-activated sintering process.* Philosophical Magazine Part B. **1994**. 69(3): p. 525-533.

Ritasalo R., M.E. Cura, X.W. Liu, O. Soderberg, T. Ritvonen et al., *Spark plasma sintering of submicron-sized Cu-powder. Influence of processing parameters and powder oxidation on microstructure and mechanical properties.* Materials Science and Engineering A, **2010**. 527: p. 2733-2737.

Ruzic J., J. Stasic, V. Rajkovic, D. Bozic, *Strengthening effects in precipitation and dispersion hardened powder metallurgy copper alloys.* Materials and Design, **2013**. 49: p. 746-754.

Sahani P., S. Mula, P.K. Roy, P.C. Kang, C.C. Koch, *Structural investigation of vacuum sintered Cu-Cr and Cu-Cr-4% SiC nanocomposites prepared by mechanical alloying.* Materials Science and Engineering, **2011**. A528: p. 7781-7789.

Samal C.P., J.S. Parihar, D. Chaira, *The effect of milling and sintering techniques on mechanical properties of Cu-graphite metal matrix composite prepared by powder metallurgy route.* Journal of Alloys and Compounds, **2013**. 569: p. 95-101.

Sato A., J. Kano, F. Saito, *Analysis of abrasion mechanism of grinding media in planetary mill with DEM simulation.* Advanced Powder Technology, **2010**. 21: p. 212-216.

Setman D., M. Kerber, H. Bahmanpour, J. Horky, R.O. Scattergood, C.C. Koch, M.J. Zehetbauer, *Nature and density of lattice defects in ball milled nanostructured copper.* Mechanics of Materials, **2013**. 67: p. 59-64.

Sharma A.S., K. Biswas, B. Basu, D.Chakravarty, *Spark plasma sintering of nanocrystalline Cu and Cu-10 Wt Pct Pb alloy*. Metallurgical and Materials Transactions A, **2011**. 42: p. 2072-2084.

Sheibani S., A. Ataie, S. Heshmati-Manesh, G.R. Khayati, *Structural evolution in nano crystalline Cu synthesized by high energy ball milling.* Materials Letter, **2007**. 61: p. 3204-3207.

Sheibani S., A. Ataie, S. Heshmati-Manesh, *Role of process control agent on synthesis and consolidation behavior of nano-crystalline copper produced by mechano-chemical route*. Journal of Alloys and Compounds, **2008**. 465: p. 78-82.

Shukla A.K., N. Murty, R. S. Kumar, K. *Mondal, Spark plasma sintering of dispersion hardened Cu-Cr-Nb alloy powders.* Journal of Alloys and Compounds, **2013**. 577:p. 70-78.

Song X., X. Liu, J. Zhang**,** *Neck Formation and Self-Adjusting Mechanism of Neck Growth of conducting powders in Spark Plasma Sintering*. J. Am. Ceram. Soc. **2006**. 89(2): p. 494-500.

Srinivasarao B., C. Suryanarayana, K. Oh-Ishi, K. Hono**,** *Microstructure and mechanical properties of Al-Zr nanocomposite materials.* Materials Science and Engineering A. **2009**. 518(1-2): p. 100–107.

Srivatsan T.S., N. Narendra, J.D. Troxell, *Tensile deformation and fracture behavior of an oxide dispersion strengthened copper alloy*. Materials and Design, **2000**. 21: p. 191.198.

Stobrawa J.P., Z.M. Rdzawski, *Characterization of nanostructured copper-WC materials.* Journal of Achievements in Materials and Manufacturing Engineering, **2009**. 2: p. 171-178.
Straffelini G., M. Pellizzari, A. Molinari, *Influence of load and temperature on the dry sliding behaviour of Al-based metal-matrix composites against friction material*. Wear, **2004**. 256: p. 754-763.

Straffelini G., L. Maines, M. Pellizzari, P. Scardi, *Dry sliding wear of Cu-Be alloys.* Wear, **2005**. 259: p. 506-511.

Sule R., P.A. Olubambi, I. Sigalas, J.K.O. Asante, J.C Garrett, *Effect of SPS consolidation parameters on submicron Cu and Cu-CNT composites for thermal management.* Powder Technology, **2014**. 258: p. 198-205.

Suryanarayana C., *Mechanical alloying and milling*. Progress in Materials Science, **2001**. 46: p. 1-184.

Suryanarayana C., T. Klassen, E. Ivanov, *Synthesis of nanocomposites and amorphous alloys by mechanical alloying.* Journal of Materials Science, **2011**. 46: p. 6301-6315.

Theisen W., *Design of wear resistant alloys against abrasion. Proceeding of abrasion*, **2008**. p. 128-138.

Ting J.M., R.Y. Lin, *Effect of particle size distribution on sintering - part I modelling*. Journal of Materials Science, **1994**. 29: p. 1867-1872.

Ting J.M., R.Y. Lin, *Effect of particle size distribution on sintering - part II sintering*. Journal of Materials Science, **1995**. 30: p. 2382-2389.

Tjong S.C, K.C. Lau, *Abrasive wear behavior of TiB_2 particle-reinforced copper matrix composites.* Materials Science and Engineering A, **2000**. 282: p. 183-186.

Tokita M., *Mechanism of spark plasma sintering*. Journal of the Society of Powder technology, **1993**. 30: p. 790-804.

Tokita M., *Development of Large-Size Ceramic/Metal Bulk FGM Fabricated by Spark Plasma Sintering*. Material Science Forum, **1999**. 308-311: p. 83-88.

Tu J.P., W. Rong, S.Y. Guo, Y.Z. Yang, *Dry sliding behavior of in situ Cu-TiB_2 nanocomposites against medium carbon steel.* Wear, **2003**. 255: p. 832-835.

Uddin S.M., Mahmud T., C. Wolf, C. Glanz, *Effect of size and shape of metal particles to improve hardness and electrical properties of carbon nanotube reinforced copper and copper alloy composites.* Composites Science Technology, **2010**. 70: p. 2253-2257.

Valiev R., *Nanostructuring of metals by severe plastic deformation for advanced properties*. Nature Materials, **2004**. 3: p. 511-516.

Wang F., Y. Li, K. Yamanaka, K. Wakon, K. Harata, A. Chiba, *Influence of two-step ball-milling condition on electrical and mechanical properties of TiC-dispersion-strengthened Cu alloys.* Materials and Design, **2014**. 64: p. 441-449.

Wang K., N.R. Tao, G. Liu, J. Lu, K. Lu, *Plastic strain-induced grain refinement at the nanometer scale in copper.* Acta Materialia, **2006**. 54: p. 5281-5291.

Wen H., Y. Zhao, Z. Zhang, O. Ertorer, S. Dong, E.J. Lavernia, *The influence of oxygen and nitrogen contamination on the densification behavior of cryomilled copper powders during spark plasma sintering.* Journal of Materials Science. **2011**. 46(9): p. 3006-3012.

Xiao X., Z. Zeng, Z. Zhao, S. Xiao, *Flaking behavior and microstructure evolution of nickel and copper powder during mechanical milling in liquid environment*. Materials Science and Engineering A, **2008**. 475: p. 166-171.

Yanagisawa O., H. Kuramoto, K. Matsugi, M. Komatsu, *Observation of particle behvaior in copper powder compact during pulsed electric discharge*. Materials Science and Engineering A, **2003**. 350: p. 184-189.

Yousefi M., S. Sharafi, A. Mehrolhosseiny, *Correlation between structural parameters and magnetic properties of ball milled nano-crystalline Fe-Co-Si powders.* Advanced Powder Technology, **2013.** 25: p. 752-760.

Yusoff M., R. Othman, Z. Hussain, *Mechanical alloying and sintering of nanostructured tungsten carbide-reinforced copper composite and its characterization.* Materials and Design, **2011**. 32: p. 3293-3298.

Zeng Q., Y.F. Xiao, S.Z. Dong, X.B. Liu, B.Q. Qui, et al., *Influence of milling conditions on magnetic properties of $Nd(Fe,Mo)_{12}N_x$ compounds*. Journal of Magnetism and Magnetic Materials, **1999**. 192: p. 321-324.

Zhang F.L., M. Zhu, C.Y. Wang, *Parameters optimization in the planetary ball milling of nanostructured tungsten carbide/cobalt powder.* International Journal of Refractory Metals & Hard Materials, **2008**. 26: p. 329-333.

Zhang J., L. He, Y. Zhou, *Highly conductive and strengthened copper matrix composite reinforced by $Zr_2Al_3C_4$ particulates.* Scripta Materialia, **2009**. 60: p. 976-979.

Zhang R., L. Gao, J. Guo, *Thermodynamic behaviour of copper-coated silicon carbide particles during conventional heating and spark plasma sintering.* Communications of the American Ceramic Society, **2003.** 86: p. 1446-1448.

Zhang Y.F., L. Lu, S.M. Yap, *Prediction of the amount of PCA for mechanical milling.* Journal of Materials Processing Technology, **1999**. 89-90: p. 260-265.

Zhang Y.S., Z. Han, K. Wang, K. Lu, *Friction and wear behaviors of nanocrystalline surface layer of pure copper.* Wear, **2006**. 260: p. 942-948

Zhang Y.S., K. Wang, Z. Han, G. Liu, *Dry sliding wear behavior of copper with nano-scaled twins.* Wear, **2007**. 262: p. 1463-1470.

Zhang Y.S., Z. Han, K. Lu, *Fretting wear behavior of nanocrystalline surface layer of copper under dry condition.* Wear, **2008.** 265: p. 396-401.

Zhang Z.H., F.C. Wang, L. Wang, S.K. Li, *Ultrafine-grained copper prepared by spark plasma sintering process.* Materials Science and Engineering A, **2008**. 476: p. 201-205.

Zhao Y.H., K. Lu, *Microstructure evolution and thermal properties in nanocrystalline Cu during mechanical attrition.* Physical Review B, **2002**. 66: p. 085404_1-8.

Zhaohui Z., W. Fuchi, W. Lin, L. Shukui, S. Osamu, *Sintering mechanism of large-scale ultrafine-grained copper prepared by SPS method.* Materials Letters. **2008**. 62(24): p. 3987–3990.

Zum Gahr K.H., *Wear by hard particles.* Tribology International, **1998**. 31: p. 587-596.

Scientific Production

International Journal:

[1] M.Pellizzari, D.Ugues, **G.Cipolloni**, *Influence of heat treatment and surface engineering on thermal fatigue behavior of tool steel*, International Heat Treatment and Surface Engineering 7:4 (2013) 180 -184. DOI: 10.1179/1749514813Z.00000000091.

[2] C.Menapace, **G.Cipolloni**, A.Molinari, *Influence of high temperature sintering on impact properties of low alloyed steels,* Materials Science Forum 802 (2014) 483-488. DOI:10.4028/www.scientific.net/MSF.802.483

[3] **G.Cipolloni**, C.Menapace, I.Cristofolini, A.Molinari, *A quantitative characterization of porosity in a Cr-Mo sintered steel by Image Analysis*, Materials Characterization 94 (2014) 58 - 68. DOI: 10.1016/j.matchar.2014.05.005

[4] **G.Cipolloni**, M.Pellizzari, A.Molinari, M.Hebda, M.Zadra, *Contamination during high energy milling of atomized copper powder and its effects on Spark Plasma Sintering*, Powder Technology 275 (2015) 51-59. DOI:10.1016/j.powtec.2015.01.063

[5] C.Menapace, **G.Cipolloni**, M.Hebda, G. Ischia, *Spark plasma sintering behaviour of copper powders having different particle sizes and oxygen contents*, Powder Technology 291 (2016) 170-177. DOI:10.1016/j.powtec.2015.12.020

Proceedings:

[1] I.Cristofolini, **G.Cipolloni**, A.Molinari, *Macro and micro-geometrical characteristics of surfaces of porous sintered parts,* Proc. Int. Conf. on Powder Metallurgy & Particulate Materials, Nashville (United State of America) 2012, pp. 714-724. ISBN: 9780985339722

[2] M.Pellizzari, D.Ugues, **G.Cipolloni**, *Influence of heat treatment and surface engineering on thermal fatigue behaviour of tool steel*, Proc. 2nd Mediterranean Conference & New Challenges on Heat Treatment and Surface Engineering, Dubrovnik (Croatia) 2013, pp. 207-214. ISBN: 9789537690021

[3] C.Menapace, **G.Cipolloni**, A. Molinari, *Influence of high temperature sintering on impact properties of low alloyed steels, Proc. Conf. on* PTECH Congress in Brazil 2013. DOI:10.4028/www.scientific.net/MSF.802.483

[4] C.Menapace, **G.Cipolloni**, A.Molinari, *Influence of the high sintering temperature on the impact properties of a low alloyed Cu-Mo steel*, Proc. European Powder Metallurgy Congress & Exhibition - EUROPM 2014, Salzburg (Austria) 2014.

[5] **G.Cipolloni**, M.Pellizzari, A.Molinari, M.Hebda, M.Zadra, *Study of the processing route of copper powder by mechanical milling and Spark Plasma Sintering*, Proc. of: European Powder Metallurgy Congress & Exhibition – EUROPM 2014, Salzburg (Austria) 2014.

[6] **G.Cipolloni**, M.Pellizzari, A.Molinari, B.T.Cao, *Produzione e caratterizzazione di compositi a matrice in Cu rinforzati con particelle di TiB_2* , Proc. of: 35° Convegno nazionale della metallurgia italiana, Roma (Italy) 2014.

[7] **G.Cipolloni**, M.Pellizzari, A.Molinari, *Tribological behaviour of TiB_2 reinforced Cu-matrix composites produced by mechanical alloying and spark plasma sintering*, Proc. of: European Powder Metallurgy Congress & Exhibition – EUROPM 2015, Reims (France) 2015.

Acknowledgments

I gratefully acknowledge Pometon Powder Company for the supply of copper powder.
This research was supported by Professor J.Kazior and his assistant M.Hebda of the Institute of Materials Engineering, Cracow University of Technology (Poland), for the thermo-gravimetrical and the quadrupole mass spectrometry analyses.
I would like to thank Netzsch group, especially Dr.C.Baldini and Dr.F.Beckstein for the thermal conductivity analysis.
Finally I would like to thank the University of Trento, especially the Department of Industrial Engineering. I gratefully acknowledge Professor Molinari and Professor Pellizzari.

…e quelli meno formali…

Un ringraziamento speciale va nuovamente al Professor Pellizzari che mi ha sostenuto in questi tre anni, e spesso mi ha indirizzato nel percorso in modo da rendere al meglio e ottenere soddisfazioni personali e professionali.

Un ringraziamento alla K4Sint di Pergine per aver sinterizzato qualsiasi polvere di rame portassi. Un grazie speciale a Mario, che con i suoi consigli professionali e concreti è stato di grande aiuto in questo percorso.

Un grazie di cuore a tutto il laboratorio di metallurgia: a chi c'era quando sono arrivata e poi se ne è andato, a chi è arrivato con me e abbiamo fatto questo cammino insieme, e a chi è arrivato dopo e rimarrà ancora un po' a lucidare.

Un grazie speciale a Cinzia per l' efficace e produttiva collaborazione, inoltre grazie per essere sempre stata disponibile e gentile. Il tuo supporto e la tua energia sono stati fondamentali per me e lo sono per tutti i boys e le girls del laboratorio.

Un grazie a Lorena e Gloria per il vostro sostegno e la vostra professionalità, il SEM e il TEM (soprattutto quelli vecchi) non renderebbero così bene senza di voi.

Ci tengo a ringraziare tutte le persone che vivono la mia quotidianità.

Prima di tutto le 'girls power' con le quali l'amicizia è cresciuta giorno dopo giorno e durerà oltre il 15/04/2016. Grazie Lorena perchè con la tua ansia e precisione mi hai fatto ricordare scadenze e impegni che altrimenti avrei totalmente dimenticato, ma soprattutto grazie per il sostegno e l'aiuto di tutti i giorni. Grazie Ali per avermi fatto capire che non c'è solo il lavoro, ma esistono anche i giorni di ferie! Grazie a Sara per essermi stata vicina sia come perfetta segretaria del DII ma in special modo come amica.

Grazie a Maida che ormai conviviamo da più di sei anni condividendo momenti up e down, ma alla fine tutto si risolve con una chiaccherata sul divano.

Anche se un po' più distanti un grazie speciale a Fede e Ali, che sono sempre presenti nella mia vita e lo saranno ancora a lungo. Siete speciali amiche mie!

Un ringraziamento dal profondo del cuore a tutta le mia famiglia, e in special modo a papà e mamma che senza il loro appoggio, sostegno e aiuto tutto questo non sarebbe stato possibile.

E un grazie particolare ad Enrico che mi è vicino in ogni istante.